LARGE SCALE INFLUENCES ON INTERANNUAL VARIABILITY, PHYSICAL MECHANISMS, POTENTIAL PREDICTABILITY AND PREDICTION OF SHORT RAINS OVER EAST AFRICA

By:

Titike Kassa

DEPARTMENT OF PHYSICS THE SCHOOL OF GRADUATE STUDIES OF ADDIS ABABA UNIVERSITY

A THESIS SUBMITTED IN PARTIAL FULFILLMENT OF THE REQUIREMENT FOR THE DEGREE OF **DOCTOR OF PHILOSOPHY (Ph.D.) IN ATMOSPHERIC PHYSICS**

November, 2014
Addis Ababa, Ethiopia

Declaration

DEPARTMENT OF PHYSICS, ADDIS ABABA UNIVERSITY

The undersigned hereby certify that they have read and recommend to the Graduate Studies in College of Natural Sciences for acceptance a thesis entitled "**Large Scale Influences on Interannual Variability, Physical Mechanisms, Potential Predictability and Prediction of Short Rains over East Africa**" by **Titike Kassa** in partial fulfillment of the requirements for the degree of **Doctor of Philosophy in Atmospheric Physics**.

Dated: November, 2014

External Examiner: _____ _____

Prof. Jianping Li
Dean GCESS, Beijing Normal
University, Beijing 100875, China

Internal Examiner: _____ _____

Prof. A. V. Gholap
Professor, Department of Physics,
AAU, AA, Ethiopia

Main Supervisor: _____ _____

Dr. Gizaw Mengistu
Associate Professor, Department
of Physics, AAU, AA, Ethiopia

Examining Chair: _____ _____

Dr. Deribie Hirpo
Assistant Professor, Department
of Physics, AAU, AA, Ethiopia

ADDIS ABABA UNIVERSITY

Date: **November, 2014**

Author: **Titike Kassa**

Title: **Large Scale Influences on Interannual Variability, Physical Mechanisms, Potential Predictability and Prediction of Short Rains over East Africa**

Department: **Physics**

Degree: **PhD** Convocation: **November** Year: **2014**

Permission is herewith granted to **Addis Ababa University (AAU)** to circulate and to have copied for non-commercial purposes, at its discretion, the above title upon the request of individuals or institutions.

Signature of Author

Declaration of originality

This dissertation contains no material which has been accepted for a degree or diploma by the University or any other institution, except by way of background information and duly acknowledged in the dissertation. Moreover, to the best of my knowledge and belief no material previously published or written by another person except where due acknowledgement is made in the text of the dissertation, nor does the dissertation contain any material that infringes copyright.

Dated: November, 2014

The Author: _____ _____

Titike Kassa

PhD Student, Department of

Physics, AAU, AA, Ethiopia

Coauthorship

Chapter 5 contains material that was published in T. k. Bahaga, G. Mengistu Tsidu, F. Kucharski, G. Tefera Diro 2014. Potential predictability of the SST-forced equatorial East African short rain interannual variability in the 20^{th} century. *Q. J. R. Meteorol. Soc. :DOI:10.1002/qj.2338.* A part of Chapter 6 contains material puplished in Bahaga et al. 2013 *NWS Science and Technology infusion Climate Bulletin Supplement, NOAA* and the rest of Chapter 6 has been submitted with minor revison for publication T. k. Bahaga, F. Kucharski, G. Mengistu Tsidu, Hongwei Yang 2014: Assessment of prediction and Predictability of Short rain over Equatorial East Africa using APCC Multi-Model Ensemble *(minor revision submitted to Theoretical and Applied Climatology).*

In all cases, the design and implementation of the research, data analysis, interpretation of the results and manuscript preparation was the responsibility of the candidate. G. Mengistu Tsidu (Atmospheric science group, Department of Physics, Addis Ababa University (AAU)) and F. Kucharski (Earth System Physics Section, Abdus Salam International Center for Theoretical Physics (ICTP)) played great role in assisting with valuable insight, direction and guidance and supervision in all aspects of the PhD and with help producing publishable quality manuscripts.

Dated: November, 2014

Main Supervisor: _____ _____

Dr. Gizaw Mengistu
Associate Professor, Department
of Physics, AAU, AA, Ethiopia

Co-Supervisor: _____ _____

Dr. Fred Kucharski
Research Scientist, Earth System
physics, ICTP, Trieste, Italy

Acknowledgements

Above all, I would like to thank the Almighty God for His unreserved gift. "Trust in the Lord with all your heart. Don't put your confidence in your own understanding. In all your way acknowledge Him, and He will direct your path." Proverbs 3:5-6.

I would like to thank first and foremost my supervisors, **Dr. Gizaw Mengistu** and **Dr. Fred Kucharski** for their valuable insight, direction, encouragement and guidance throughout these years. It is with great appreciation that I thank Dr. Gizaw Mengistu not only for sharing his wisdom, experience and enlightening discussion all the way through from the beginning but also for his tireless effort, commitment and great contribution in advancing Atmospheric Science in AAU in particular and throughout the country at large. I would also like to express my admiration and thanks to Dr. Fred Kucharski for his constant dedication, invaluable advise, thoughtful comments and tremendous mentor for the successful completion of this study.

The authors thank all anonymous reviewers for their time, expertise in making a thorough revision and constructive comments, which greatly helped improve the quality of the published manuscripts which are included in Chapter 5 and Chapter 6 of this dissertation.

My great acknowledgment goes to Sandwich Training Educational Program (**STEP**) for providing financial support for the duration of my research visits to **ICTP**. I am highly indebted to ICTP and all people behind the institution who support and implement the idea which contributes greatly to science in the developing world by creating opportunities to those who lacked it so that they in turn will play their part. I am also thankful to Earth System Physics Section at ICTP for offering me the opportunity, providing infrastructure, research facilities and fascinating research environment.

I gratefully acknowledge the Asian Pacific Climate Center (**APCC**) for providing me financial support, opportunity, facilities and engaging research environment during my visit to their center

in Busan, South Korea on Young Scientist Support Program (YSSP). I am also highly indebted to APCC for providing the coupled models hindcast datasets used in Chapter 6 of this dissertation, which are collected from different operational numerical weather prediction (NWP) centers.

Special thanks go to school of graduate studies in AAU for accepting my application as PhD student and in particularly academic and administrative staff of Department of Physics. I would also wish to thank previous Department Head Dr. Lemi Demiyu and Dr. Belayneh Mesifin current head for their consistent help, support and for every opportunity for successful completion of my work. Special mention and thank also given to w/r Tsilate Adinew, secretary Department of Physics for her efforts in facilitating my dealings with the department and providing resources and research facilities.

I acknowledge Jigjiga University for offering me the opportunity for study leave and their consistent financial support over the last five years for the PhD fellowship, in general for investing so much resource to train me as a part of academic staff development.

Special thanks must go to Institute of Geophysics, Space Science and Astronomy (**IGSSA**) and staff members for providing me with computational facilities, office and suitable research environment.

I also thank all institutions around the world that maintain and allow public access to observational, reanalysis, reconstructed and/or other datasets used in this study.

This dissertation work is dedicated to my incredibly wonderful wife, Meron, who has been a constant source of support and encouragement during the challenges of my research and Sileshi, who has always been a source of inspiration over the years to get me to where I am now through your encouragement.

Lastly, I would like to pay tribute to my parents, office mates, class mates and friends for their continuing support and tolerance. To my brothers and sister who have been a source of strength and motivation from the beginning, and to all people who supported me with this dissertation.

List of supporting publications

Bahaga, TK, Mengistu Tsidu G, Kucharski F, Diro GT. 2014. Potential Predictability of the SST-Forced Equatorial East African Short Rain Interannual Variability in the 20^{th} Century. *Q. J. R. Meteorol. Soc. :DOI:10.1002/qj.2338*

Bahaga, TK, Mengistu Tsidu G, Kucharski F, Hongwei Y. 2013. Prediction of short rains over East Africa using multi model ensemble. *NWS Science and Technology infusion Climate Bulletin Supplement, NOAA.*

Bahaga, TK, Kucharski F, Mengistu Tsidu G, Hongwei Y. 2014. Assessment of Prediction and Predictability of short rains over Equatorial East Africa using Multi-Model Ensemble. *(minor revision submitted to Theoretical and Applied Climatology)*

Abstract

The climate of the East Africa exhibits marked interannual fluctuations that provoke droughts or flooding which lead to enormous impact on socio-economic activities over the region. Therefore, understanding of the mechanisms that produce this variability and developing both dynamical and statistical approaches for extended range forecast and projected information on future climate is of great importance. In the first part of this study observational datasets and a series of Sea Surface Temperature (SST) forced Atmospheric General Circulation Model (AGCM) ensemble simulations for the whole 20^{th} century are analyzed to investigate the physical mechanism and potential predictability of East African short rains variability.

It is found that there is substantial skill in reproducing the East African short rains variability given the SSTs are known. Consistent with recent previous studies it is found that the Indian Ocean (IO) and in particular the western pole of the Indian Ocean dipole (IOD) play a dominant role for the prediction skill, whereas SST outside the IO play a minor role. The physical mechanism for the western IO influence on East African rainfall in the model is consistent with previous findings and consists of a gill-type response to a warm (cold) anomaly that induces a westerly (easterly) low-level flow anomaly over equatorial Africa and leads to moisture flux convergence (divergence) over East Africa. On the other hand a positive El Niño-Southern Oscillation (ENSO) anomaly leads to a spatially non coherent reducing effect over parts of East Africa, but the relationship is not strong enough to provide any predictive skill in our model.

The East African short rains prediction skill is also analyzed within a model derived potential predictability framework and it is shown that the actual prediction skill is broadly consistent with the models potential prediction skill. Low frequency variations of the prediction skill are mostly related to SSTs outside the IO region and likely due to an increased interference of ENSO with the IO influence on East African short rains after the mid-70s climate shift.

Based on results from a series of AGCM experiments, the performance of dynamical seasonal forecast systems are evaluated for the prediction of SSTAs over tropical IO and short rains anomalies over equatorial East Africa. The evaluation is based on ob-

servational datasets and the Asia-Pacific Climate Center (APCC) Ocean-Atmosphere-Land coupled Multi-Model Ensemble (MME) retrospective forecasts (hindcasts) using common years for all models from 1982 to 2005.

The coupled climate models ensemble reproduces seasonal characteristics of low level wind, the spatial distribution of SON mean rainfall and seasonal climate variations over equatorial East Africa with further improvement in MME mean. Ensemble mean of individual coupled models and MME mean also show statistically significant skill in forecasting sea surface temperatures anomalies (SSTAs) over the western and eastern parts of the tropical IO, giving significant correlation at 99% confidence level for IOD. Moreover, five out of ten coupled models and MME mean show statistically significant skill in predicting equatorial East Africa short rains. The fidelity of hindcasts is further measured by Anomaly Correlation Coefficient (ACC) and four models as well as MME mean show significant skill over East Africa. It is shown that the reproduction of the observed variability in the East African region is mainly due to a realistic relationship of East African rainfall with the IOD. Overall, the skill of the dynamical models is attributed to the fact that slowly evolving SSTs are the primary source of predictability, and to the fact that coupled climate models produce skillful predictions of SON SST anomalies over tropical IO.

This study therefore provides insight into interannual rainfall variability and predictability over East Africa, in view of tropical Indian Ocean-Atmosphere climate patterns and underlying mechanisms. In addition, the information on coupled forecast systems will open the possibility of using readily available seasonal forecasts as skillful predictions of equatorial East Africa short rains. On the whole, the results found in this study will feed into real-time monitoring and forecasting at seasonal to interannual timescales to enhance early warning and disaster preparedness activities and minimize the impacts of climate-related catastrophes that are prevalent in the region.

Contents

List of Figures

List of Tables

Chapter 1

Introduction

East African countries are facing recurrent extreme climate events with extensive economic and social consequences. In particular, persistent interannual fluctuation of short rains over equatorial East Africa affect rain-fed agriculture, drinking water, health, generation of pasture and the very livelihood of highly vulnerable society. The 2010-2011 droughts in East Africa (Famine Early Warning System Network, East Africa), by some measures the worst drought in 60 years, is a reminder that rainfall in this politically and socioeconomically vulnerable region can fluctuate dramatically. These variations and extremes are related to a lack of or an excess of rainfall which often lead to severe disasters such as flooding or drought. This makes understanding of the mechanisms that produce this variability and developing both dynamical and statistical approach for extended range forecast of short rains from a month to seasons be vital for agricultural productivity, management of water resources, disaster prevention and mitigation, and better socio-economic planning. In addition, the successful prediction of short rains and timely availability of information prior to the rainy season is very important for the region (Jury, 2002), ranging

from reasonable advices for lending money from banks for seed to local management of epidemic diseases (Morse *et al.*, 2003) and flood/drought controls (CLIVAR, 1999).

The mean climate patterns over Equatorial East Africa are closely linked to regional factors and the inter-tropical convergence zone (ITCZ). ITCZ sweeps across the region twice a year and has significant influence on the climatological rainfall pattern. The influence of ITCZ is largely responsible for the bimodal rainfall pattern experienced over many parts during March to May (long rains) and September to November (short rains). The amount of rainfall is larger during the season of long rains, as compared to that of the short rains (Hastenrath *et al.*, 1993). Moreover, the long rains bring several weeks of heavy rainfall associated with the relatively slow northward movement of the ITCZ. In contrast, during the core of the short rains, the southward migration of the ITCZ is more rapid (Black *et al.*, 2003) and exhibits more intense variability (Hastenrath *et al.*, 2007). Although the averaged rainfall amount is larger during the long rains than during the short rains, the latter shows more interannual variability (Hastenrath *et al.*, 1993; Black *et al.*, 2003) and has a larger impact on the society through changes of the regional hydrological cycle (Behera *et al.*, 2005).

Rainfall variability over East Africa is dominated by changes on the large-scale with a clear link to tropical Ocean-Atmosphere variability. The interannual variability of East Africa rainfall and its relationship with SST has been examined extensively using a statistical approach (e.g., Ropelewski and Halpert, 1987; Hastenrath *et al.*, 1993; Mutai *et al.*, 1998; Ogallo, 1988; Diro *et al.*, 2008, 2011). These studies focus on the role of ENSO in controlling the East African rainfall.

However, Saji *et al.* (1999) reported the co-existence of IOD and some exceptional short rains events over East Africa. In view of this new mode, the focus has been shifted to the IO for

understanding variability of the short rains (Black *et al.*, 2003; Yamagata *et al.*, 2004; Behera *et al.*, 2005; Ummenhofer *et al.*, 2009). These studies concluded that rainfall over East Africa (Indonesia) is increased (decreased) during a positive IOD event and the reverse Ocean-Atmosphere condition happens in negative IOD event.

On the other hand, it is clearly important to be able to assess where on the globe atmospheric variations are sufficiently affected by oceanic forcing to enable practical seasonal prediction. This requires measurements of atmospheric potential predictability (potential indicates that this also depends on predictions of anomalous oceanic forcing), whose definition and mapping have been topics of ongoing research in the climate community (Rowell, 1998). Predictability of East Africa short rains has been analyzed in previous studies. Mutai and coworkers (Mutai *et al.*, 1998; Mutai and Ward, 2000) used global SST as input to empirical orthogonal function (EOF) analysis aimed at the seasonal forecasting of the East African rainfall. The short rains of the East African coast have a concurrent correlation of -0.85 with the equatorial surface westerlies (Hastenrath *et al.*, 1993). Consequently, empirical circulation diagnostics has been applied by Philippon *et al.* (2002). Moreover, Hastenrath *et al.* (2004) explored the predictability of short rains using different indices derived from observation and reanalysis data, and found that the sudden development of the zonal circulation cell and the lack of long-lived precursors seriously hamper its usefulness as predictors for East African short rains. On the other hand, a temporally limited potential dynamical predictability of short rains has been indicated using a Coupled Ocean-Atmosphere General Circulation Model (CGCM, Behera *et al.* (2005)). They showed that the July-August signal of the IOD in the SST dipole mode index have high prediction skill for the variations of short rains.

The scientific basis for such skillful dynamical seasonal forecasting is slowly varying lower-boundary forcing including SST, land-surface temperature and albedo, vegetation cover and type, soil moisture and snow cover, which cause atmospheric perturbations, having longer memory than the atmospheric perturbations themselves, and the response of the Atmosphere to these forcing being detectable (Murphy *et al.*, 2001). Among these slowly varying boundary forcing, SSTs are believed to have the strongest relationship with East Africa rainfall because of their coupling to the deep convection and hence to the large-scale dynamics of the Atmosphere (Diro *et al.*, 2008; Segele *et al.*, 2009). Several observational and modeling studies (Charney and Shukla, 1981; Palmer and Anderson, 1994) provide evidence that boundary forcing, particularly in the tropics, contributes significantly to the interannual variability and predictability of the tropical climate and the monsoon circulations.

Regardless of the numerous studies discussed above, there are many unsettled questions regarding to what extent IOD and ENSO influence equatorial East African short rains. Though some studies have shown the importance of western part of the Tropical Indian Ocean (TIO) for short rains anomalies over East Africa, the relative importance of easterly versus westerly low-level wind anomalies induced by the warm anomaly over western IO has not been sufficiently addressed. Moreover, there is lack of reports regarding assessment of potential predictability and its decadal changes of SON rainfall based on AGCM ensemble experiments for the whole 20^{th} century. Furthermore, the study by Desole and Shukla (2012) on predictability of Indian monsoon also showed dynamical models extract more predictive information than statistical models for seasonal prediction. Despite the relative advantage and availability of full coupled GCMs, predictability and prediction of equatorial East Africa short rains has not been evaluated using

MME forecast systems. There is also a growing evidence of the role of IOD for driving predictable climate variability over regions surrounding IO.

Therefore, the main purposes of this dissertation are (1) to investigate further the relative influence of IO compared to that of the Pacific Ocean as well as their combined effect on the interannual variability of short rains over East Africa, (2) to evaluate potential predictability as well as its decadal changes of short rains over equatorial East Africa using ensembles of long AGCM simulations for the whole 20^{th} century, (3) to confirm and refine previously identified physical mechanisms by which IOD impacts East African short rains with a focus on the implication for seasonal predictability and (4) in light of usefulness of IOD for seasonal prediction and research gaps in the evaluation on the performance of coupled MME dynamical seasonal forecast systems, we have also explored deterministic prediction of SSTAs in the IO and short rains anomalies over equatorial East Africa.

The dissertation is organized such that in Chapter 2 a description of observational and reanalysis datasets used, explanation of ICTPAGCM, its physical parametrization and experimental set-up is given. In addition, a brief report on operational seasonal forecast systems and statistical methods used is also presented. Chapter 3 examines the the dynamics of East Africa mean climate, climate controlling systems and large scale atmospheric circulation climatology.

A literature review follows in Chapter 4 on the current state of knowledge of East Africa rainfall variability, predictability and the influences of tropical Ocean-Atmosphere climate patterns and underlying mechanisms. Results on analysis of climatological features of observation and ICTPAGCM simulations over IO basin and East Africa during SON season are given in Chapter 5. In this Chapter the responses of the Atmosphere for individual ICTPAGCM experiments

and anomalies associated with extremes in the East Africa short rains and the physical mechanism for the change in circulation pattern are also explored. Moreover, assessment of potential predictability of short rains with ICTPAGCM ensemble experiments is given.

In Chapter 6, a validation of individual coupled models and MME mean in simulating SON seasonal mean climate over Africa as well as in the IO basin and the seasonal cycle over East Africa is shown. An assessment on the skill of coupled models and MME mean in forecasting SON SST anomalies over tropical IO is also discussed. The effort on evaluation of real time prediction of equatorial East Africa short rains with coupled model ensembles and MME mean is also presented. Finally, the conclusions and summary are given in Chapter 7.

Chapter 2

Datasets, Models and Methodology

Various observation and reanalysis dataset have been used to understand East African climate, to evaluate the performance of both the AGCM and coupled dynamical forecast systems, to identify the key systematic bias and to provide a description of East African rainfall variability, predictability and its teleconnections with ENSO and IOD. The monthly data from the period 1920-2009 AGCM results and seasonal forecast systems with common period 1982 to 2005 are also used in this study. Some of observed dataset used includes, Climatic Research Unit (CRU; Mitchell and Jones, 2005) precipitation and Merged Analysis of Precipitation (CMAP) (Xie and Arkin, 1996). In addition, NCAR reanalysis wind, sea level pressure from HadSLP2, two observed SSTs are also incorporated. The details and technical information about the dataset used, models and methods are summarized in the following section.

2.1 Observed datasets

2.1.1 Rainfall

2.1.1.1 Tropical Rainfall Measuring Mission (TRMM)

In Chapter 2 we have used TRMM observed dataset to describe the spatial patterns of seasonal rainfall and annual characteristics over East Africa. TRMM is a joint U.S.-Japan satellite mission which is launched on 27 November 1997, to provide the first detailed and comprehensive dataset of the four-dimensional distribution of rainfall and latent heating over vastly under sampled tropical and subtropical oceans and continents (40^oS-40^oN). Over the past 14 years, TRMM has been a major data source for meteorological, hydrological, and other research and application activities around the world (Liu *et al.*, 2012). Monthly time series for 1989-2012 is downloaded from http://disc.sci.gsfc.nasa.gov/services/opendap/TRMM/trmm.shtml.

2.1.1.2 University of East Anglia (CRU)

In Chapter 5 of this thesis an analysis is made on a long year Atmospheric General Circulation Model (AGCM) ensemble simulations. These AGCM experiments are performed to understand the physical mechanism of large scale influences on East Africa rainfall variability. To evaluate the performance of the model in simulating climatological feature of rainfall, characteristics of low level flow and interannul rainfall variability over East Africa we have used Climatic Research Unit (CRU; Mitchell and Jones, 2005) precipitation based on gauge observations. CRU is a global dataset of monthly time series of precipitation. These are calculated on high-resolution 0.5^o x

0.5^o latitude/longitude grids, which are based on analysis of over 4000 individual weather station records distributed around the world. Many of the input records have been homogenized and span the period 1901-2009.

2.1.1.3 Climate Prediction Center (CPC) Merged Analysis of Precipitation (CMAP)

In Chapter 6 an assessment is made on the seasonal rainfall hindcast skill available from the Asia-Pacific Economic Cooperation (APEC) Climate Center (APCC) system. These hindcasts are available on a 2.5^o x 2.5^o latitude/longitude grid. Moreover, the forecast systems have different hindcast periods; here we have selected common years from 1982 to 2005. Climate Prediction Center (CPC) Merged Analysis of Precipitation (CMAP) (Xie and Arkin, 1996) is used as verification based on its availability over land and Ocean points, its data record match with the study period and its agreement with other gridded products. CMAP dataset contains monthly analyses of global precipitation in which observations from rain gauges are merged with precipitation estimates from several satellite based algorithms. CMAP analyses are on a 2.5^o x 2.5^o latitude-longitude grid and extend back to 1979. Otieno and Anyah (2013) made a brief analysis on the performance of CMAP dataset in representation of rainfall distribution and intensity over East Africa compared against different satellite-gauge rainfall products and they have found agreement between observations over the East Africa. CMAP data are provided by the Physical Sciences Division (PSD) of the Earth System Research Laboratory (ESRL), which is based at the National Oceanic and Atmospheric Administration (NOAA), Boulder, Colorado, USA. The data are available from http://www.cdc.noaa.gov/data/gridded/data.cmap.html.

2.1.2 Reanalysis wind

The National Centers for Environmental Prediction/National Center for Atmospheric Research (NCEP/NCAR) reanalysis wind are used to review the modeled wind climatologies at 200, 850, and 950hPa level and circulation anomalies around Indian Ocean basin associated with East Africa rainfall variability. The reanalysis dataset is generated using a state-of-the-science data assimilation scheme and numerical model (Kalnay *et al.*, 1996). This Climate Data Assimilation System employs T62 horizontal resolution (about 210 km, interpolated to a 2.5^o x 2.5^o latitude-longitude). The wind fields were assessed to have a high confidence rank by the authors of the reanalysis dataset (Kalnay *et al.*, 1996). The reanalysis dataset are available for 1948-2012.

2.1.3 Sea level pressure (SLP)

We also utilized Hadley Center Sea Level Pressure dataset (HadSLP2; Allan and Ansell, 2006) to examine the robustness of model simulation.

2.1.4 Sea surface semperature (SST)

2.1.4.1 NOAA ERSST

The SST dataset used in this study includes the Extended Reconstructed Sea Surface Temperature (ERSST.v3) dataset which is a global monthly sea surface temperature analysis derived from the International Comprehensive Ocean-Atmosphere Dataset with missing data filled in by statistical methods (thses dataset also includes satellite data) of (Smith *et al.*, 2008), with

a spatial resolution of 2^o latitude-longitude squares. This monthly analysis includes anomalies computed with respect to a 1971-2000 monthly climatology. This data was downloaded from http://www.ncdc.noaa.gov/ersst/ and is available from 1871 to present.

2.1.4.2 UK Met office HadISST

The Hadley Centre Sea Ice and Sea Surface Temperature data set (HadISST), contains in situ sea surface observations and satellite derived estimates at the sea surface (Rayner *et al.*, 2003) are included in the analysis to form a global SST observation dataset. HadISST (Version 1.1) is a combination of monthly globaly complete fields of SST and sea ice concentration. This data set gives global, reanalysis 1^o longitude $\times$ 1^o latitude gridded, sea-surface temperature (SST) data from 1870 to present.

2.2 Climate models

2.2.1 Atmospheric General Circulation Model (AGCM)

In this study the International Center for Theoretical Physics Atmospheric General circulation Model (ICTPAGCM) used to understand large scale influences and the underpinning physical mechanism of climate variability and predictability over East Africa. The ICTPAGCM version 41 (Kucharski *et al.*, 2013) (formerly known as "SPEEDY", for "Simplified Parameterizations, privitivE-Equation DYnamics") has been described in detail in Molteni (2005) in its 5-level version and in Kucharski *et al.* (2006) in its current 8-level version. The ICTPAGCM is based on a spectral

dynamical core developed at the Geophysical Fluid Dynamics Laboratory (see Held and Suarez (1994)). It is a hydrostatic, sigma (σ)-coordinate, spectral-transform model in the vorticity-divergence form described by Bourke (1974).

2.2.1.1 Overview of physical parameterizations.

The parametrized processes include short- and long-wave radiation, large-scale condensation, convection, surface fluxes of momentum, heat and moisture and vertical diffusion. Convection is represented by a mass-flux scheme that is activated where conditional instability is present and boundary-layer fluxes are obtained by stability-dependent bulk formulae. A set of physical parametrization schemes has been developed starting from basic principles used in more complex GCMs, with a number of simplifying assumptions which are suited to a model with a coarse vertical resolution. A more detailed and quantitative description can be found in (users.ictp.it/∼kucharsk).

2.2.1.2 Boundary conditions

As any atmospheric model, ICTPAGCM requires appropriate boundary conditions to determine the fluxes of momentum, heat and moisture at the surface, and the flux of incoming solar radiation at the top of the atmosphere. At the surface, in addition to topographic height and (fractional) land-sea mask, the model requires climatological fields of the following variables:

- sea surface temperature (SST);
- sea ice fraction;
- soil temperature in the deep soil layer (about 1 m);

- moisture in the top soil layer and the root-zone layer;
- snow depth;
- bare-surface albedo (in the absence of snow or sea ice);
- fraction of land-surface covered by vegetation.

For the last two fields, annual-mean values are used, while all other fields are specified as monthly means and are linearly interpolated to get daily-updated values. The bare-surface albedo is linearly combined with assigned values of sea-ice and snow albedo to get a net surface albedo, using weights which are linearly dependent on sea-ice fraction and snow cover respectively. Similarly, the soil moisture in the top soil layer and in the root zone are linearly combined (using the vegetation fraction) to define a soil moisture availability index, which is used to compute evaporation over land.

All climatological fields have been computed by averaging the corresponding data from the European Center for Medium-Range Weather Forecasts re-analysis (ERA15; see Gibson *et al.* (1997)) in the period 1981-90. This period has been chosen (instead of the full 1979-93 period cover by ERA15) to have a better balance between warm and cold ENSO events in the SST field.

For soil and sea ice, the temperature the upper layer (1m for soil and 1.8 m for sea ice) are estimated using an extended force-restore type approach.

The model allows a time-varying SST anomaly to be superimposed to the climatological SST; the anomaly can be either specified from an input file or computed by a coupled ocean model. As an option, speedy employs a slab Ocean model, with a depth of 50 m. Ocean temperature

anomalies are calculated due to net heatflux anomalies at the ocean surface. In order to determine the heatflux anomalies, SPEEDY has to be run previously using prescribed SSTs.

At the top of the atmosphere, the incoming flux of solar radiation is computed daily from astronomical formulae (the model has no daily cycle). Empirical, seasonally varying functions are used to define the absorption of solar radiation by ozone in the stratosphere, and the latitudinal variations of the optical depth for solar radiation depending on the daily-averaged zenith angle. The use of a proper ozone climatology is planned for future model versions.

2.2.2 Coupled dynamical seasonal forecast systems

The coupled dynamical models that are examined in this thesis are ten state-of-the-arts fully coupled Atmosphere-Ocean-Land seasonal prediction systems and are obtained from operational seasonal prediction models participating in the APCC MME seasonal forecast (Kang *et al.*, 2009; Lee *et al.*, 2010; Min *et al.*, 2011; Sohn *et al.*, 2011). These are among models participated in climate Prediction and its Application to Society (CliPAS) project, which was a multi-model inter-comparison and synthesis project sponsored by Asian-Pacific Economic Cooperation (APEC) Climate Center (APCC). The APCC/CliPAS project was formally established in April 2005 as a research and development component of APCC. One of the objectives of CliPAS was to develop a well-validated MME prediction system and to study the predictability of the seasonal and sub-seasonal climate variations (Wang *et al.*, 2009). Moreover, these models also have been used in the semi operational real-time long-lead coupled prediction at APCC (Sohn *et al.*, 2012). Table 2.1 presents a brief summary of each model. For more details of the models, the readers are referred to the relevant literatures cited in the Table 2.1. The models resolutions are different but interpolated

onto a common 2.5x2.5 grid prior to analysis. Each model have ensemble of different integrations and each ensemble member has been created using different atmospheric initial conditions, the size of individual model ensemble is given in column 7 of Table 2.1. We are interested in the skill of individual model ensembles and their Multi-Model ensemble mean during the common hindast period which covers the 24-year period from 1982 to 2005. These models have retrospective forecasts (hindcasts) with 6 month lead integration and are initialized in different month, but here we are interested to evaluate seasonal forecast initialized on first of August, averaged over predicted SON means, as these are most relevant to equatorial East African short rains prediction. The models Equatorial East Africa rainfall index (EEARI) is estimated by averaging individual models and the Multi-Model ensemble mean precipitation over the same domain.

2.3 Methodology

This study has employed different statistical methods to investigate large scale influences on interannul variability, to understand underlying physical mechanisms and to evaluate potential predictability and prediction of short rains over East Africa. Spectral analysis methods is used to demonstrate none randomnous of interannul fluctuations of short rains over East Africa. It also uses Empirical Orthogonal Function (EOF) analysis, also known as principal component analysis to investigate the dominant mode of variability on seasonal mean SSTAs over tropical Indian Ocean. Besides ICTPAGCM ensemble experiments we have employed other simple statistical methods and techniques including: correlation, regression and composite analysis to understand the drivers of interannul variability and to determine the potential predictability of short rains over East Africa. In addition, we have identified and applied standard forecast verification tools

Institute	*Model*	*AGCM*	*Resolution*	*OGCM*	*Resolution*	*Ensemble*	*Reference*
APCC	CCSM3	CAM3	T85L26	POP1.3	gxlv3L40	5	(Jeong *et al.*, 2008)
NCEP	CFS	GFS	T62 L64	GFS	1/3 °ltX5/8 °lnL27	15	(Saha *et al.*, 2006)
SNU	SNU	SNU	T42 L21	MOM2.2	1/3 °ltX1 °lnL32	6	(Ham and Kang, 2010)
NASA	NASA	NSIPP1	2 °ltx2.5 °lnL34	PoseidonV4	1/3 °lt5/8 °lnL27	8	(Vintzileos *et al.*, 2003)
UHT1	UHT1	ECHAM4	T31L19	UH Ocean	1 °ltx2 °lnL2	10	(Fu and Wang, 2004)
FRCGC	SINTEX-F	ECHAM4	T106 L19	OPA8.2	2 °cos(lt)x2 °lnL31	9	(Luo *et al.*, 2005)
BMRC	POAMA1.5	BAM 3.0d	T47 L17	ACOM2	0.5-1.5 °ltx2 °lnL31	10	(Zhong *et al.*, 2005)
PNU	PNU	CCM3	T42L18	MOM3	2.8125 °L29	5	(Sun and Ahn, 2011)
MSC	CanCM4	AGCM4	T63L35	OGCM4	1.41x0.94,L40	10	(Scinocca *et al.*, 2008)
MSC	CanCM3	AGCM3	T63L31	OGCM4	1.41x0.94,L40	10	(McFarlane *et al.*, 2005)

Table 2.1: Description of the coupled models and their retrospective forecast used in this thesis.

to measure and quantify the the skill of coupled dynamical forecast systems over the region.

In this section we give a brief description for some of these data analysis methods whereas the detailed discussion on the remaining of statistical methods and tools used in this study are given in the respective Chapters where they are used.

2.3.1 EOF method

We have used EOF method (Dommenget and Latif, 2002) to isolate the dominant modes of the interannual variability in the observed SSTAs over Indian Ocean basin. EOF analyses is widely used in climate research. In recent years there have been several studies in which EOF analyses were used to highlight potential physical mechanisms associated with climate variability. In EOF analysis it is assumed that the modes are orthogonal in space and time, and that the first mode is the mode that maximizes the explained variance over the total dataset.

The interannual variability of SSTAs derived from HadISST monthly dataset is analyzed based on seasonal mean data for the SON season. We have performed EOF analysis on a 62-years monthly SST (1950 -2012) over Indian Ocean basin to refine previous interpretation on physical mechanism associated with the spatial and temporal patterns of the first two EOF modes. The detailed discussion following the results of this analysis are given in section 4.2.

2.3.2 Spectral analysis

Spectral analysis is concerned with estimating the unknown spectrum of the process from the data and with quantifying the relative importance of different frequency bands to the variance of the process. The spectrum of a time series is the distribution of variance of the series as a

function of frequency. Apart from providing the spectral composition of a signal, spectral analysis also makes it possible to filter the signal in a selected band (or bands) and analyse the filtered signal, as well as to estimate qualitatively the relative contribution of the variance of the signal in a particular band into the total variance of the signal. Applications of spectral analysis in practice are commonly done or based on the Fourier Transform.

Applications of the spectral analysis methods in this study is limited to seasonal mean rainfall time series over East Africa. East Africa seasonal rainfall variability that is frequency-dependent, and understanding the frequency dependence may yield information about the underlying physical mechanisms. The discussion on spectral analysis is given in section 4.3.1.

Chapter 3

The Dynamics of East African Climate

The dynamics of climate at any location is determined by the space-time characteristics of the general circulation; which controlled by complex interaction between ecosystem, land, oceanic and atmospheric process. East Africa sub-regions covering Ethiopia highlands, Horn of Africa, Equatorial East Africa and southern East Africa has complex topography (Figure 3.1) compared to the rest of the continent. The sub-region roughly covers an area bounded between 12^o S to 12^o N latitudes and 29^o to 51^o E longitudes. The sub-region comprises of ten countries; Kenya, Uganda, Tanzania, Ethiopia, Eritrea, Djibouti, Rwanda, Sudan, Somalia and Burundi. The large-scale tropical controls, which includes several major convergence zones, are superimposed upon regional factors associated with lakes, topography and maritime influence. As a result, the climatic pattern are markedly complex and change rapidly over short distances.

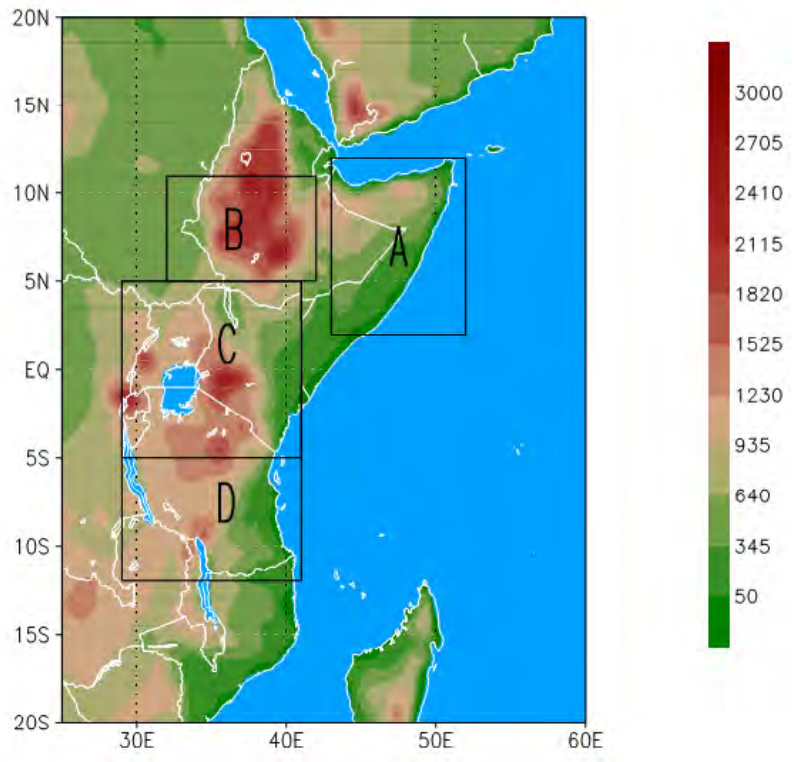

Figure 3.1: Map of East Africa showing the homogeneous rainfall regions. Region A (Horn of Africa); region B (Northern East Africa); region C (Equatorial East Africa); and region D (Southern East Africa). Rainfall was delineated into regions by using topography.

3.1 Regional climate systems

The climate of East Africa is dominated by planetary scale features such as the meridional overturning of the Hadley Circulation, Walker Circulation, the influences of the Atlantic and Indian Ocean monsoons, the Inter-Tropical Convergence Zone (ITCZ), teleconnections with sea-surface temperature (SST), subtropical anticyclons, tropical cyclones, jet streams and Easterly/westerly wave perturbations (Glantz, 1988; Nicholson *et al.*, 1988; Hastenrath, 1991). The characteristics of the general circulation are generally determined by individual locations by regional and local factors like topography and large water bodies, while the larger scale climate variability is sensitive to the large scale modes of variability. In addition, the latitude of each country is a major factor

in the distribution of the rainy seasons across the year, which is linked to the passage of the sun in the tropics.

In Ethiopia highland rainfall climatology is determined mainly by seasonal changes in large-scale circulation, part of which involves the seasonal north-south movement of the ITCZ. Main rainy season June-September (JJAS) (Figure 3.2c), which is associated with Indian summer (south-west) monsoon and locally known as Kiremt, this seasonal monsoon in Ethiopia is controlled by several climatological features in the lower and upper troposphere (e.g., Hastenrath, 1991; Segele *et al.*, 2009). These include the following: 1) seasonal northward advance of the ITCZ, persisting over Ethiopia; 2) formation of heat lows over the Sahara and Arabian landmasses; 3) establishment and intensification of subtropical high pressure over the Azores, St. Helena, and Mascarene; 4) well-developed southerly/southwesterly cross-equatorial moisture flow from the southern Indian Ocean, central tropical Africa, and the equatorial Atlantic; 5) upper-level Tropical Easterly Jet (TEJ) flowing over Ethiopia; 6) low-level jet (Somali jet). These synoptic systems arising from these seasonal circulations have been discussed (National Meteorological Agency NMA, 1996; Gissila *et al.*, 2004; Segele and Lamb, 2005; Segele *et al.*, 2009). Moreover, the spatial distribution of rainfall in Ethiopia is significantly influenced by topography which also has many unexpected changes in the Rift Valley (Kassie *et al.*, 2013).

3.1.1 Rainfall climatology

Seasonal mean rainfall derived from Tropical Rainfall Measuring Mission (TRMM) climatology over large part of East Africa is shown in Figure 3.2, brief description of this rainfall dataset is given in Chapter 2. It is readily seen that the dominant pattern is a seasonal south-north

movement of rainbelt, a consequence of the dominant influence of ITCZ.

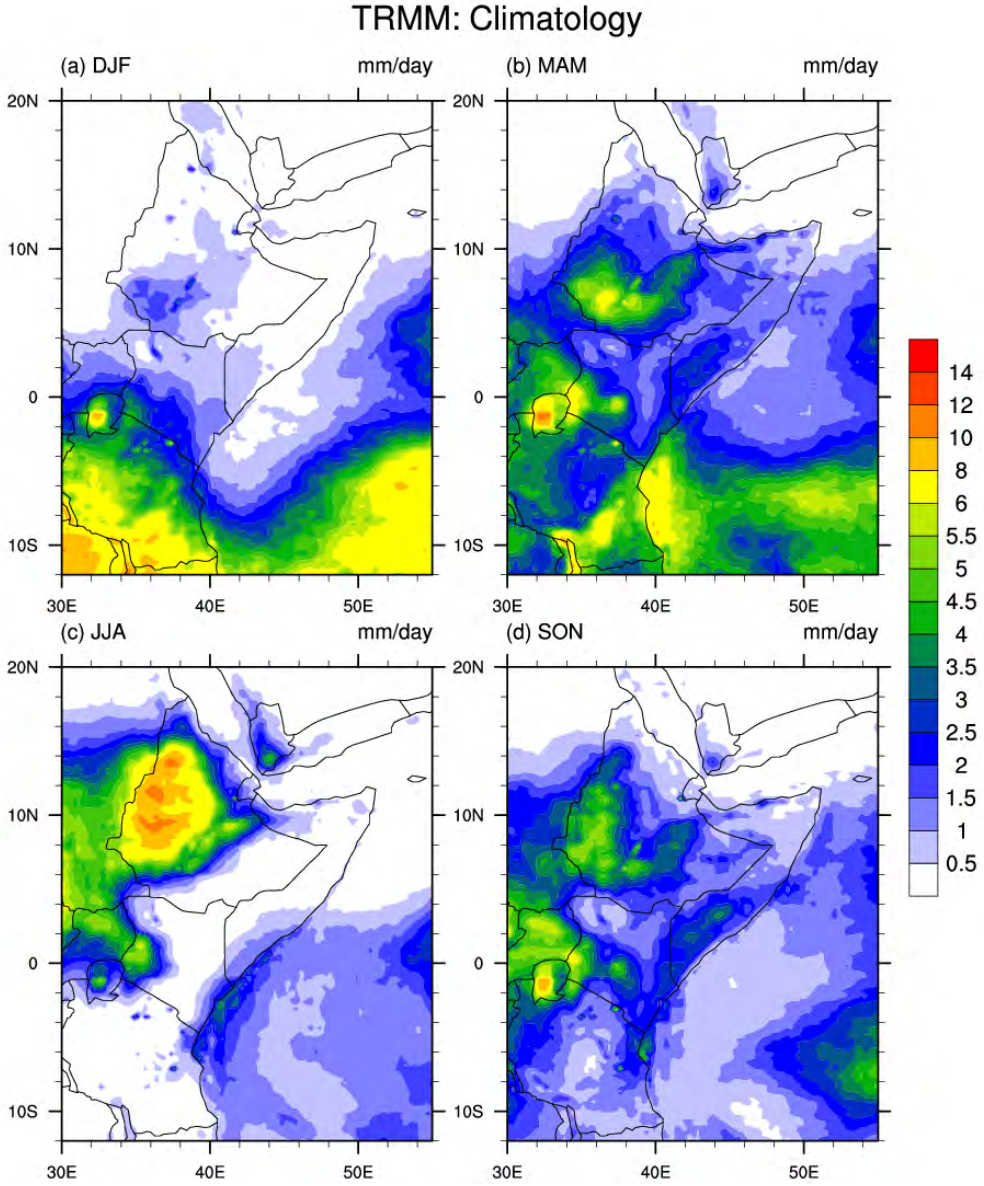

Figure 3.2: Seasonal mean TRMM rainfall distribution over East Africa for 1998 - 2012. (a) December - January - February (DJF), (b) March - April - May (MAM), (c) June - July - August (JJA) and (d) September - October - November (SON). Unit are given in $mm(day)^{-1}$.

Throughout December - January - February (DJF) most part East Africa are dry and the northeast monsoon brings dry continental air into East Africa, and consequently, the rainfall during these months is low (Figure 3.2a), except occurrence of heavy rainfall in southeastern hemisphere sector (Figure 3.2a). Equatorial East Africa region has bimodal rainfall distribution the "long

rains" in March-May (MAM) and the "short rains" in September-November (SON) (Figure 3.2b and d). This seasonal rainfall distribution influenced by the movement of the ITCZ, which migrates between 15^{o}S and 15^{o}N between January and July respectively, and by the monsoon circulation. These rainy seasons occur during the transitions between the winter and summer monsoons, when air in both hemispheres confluence near the equator (Hastenrath *et al.*, 2004). The timing of maximum rainfall lags the migration of the sun by approximately one month (Black *et al.*, 2003). During the so-called long rains, the ITCZ moves slowly north- wards, bringing several weeks of heavy rainfall. In contrast, during the short rains the ITCZ migration is relatively faster (Black *et al.*, 2003). On the other hand, the southwest monsoon starts in June and persists until September, during June - July - August (JJA) the moisture influx from the Atlantic and Indian Ocean results in high rainfall over Ethiopian highlands (Figure 3.2c; Segele *et al.*, 2009; Mengistu Tsidu, 2012). However, southern, southeastern and horn part of the East Africa are dry during southwest monsoon season because the monsoon flow is diverted by the high topography of Madagascar and the East African coast (Figure 3.2c).

3.1.2 Annual cycle of rainfal climatology

Figure 3.3 shows the average seasonal cycle in precipitation rate from TRMM for 1998-2012 averaged over four regions, (a) Ethiopian Highland (6-12^{o}N, 35-40^{o}E), (b) Horn of Africa (2-12^{o}N, 40-50^{o}E), (c) Equatorial East Africa (5^{o}S-5^{o}N, 35-46^{o}E) and (d) Southern East Africa (5^o-12^{o}S, 32-42^{o}E). Since East Africa lies in the tropics, each region has distinct annual rainfall cycle driven by the motion of the sun and associated changes in Oceanic and Atmospheric circulation caused by a degree of solar isolation (Figure 3.3; Black *et al.*, 2003). Moreover, the seasonal cycle of rainfall

in East Africa is controlled by large-scale monsoon circulations, the migration of the ITCZ, and by regional orography (Figure 3.1; Nicholson *et al.*, 1988; Black *et al.*, 2003).

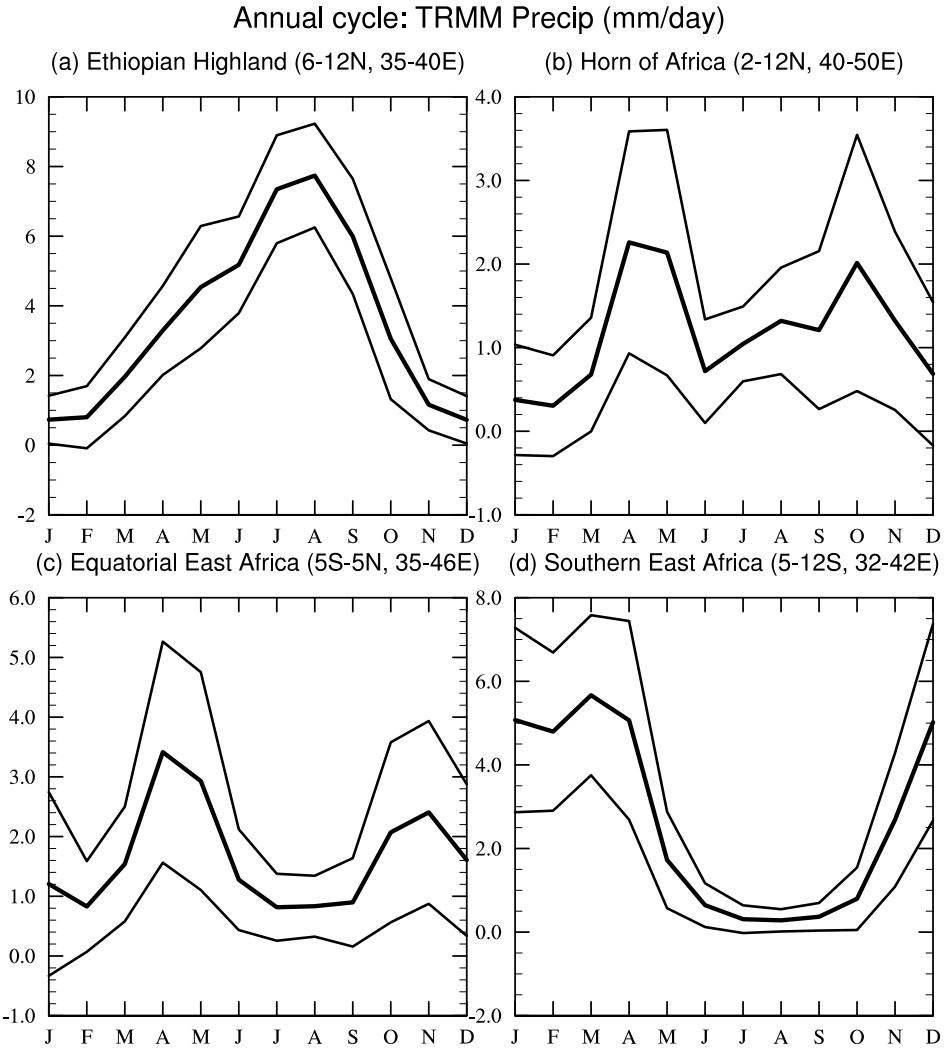

Figure 3.3: Annual cycle in East African rainfall for (a) Ethiopian Highland, (b) Horn of Africa, (c) Equatorial East Africa, and (d) Southern East Africa. The thick line denotes the climatological mean, and the thin lines show ± one standard deviation of the interannual variability. Rainfall is derived from TRMM and the unit is given in $mm(day)^{-1}$.

It is clearly seen that there is a marked contrast in the seasonal cycle between the northernmost region and the other three, reflecting the strong influence of the southwest monsoon circulation on rainfall in Ethiopian highland during JJA (Figure 3.3a). The other regions are dry during the southwest monsoon and instead show a semiannual distribution to the rainfall,

which is particularly marked for the equatorial East Africa and Horn of Africa (Figure 3.3c and d). On the other hand, Southern East Africa is dry throughout both southwest monsoon and equatorial transition period, this region receives significant amount of rain during boreal winter (Figure 3.3d).

Figure 3.3 also shows the interannual standard deviation. It is clear that the short rains are highly variable interannually. Indeed, in percentage terms, they are more variable than the long rains. The possible reasons for this are discussed later in the context of the interannually variability and predictability in Chapter 4.

3.2 Large-scale atmospheric circulations climatology

Figure 3.4 shows the seasonal mean reanalysis winds derived from National Centers for Environmental Prediction (NCEP) at the surface (925 hPa) and sea level pressure derived from Hadley Center Sea Level Pressure (HadSLP2) over the Indian Ocean region and Africa. The unique geography of the Indian Ocean region and Africa, being bounded to the north by the Asian continent, leads to a complex annual cycle associated with substantial seasonal reversals of the annual monsoon winds. The seasonal cycle is dominated by the Asian monsoon with its dramatic reversals of the wind from northeasterly in DJF (Figure 3.4a) to southwesterly in JJA (Figure 3.4c).

The wind and pressure patterns governing Equatorial East Africa climate include three major air streams and three convergence zones (Figure 3.4b and d). The air streams are Congo air

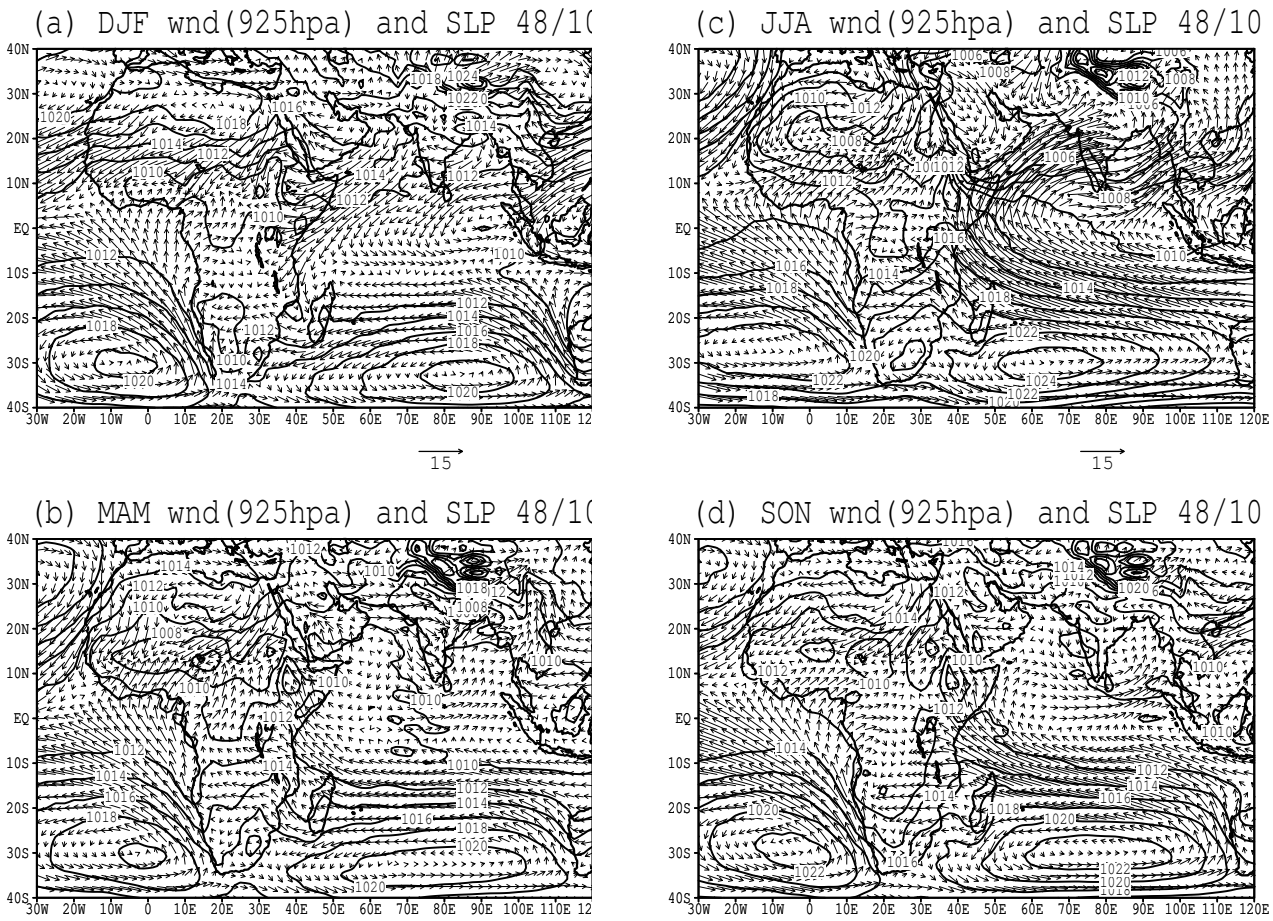

Figure 3.4: Seasonal mean low level wind and sea level pressure climatology for 1948 - 2012. (a) December - January - February (DJF), (b) March - April - May (MAM), (c) June - July - August (JJA) and (d) September - October - November (SON). Sea level pressure fields derived from HadSLP2 and wind fields are derived from NCEP/NCAR reanalysis data, a brief description of these dataset is given in Chapter 2. Unit are hPa for pressure and ms^{-1} for wind.

with westerly and southwesterly flow, the northeast monsoon and the southeast monsoon. Both monsoons, unlike the southwest monsoon of Asian, are thermally stable and associated with subsiding air; they are therefore relatively dry. In contrast, the flow from the Congo is humid, convergent, thermally unstable and therefore associated with rainfall. These air streams are separated by two surface convergent zones, the ITCZ and Congo air boundary; the former separate the two monsoons, the later, easterlies and westerlies (Figure 3.4b and d; Nicholson *et al.*, 1988).

A third convergence zone separates the dry, stable northerly flow of Saharan origin and the moister southerly origin (Figure 3.4b and d; Nicholson *et al.*, 1988)

3.2.1 Low level flow

In boreal winter the northeast dry monsoon winds sweep the northern Indian Ocean, cross the equator, and recurve to meet the southeast trade winds in a confluence zone around 10^{o}S overlying a band of warmest surface (Figure 3.4a). Moreover, the northeast monsoon brings dry continental air into East Africa, and consequently, the rainfall during these months is low (Figure 3.2a; Figure 3.4a; Hastenrath *et al.*, 1993). In boreal summer the southeast trade winds cross the equator and curve back to become the southwest monsoon penetrating into the southern part of the Asian continent (Figure 3.4c). The surface winds are easterlies south of the equator in the eastern and central Indian Ocean but veer northwestward toward East Africa during both transition seasons of MAM (Figure 3.4b) and SON (Figure 3.4d). The regional veer coincides with development and retreat of the boreal summer monsoon and leads to moisture convergence over Equatorial East Africa, enhancing the atmospheric convection and rainfall there (Hastenrath *et al.*, 1993; Behera *et al.*, 2005).

3.2.2 Sea level pressure

The main driver of the marked seasonality in winds and rainfall seen in Figure 3.2 and Figure 3.4, is the change in the distribution of surface pressure between winter and summer (Figure 3.4a and c), primarily associated with seasonal variations in the position of the Sun. The southeasterly trades that blow across the Southern Indian Ocean and represent the northern side of the Mascarene High migrate equator wards and strengthen as the Asian summer monsoon

develops in JJA (Figure 3.4c). The Mascarene High moves from its position over the southeastern Indian Ocean centered near 85^{o}E, 30^{o}S in DJF (Figure 3.4a), to lie over the southwestern Indian Ocean centered near 55^{o}E, 30^{o}S in JJA (Figure 3.4c; Segele *et al.*, 2009). Another key factor in the intensity of the Asian monsoon winds is the Tibetan Plateau, which acts as an elevated heat source and hence low sea level pressure during northern summer, and has a profound influence on the establishment and maintenance of the Asian summer monsoon circulation (Figure 3.4c).

Chapter 4

Interannual Variability and Predictability of Short Rains

This Chapter will cover a literature review to understand what causes ineranual variability rainfall over East Africa including Ocean-Atmosphere climate patterns, potential predictability, and underlying Physical mechanisms. This revision greatly pave our way of the experiments and different analysis performed to investigate further the relative influence of Indian Ocean compared to that of the Pacific Ocean as well as their combined effect on the variability of short rains over East Africa and to confirm and refine previously identified physical mechanisms by which IOD impacts East African short rains with a focus on the implication for seasonal predictability. The brief description of tropical Ocean-Atmosphere interaction is given in section 4.1. Section 4.2 then progresses to state SST forced interannual variability of East Africa rainfall, whilst the potential predictability of East Africa rainfall will be briefly described in section 4.3.

4.1 Tropical Ocean-Atmosphere variability

Tropical Oceans play major roles in the natural variability of the world climate. It is a well-established fact that anomalous coupled Ocean-Atmosphere phenomena generated in the tropical Oceans produce global Atmospheric and Oceanic circulation changes that influence regional climate conditions even in remote regions. On the interannual time scale, the El Niño-Southern Oscillation (ENSO) of the tropical Pacific Ocean is known as one typical example of such phenomena and has so far received worldwide attention because of the enormous societal impact.

4.1.1 Climatology in pacific basin

Figure 4.1 shows the tropical Pacific climatology for 30-years average SST and low level wind observed during October-December (Figure 4.1 upper panel), the average SST and low level wind observed during the five warmest October-December seasons (Figure 4.1 middle panel), and (Figure 4.1 lower panel) the difference between the patterns (Figure 4.1 middle panel) and (Figure 4.1 upper panel), that is, the mean SST anomaly observed during the five warmest October-December seasons as measured in the Nino3 region. It is clear (see Figure 4.1 upper panel), there is an obvious asymmetry in the SST and wind distribution, with the ITCZ and warmest SSTs being located in the western part of the basin. The easterlies drive Ekman divergence along the equator and coastal upwelling along the coasts of South America, resulting in the formation of the east Pacific cold tongue and Peruvian coastal upwelling.

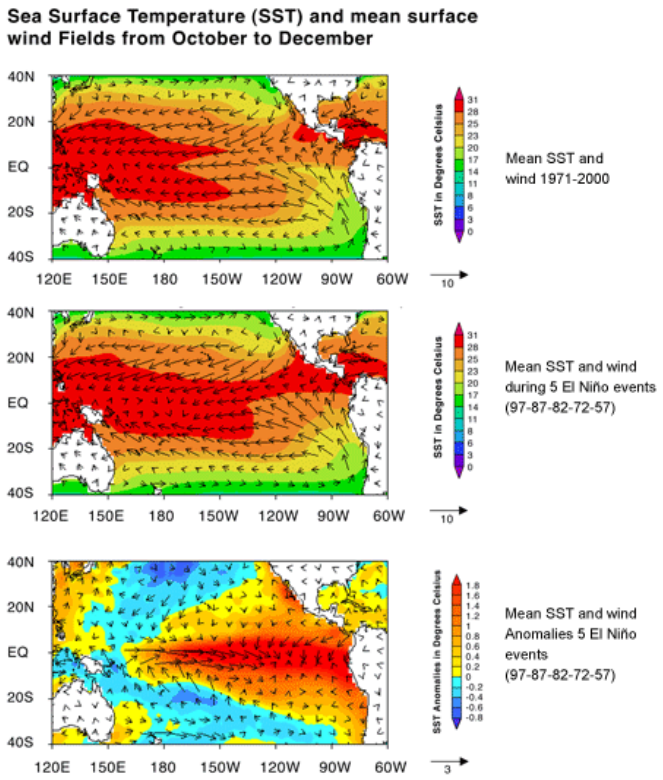

Figure 4.1: Maps October-December seasonal mean and anomalies of observed SST and low level wind over Pacific Ocean basin for 30-year average during 1971-2000. This figure is taken from $http://ccnmtl.columbia.edu/projects/climate/course\_html/module\_22\_lesson_3 61.html$.

4.1.2 El Niño-Southern Oscillation (ENSO)

Before considering the impact of ENSO on the East African rainfall, a more detailed description of the oscillation will be given here. ENSO is the largest coupled Ocean-Atmosphere phenomenon and described as the primary global mode of natural climate variability on a time scale ranging between 2-7 years; and is defined by sea surface temperature anomalies in the eastern tropical Pacific (Ropelewski and Halpert, 1987; Glantz, 2001). This phenomenon contributes significantly to seasonal to interannual climate fluctuations in many regions of the globe. This wide ranging influence of ENSO has attracted the attention of the global climate community, particularly due to the well-documented economic and societal impacts, both today and throughout historical times,

recorded locally and globally, within a wide latitudinal band about the equator.

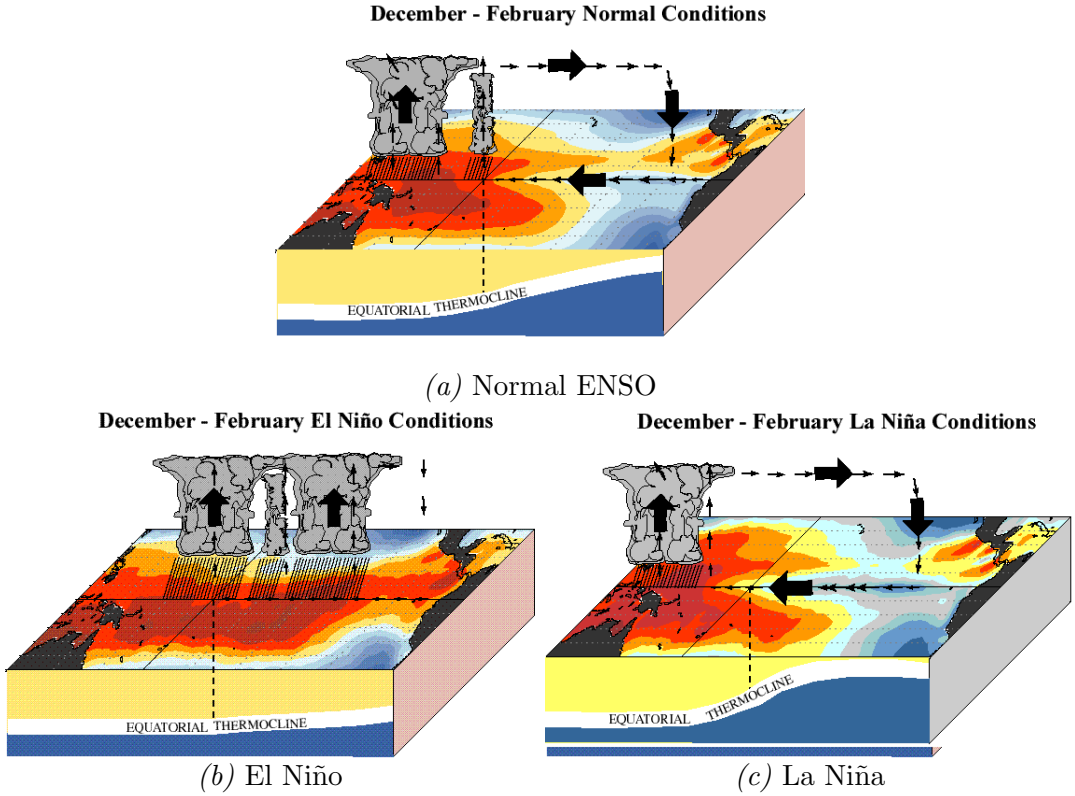

(a) Normal ENSO

(b) El Niño

(c) La Niña

Figure 4.2: Schematic diagrams of (a) Normal, (b) El Niño and (c) La Niña in the equatorial Pacific and sub-surface waters during boreal winter. This figure is taken from *http* : *//www.pmel.noaa.gov/tao/elnino/el − nino − story.html*.

El Niño and La Niña event are opposite phases of the ENSO cycle, with El Niño sometimes referred to as the warm phase of ENSO (warm sea surfce temperature anomalies in the central and east Pacific) while the converse explains the La Niña event. The interaction of the Atmosphere and Ocean is an essential part of El Niño and La Niña events (the term coupled system is often used to describe the mutual interaction between the Ocean and Atmosphere). During an El Niño, sea level pressure tends to be lower in the eastern Pacific and higher in the western Pacific while the opposite tends to occur during a La Niña. This see-saw in atmospheric pressure between the eastern and western tropical Pacific is called the Southern Oscillation (SO) (Walker, 1924). In common with earlier work, Sallinger (2005) describes the Southern Oscillation Index (SOI) as the

normalized pressure difference between Tahiti and Darwin (which measures whether the climate system is in El Niño or La Niña state).

Schematic diagrams of ENSO phases are shown in Figure 4.2. Equatorial oceans are strongly heated near the surface and stirred by trade winds. Under normal climatic state in and over the Pacific ocean (shown for boreal winter in Figure 4.2a), a tropical Pacific-wide circuit of air proceeds westward at the surface and rises over the west Pacific warm pool, where there is persistent convective rainfall. This rising air is characterized by a surface low pressure. As it rises, it reaches the tropopause and returns eastward aloft, completing the circuit by descending over the cool eastern Pacific, leading to high pressure at the surface. This phenomena is called the Walker circulation (Gill, 1982). The winds across the Pacific blowing westward into the region of low pressure cause equatorial upwelling, replenishing the cool waters in the central region (Figure 4.2a). Also, the easterly winds cause an increased sea-surface height in the west, as warm waters pile there. Thermocline features a mean west-east tilt as shown in Figure 4.2a.

A typical El Niño event is shown in Figure 4.2b. As mentioned before, El Niño is a warm phase of ENSO. It is due to a failure of the eastern Pacific to stay cold, such that temperatures across the entire tropical Pacific become almost uniform to temperatures of the western Pacific. A coupled response to east warming Pacific involves a shift in the tropical Walker circulation. This shift causes low level convergence over the equatorial Indian ocean, resulting in a stronger Hadley circulation. During an El Niño, the rising arm of the Walker cell shifts towards the warmer eastern and central waters of the Pacific, taking with it tropical convection. The normally high sea-level pressure (SLP) of the eastern Pacific becomes lower and the SLP difference between the west and the eastern Pacific decreases ($SOI < 0$). Consistent with this decrease, is the weakening

of the Walker circulation and the relaxation of the easterly trade winds (Figure 4.1 lower panel). As the edge of the warm pool moves further east and less equatorial upwelling is produced by the Kelvin wave, there is therefore, less cooling. An idea that El Niño is remotely forced by a relaxation in equatorial wind strength was first proposed by Wyrtki (1973). Associated with these changes at sea-level are changes to the sub-surface. The thermocline responds to the advancing westerly warm water by a drop in gradient; a depression in the eastern Pacific and a shoaling in the west evident in Figure 4.2b. This evolution of the thermocline during warm episodes was first described by Bjerknes (1966). This eastward displacement of the Atmospheric source overlying the warm waters influence the global Atmospheric circulation (teleconnections) by altering the weather patterns far from the tropical Pacific ocean (Ropelewski and Halpert, 1987).

Theories behind the dynamics of the teleconnection of ENSO to the Indian Ocean and East African rainfall have been developed in several paper. Black *et al.* (2003) suggests that El Niño events are associated with a general warming of the Indian Ocean and that anomalous cold SSTs are introduced to the south Indian Ocean around the Maritime Continent via the Indonesian through flow. These cold SST anomalies could be a response to anomalous along-shore southerly winds (Black *et al.*, 2003) causing upwelling of colder waters (Xie and Annamalai, 2002). This generates an east-west sea-level pressure gradient that drives moist easterly wind across the Indian Ocean towards East Africa. Black *et al.* (2003) expands on this idea by suggesting that the observed link between ENSO and East African rainfall is actually a manifestation of the link between ENSO and the Indian Ocean Dipole (IOD). This theory has gathered support in the literature since the discovery of the IOD in 1999 (Saji *et al.*, 1999; Webster *et al.*, 1999). The following sub-section presents the IOD as a potential driver and predictor for East African short

rains.

4.2 Variability over Tropical Indian Ocean

The climate of the tropical Indo-Pacific region exhibits a marked interannual variability, which has an enormous impact on food production and water resources in most of the tropical and subtropical countries. Therefore, understanding of the mechanisms that produce this variability is of great importance, as well as the ability to simulate and, possibly, to forecast it with coupled climate models. Reverdin *et al.* (1986) showed that interannual fluctuations of the zonal SST distribution were occurring in the equatorial Indian Ocean accompanied by strong surface wind and convective anomalies. Similar anomalous conditions of the tropical Indian Ocean have also been observed during 1994 and 1997 (Saji *et al.*, 1999; Webster *et al.*, 1999). In particular, Saji *et al.* (1999) have identified a mode of variability of the SST characterized by a zonal bipolar structure, that they called Indian Ocean dipole mode (IODM), and which explains a substantial part of the total SST variance in the tropical Indian Ocean. The extremes of this dipole are located over the eastern and western tropical Indian Ocean. In its positive phase, the dipole is characterized by warm SST anomalies in the western Indian Ocean and cold anomalies in the eastern Indian Ocean.

Although the main purpose of this study is not the detailed discussion of variability over Indian Ocean, we have applied empirical orthogonal function (EOF) analysis of SSTs over Indian Ocean basin to give a brief discussion on spatial and temporal variability. Figure 4.3 demonstrates the result for the two leading mode of variations of EOF computed for the period of 1950-2012.

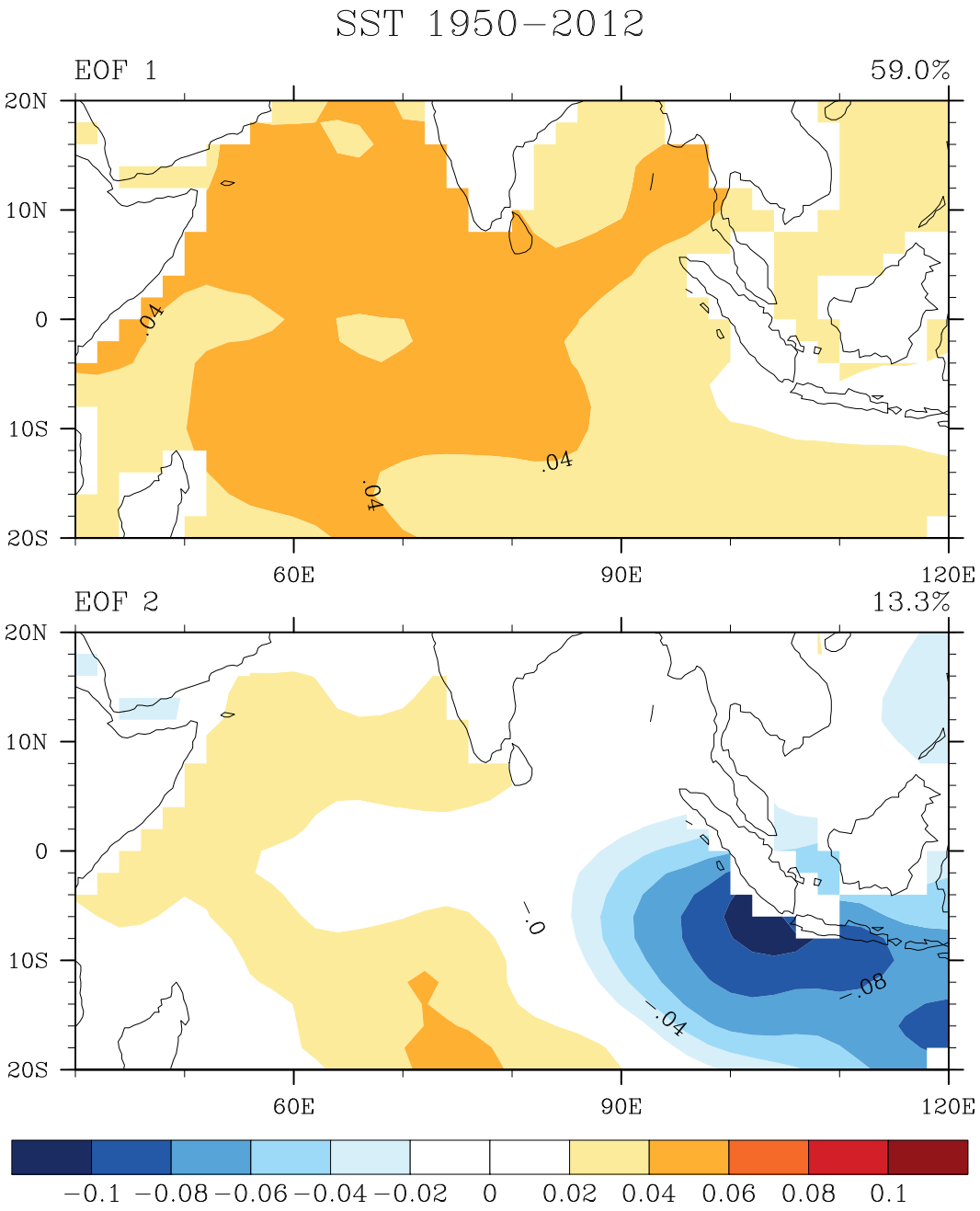

Figure 4.3: The two leading mode of Empirical Orthogonal Function (EOF) analysis derived from monthly HadISST anomalies over Indian Ocean Basin. (a) Top panel is the spatial pattern for EOF-1, and (b) bottom panel is spatial pattern for EOF-2.

EOF-1 explains about 59% of variation and represent the basin wide uniform distribution of SSTAs and it is associated with forced mode due to ENSO (Figure 4.4 top panel, Saji *et al.*, 1999; Xie and Annamalai, 2002), the corresponding PC-1 indicates the warming trend over central Indian

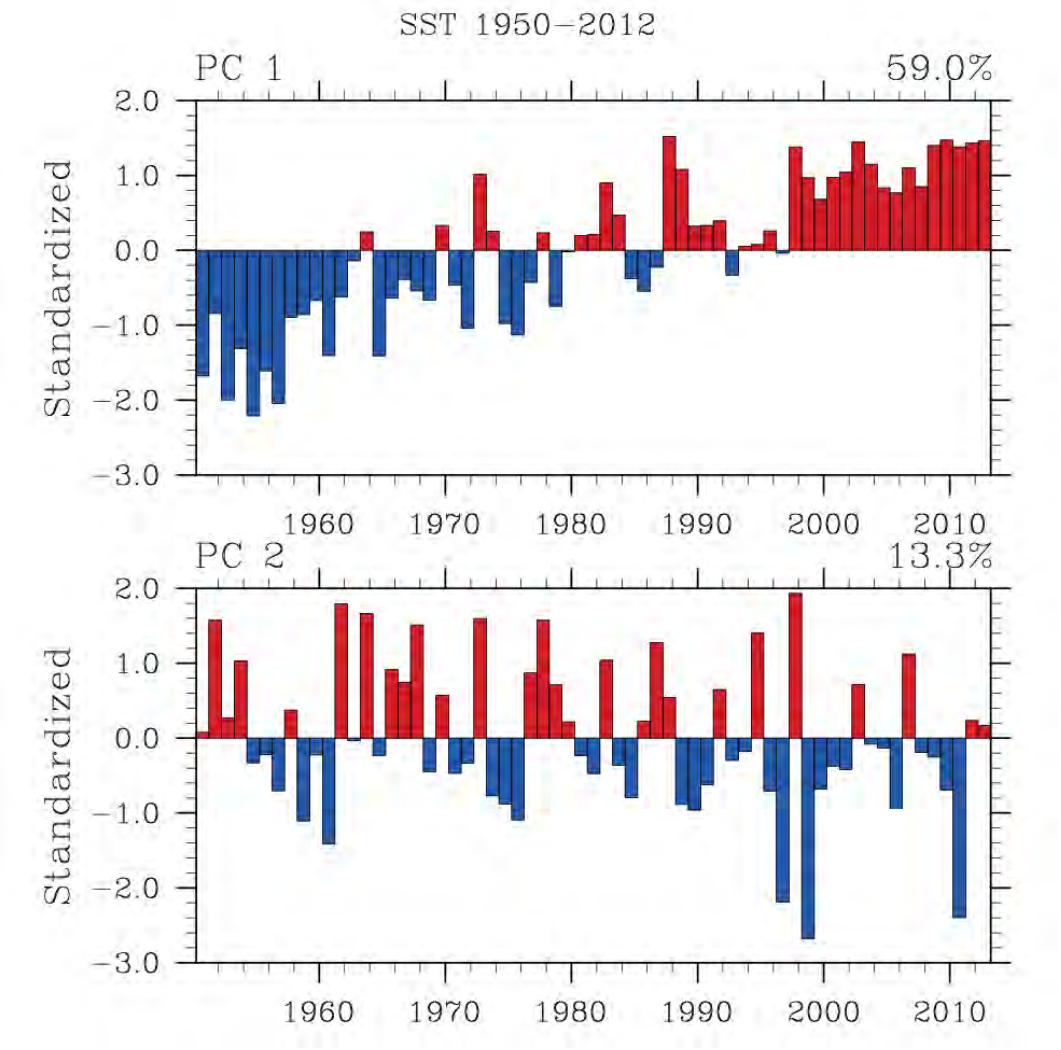

Figure 4.4: The two leading mode of Principal Components (PCs) derived from from monthly HadISST anomalies over Indian Ocean Basin. (a) Top panel is the time series for PC-1, and (b) bottom panel is the time sries for PC-2.

Ocean (Figure 4.4 top panel). On the other hand, EOF-2 explains 13.3% of variation which shows the dipole mode pattern (Figure 4.3 bottom panel), and the corresponding PC-2 have similar trend with Dipole Mode Index (DMI) over Indian Ocean basin as explained by bottom panel of Figure 4.4 and Saji *et al.* (1999). This statistically lower position of EOF-2 is due to less frequent occurrence of the events compared to ENSO events. Moreover, if we compare Figure 4.8 and lower panel of Figure 4.4, PC-2 we evidently see similar forms of variability, that support the second

mode of variability explains Indian Ocean dipole which is strongly associated with short rains interannual variability over East Africa.

4.2.1 Historical overview of IOD

The IOD is a coupled ocean-atmosphere phenomenon in the Indian Ocean characterized by an anomalous cold SST in the south-eastern equatorial Indian Ocean and anomalous warming of the western equatorial Indian Ocean. This anomalous pattern was first described as a "dipole" or "zonal" mode independently in two studies in 1999, by groups from the USA (Webster *et al.*, 1999) and Japan (Saji *et al.*, 1999). Both studies suggested that IOD is a native mode of the Indian Ocean that exists independently from the Pacific. The term IOD itself was introduced by Saji *et al.* (1999). It reflects a zonal structure of the phenomena with two maxima of different "polarity". This anomaly can be found not only in SST but also in other oceanic and atmosphere fields over the Indian Ocean, such as sea surface heights (SSH), wind, pressure, rainfall, and outgoing long wave radiation. Later, some authors referred to the anomalous pattern as proposed by Webster *et al.* (1999) the Indian Ocean Zonal Mode (IOZM) (e.g., Black *et al.*, 2003; Clark *et al.*, 2003), or Indian Ocean Dipole Zonal Mode (Annamalai *et al.*, 2005) because it matches the out-of-phase development of the SST extreme in the east and west Indian Ocean. The term dipole, on the other hand, suggests simultaneous variation in the east and west so that Clark *et al.* (2003), claim that the IOD does not represent a consistent oscillation phenomena (sea-saw) pattern, as for example, North Atlantic Oscillation, and therefore cannot be referred to as a dipole. Also it was found that anomalies along Sumatra-Java coast is a persistence property of IOD events, while the SST anomaly in the western part of the Indian Ocean varies significantly from event to event (Huang and Kinter, 2002). This property agrees, and partly overlaps with the previous study of

Reverdin *et al.* (1986) which described the anomalous interannual condition of wind and rainfall over the eastern and central equatorial Indian Ocean in October and November of certain years. Nevertheless, IOD is now the common name for this phenomenon in the scientific literature.

Prior to Webster *et al.* (1999) and Saji *et al.* (1999), investigations of the interannual variability of the Indian Ocean were mainly focused on understanding its response to the ENSO variability (Latif and Barnett, 1995). Although anomalous dipole-like patterns of SST variability between the Indonesian region and central Indian Ocean were noticed and suggested to be independent from ENSO before 1999 (Hastenrath *et al.*, 1993), these studies did not attract wide attention. Only the huge climate anomalies in 1994 and 1997 have been finally connected with the SST anomaly in the southeast Indian Ocean, stimulating interest in Indian Ocean research. Saji *et al.* (1999) and Webster *et al.* (1999) were the first to provide a comprehensive ocean-atmosphere description and identify a plausible mechanism for independent behavior of the Indian Ocean. These publications provoked debate about the interannual variability of the Indian Ocean. The main questions to answer were whether IOD is an independent or dependent mode of the Indian Ocean (from ENSO), and what is the triggering/driving mechanism of IOD (Yamagata *et al.*, 2004).

4.2.2 Quantitative description

For a quantitative analysis of IOD, a Dipole Mode Index (DMI) was introduced by Saji *et al.* (1999). It is calculated as the anomalous SST gradient between the western equatorial Indian Ocean (WIO) (50^{o}E -70^{o}E and 10^{o}S -10^{o}N) and the eastern equatorial Indian Ocean (EIO) (90^{o}E-110^{o}E and 10^{o}S-0^{o}N). For clarity and consistency in this study IOD as representation of both inherent Ocean-Atmosphere interaction and west-east SSTAs gradient in the Indian Ocean are

assumed.

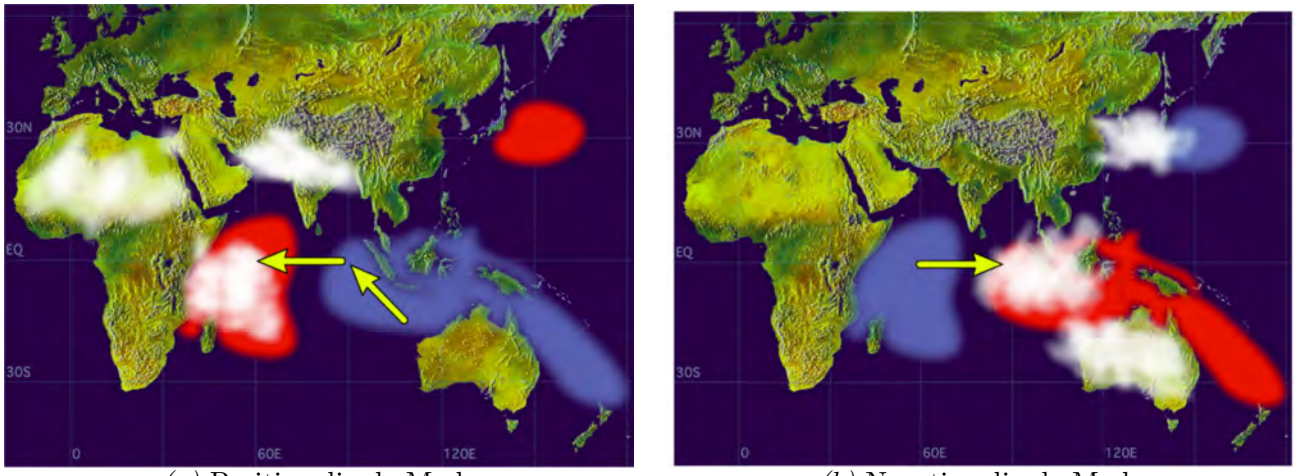

(a) Positive dipole Mode *(b)* Negative dipole Mode

Figure 4.5: Schematic diagram of the Indian Ocean Dipole (IOD). (a) Its associated warming (red shading;positive) and (b) cooling (blue shading;negative). White patches indicate areas of increased convection activity. Surface wind direction is denoted by the yellow arrows. Figure adapted from http://www.jamstec.go.jp/frsgc/research/d1/iod/IOD1. html. JAMSTEC Research Institute for Global Change.

Seasonal phase locking is important characteristic of IOD, the SST anomalies appear in the summer (around June), intensify through July- September, peak in the October, and terminate rapidly early winter (Figure 4.6; Saji *et al.*, 1999). These SST anomalies force changes in atmospheric circulations and rainfall patterns across the Indian Ocean, East Africa, south India and Indonesia. Figure 4.5 shows the SST, wind and precipitation anomalies associated with the IOD. IOD as any tropical phenomena is strongly locked to the annual cycle, reaching a peak during boreal autumn in October (Figure 4.6c; Saji *et al.*, 1999). The pattern has positive and negative phases. During a positive IOD event, cooler than normal SSTs are observed in the equatorial eastern Indian Ocean and warmer than normal in the equatorial western Indian Ocean (Figure 4.5a). Conversely, during a negative IOD event, negative (cooler) SST anomalies are observed in the western tropical Indian Ocean with positive (warmer) anomalies in the eastern tropical Indian

Ocean (Figure 4.5b). Behera *et al.* (2005) and others showed that a positive IOD event drives an atmospheric circulation with westward low-level winds. Rising motion is enhanced over warmer SSTs (positive anomalies) in the tropical western Indian Ocean. Convective activity and rainfall amounts are enhanced in this area, including parts of East Africa, with a deficit in the equatorial eastern Indian Ocean during the short rains season (Black *et al.*, 2003; Yamagata *et al.*, 2004; Behera *et al.*, 2005; Ummenhofer *et al.*, 2009).

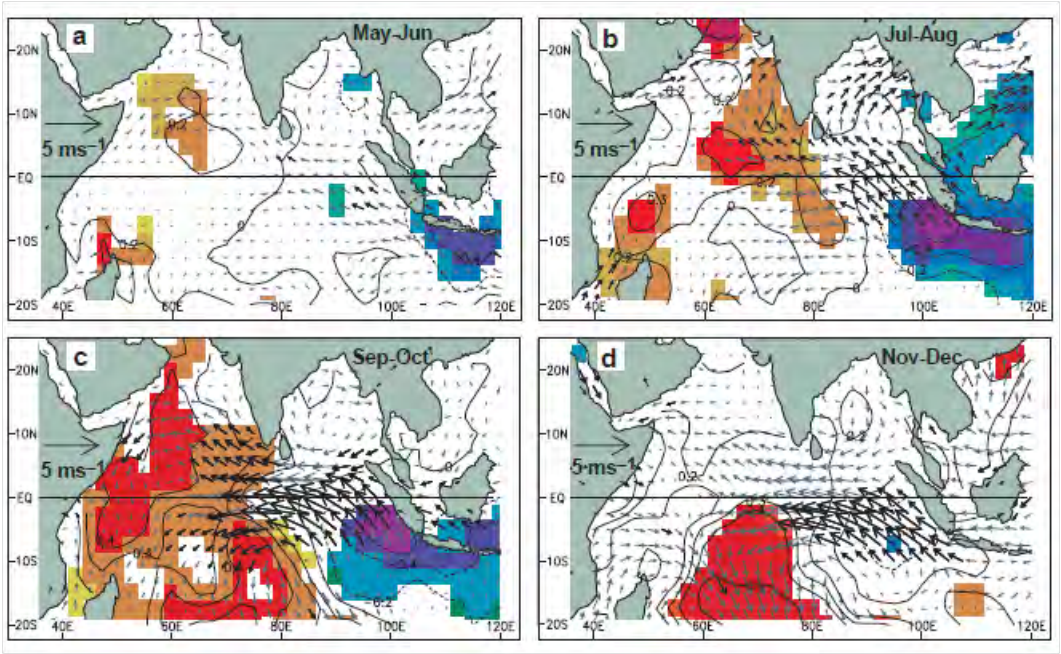

Figure 4.6: A composite dipole mode event. a-d, Evolution of composite SST and surface wind anomalies from May-June (a) to Nov-Dec (d). The statistical significance of the analyzed anomalies were estimated by the two-tailed t-test. Anomalies of SSTs and winds exceeding 90% significance are indicated by shading and bold arrows, respectively. This figure is taken from Saji *et al.* (1999).

During the negative mode of an IOD, the SST gradient drives an atmospheric circulation with eastward low-level wind anomalies. Rising motion and convective activities are enhanced over the equatorial eastern Indian Ocean (Figure 4.5b). The low level wind flow suppresses the convective activity in the western Indian Ocean, transporting moisture away from the African

continent; leading to enhanced subsidence over East Africa which results in East African rainfall reduction (Hastenrath *et al.*, 2004).

4.2.3 Relation between IOD and ENSO

Figure 4.7 demonstrate SST anomalies representative of the central and eastern equatorial Pacific (Nino3 region) against the IOD index time series. Note the significant dipole mode events of 1961, 1967 and 1994 coinciding with no ENSO, La Niña and a weak El Niño respectively (Saji *et al.*, 1999). There are years in which dipole mode events coincide with strong ENSO events as in 1972 or 1997. During dipole mode events, the surface wind field over the tropical Indian Ocean experiences large changes, especially in its zonal east-west component over the Equator. Figure 4.7 also demonstrate area-averaged equatorial zonal wind anomalies (Ueq) over (70^{o}E-90^{o}E and 5^{o}S-5^{o}N) region. It is clear that the intensity of the SST dipole mode and the strength of the zonal wind anomaly over the Equator are strongly dependent on each other (Figure 4.7; Saji *et al.*, 1999).

The burning issue is whether IOD is related to ENSO. There is a controversy going on about their relationship in the literature, with the scientific community split between the IOD being dependent on ENSO (Baquero-Bernal *et al.*, 2002; Xie and Annamalai, 2002) and independent of ENSO (Saji *et al.*, 1999; Saji and Yamagata, 2003). Previous work suggests IOD and ENSO seem to be linked to some extent. Baquero-Bernal *et al.* (2002) questioned the independence of an IOD event from ENSO. They found out that an oscillatory dipole mode exists in the tropical Indian Ocean. Their conclusion was this dipole-like variability can be explained as an oscillatory mode only in the context of ENSO. Based on their data analysis, Xie and Annamalai (2002) conclude

that most of the Indian Ocean variability is due to downwelling Rossby waves that propagate from the east to the west and are forced by ENSO. There Rossby waves are thought to interact with the atmosphere after reaching the western tropical Indian Ocean.

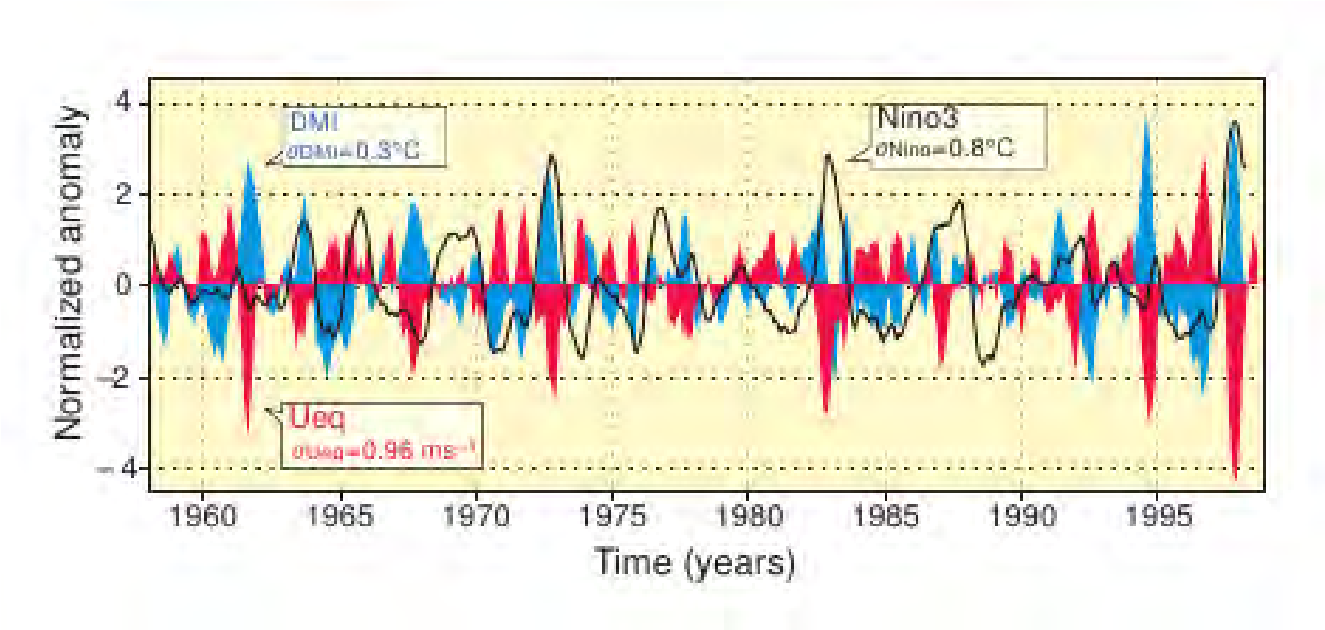

Figure 4.7: Dipole mode and El Niño events since 1958, Plotted in blue, the dipole mode index (DMI) exhibits a pattern of evolution distinctly different from that of the El Niño is represented by the Nino3 SSTAs (black line). On the other hand, equatorial zonal wind anomalies Ueq (plotted in red) coevolves with the DMI. All the three time series have been normalized by their respective standard deviations. This figure is taken from Saji *et al.* (1999).

On the other hand, after analyzing observations, Saji and Yamagata (2003) concluded that 11 out of 19 episodes occurred independently of ENSO. Studies undertaken by Black *et al.* (2003) and Behera and Yamagata (2003) suggest that IOD events may sometimes evolve without ENSO external forcing. Although there are IOD events that do not coincide with ENSO, such as 1961, the authors agree that there are instances when it does interact with ENSO, possibly through the Walker Circulation to the west and/or via the associated flow of the warm tropical ocean waters from the Pacific into the Indian Ocean (ie., the Indonesian through-flow). Moreover, Behera and Yamagata (2003) add to the debate by suggesting that the IOD can be induced by both ENSO

and local Indian Ocean circulations, although the resulting spatial IOD structures may be slightly different. This idea is supported by Xie and Annamalai (2002) and Black *et al.* (2003) who put forward that the occurrence of IOD events with no ENSO, such as in 1961, may suggest that the IOD can be triggered by factors other than ENSO. However, here we do not intend to give the detail analysis on the relation between ENSO and IOD which is beyond the scope of this study.

4.3 SST forced interannual short rains variability

Like other tropical regions, interannual variability of rainfall in East Africa results from complex interactions of forced and free atmospheric variations. These include interactions between sea surface temperature (SST) forcing, large-scale atmospheric patterns, and synoptic-scale weather disturbances including monsoon and trade winds, persistent mesoscale circulations, tropical cyclones, subtropical anticyclones, easterly/westerly wave perturbations, and extra-tropical weather systems. However, the interannual variability of short rains is mainly associated with perturbations in the global SSTAs, especially over the equatorial Pacific and India Ocean basins, and the Atlantic Ocean to some extent (e.g., Ogallo, 1988; Mutai and Ward, 2000; Saji *et al.*, 1999; Goddard and Graham., 1999; Black *et al.*, 2003; Behera *et al.*, 2005) among others.

Figure 4.8 shows the interannual variability in the short rains averaged in 5^0S-5^0N, 35-46^0E domain over equatorial East Africa. The time series is extended back to 1901 and forwarded to 2011 using CRU gridded precipitation dataset. For both in the anomaly and the standardized anomaly (Figure 4.8a and b), the temporal variability of the short rains is far from Gaussian and the distribution is positively skewed with more extreme wet events (Figure 4.8; Black *et al.*, 2003).

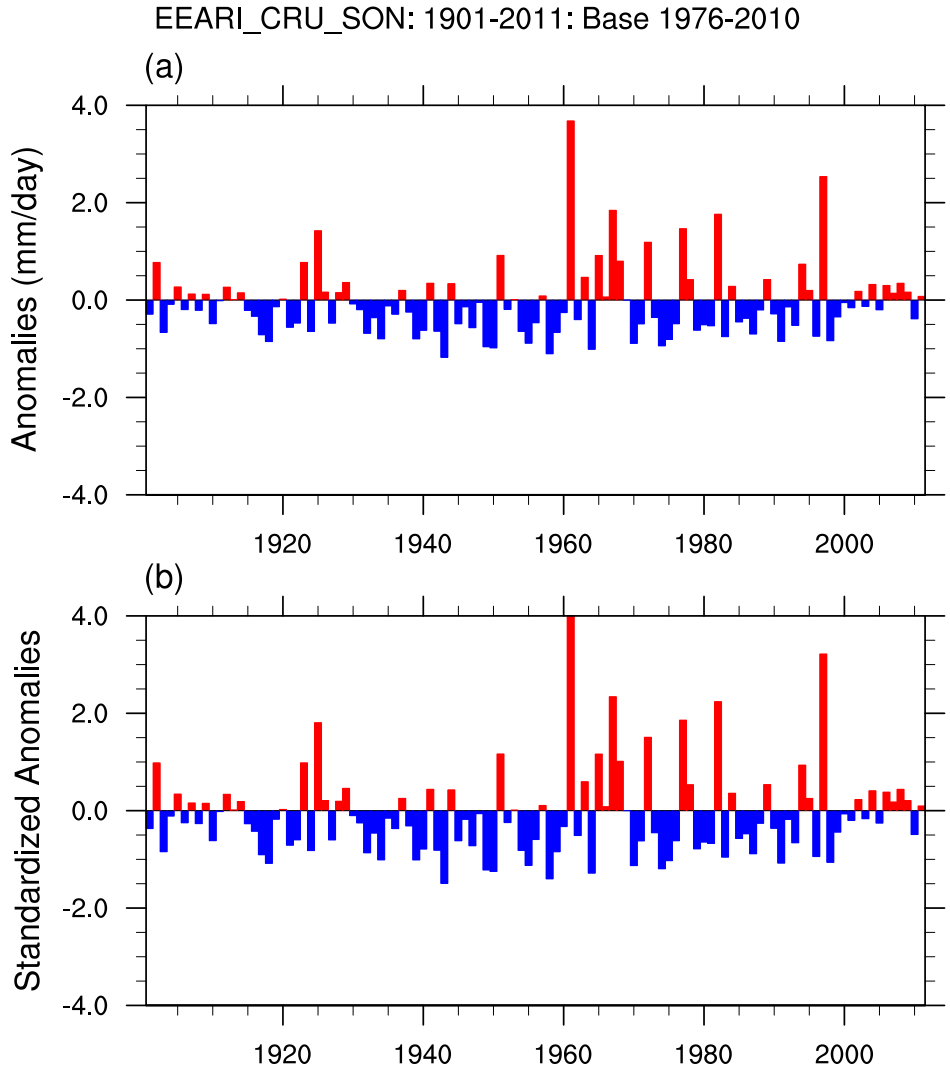

Figure 4.8: Time series of the seasonal mean East African rainfall for SON and averaged over 5^0S-5^0N, 35-46^0E for (a) Anomaly and (b) standardized anomaly. The rainfall is derived from CRU and the unit is given in $mmday^{-1}$.

On other hand, unlike other parts of Africa, such as the Sahel (e.g., Kucharski *et al.*, 2012), there is little evidence of decadal or longer-term variability. Although the extreme rainfall year of 1961 and 1997 are the most extreme wet years, clearly there are a number of wet and dry years (Figure 4.8a and b). In addition, it should be noted that most of the peaks of rainfall corresponds to positive IOD yeas, e.g., 1961, 1963, 1967, 1972, 1977, 1982, 1994, 1997 and the dry years correspond to negative IOD years, e.g., 1943, 1958, 1964, 1970, 1989 1992, 1996, 2010 (Figure 4.8;Table 5.1;

Saji and Yamagata, 2003). The second characteristic of the interannual variability is its extreme magnitude in the individual years. This is illustrated by the condition of 1961, a year in which lake Victoria rose several meters and reached levels unattained in the nineteenth century (Figure 4.8; Nicholson *et al.*, 1988). Moreover, the importance of short rains interannual variability is also underscored with analysis of linear temporal correlation: the correlation between short rains anomalies and annual departure is 0.72 compared to 0.65 between long rains anomalies and annual departure.

4.3.1 Spectral analysis of East Africa rainfall

The analysis here is of interest because East Africa short rains variability that is frequency-dependent, and understanding the frequency dependence may yield information about the underlying physical mechanisms. A number of studies have utilized spectral analysis to demonstrate that these rainfall fluctuations over East Africa are not completely random, but rather occur on preferred time scales (e.g., Nicholson *et al.*, 1988). The spectrum for both short rains and long rains over Equatorial East Africa shown in Figure 4.9. A peak in the spectrum represents relatively high variance in a frequency band centered on the peak. The short rains dominated by a strong peak at 5 to 6 years, but significant peaks at about 2.6 and 2.2 years are also evident (Figure 4.9).

The 5-6 years peak is also the dominant one in the spectrum of the first principal component (Nicholson *et al.*, 1988). This suggests that some forcing mechanism acting quasi-periodically with a time scale of 5-6 years is responsible for most of interannual variability of short rains in East Africa and the relative coherence throughout the domain. On the other hand, the peak in the

spectrum of long rains is dominated by 3.5 years, but significant peaks at about 2.2, 5, and 10 years are also evident (Figure 4.9).

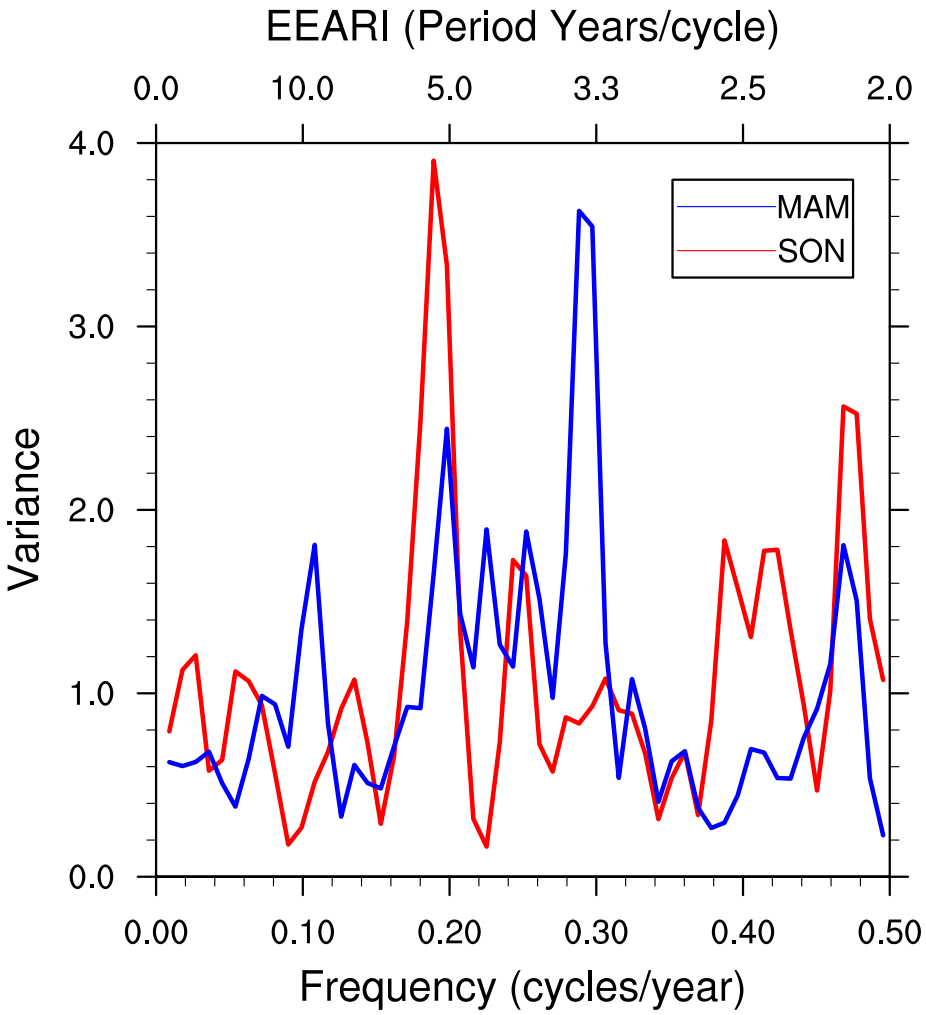

Figure 4.9: Spectrum of EEARI time series, the distribution is given variance of the series as a function of frequency for both short rains (plotted in red) and long rains (plotted in blue). Rainfall index is derived from CRU for 1901-2011, brief description of CRU rainfall is given in Chapter 2.

4.3.2 The role of ENSO

The interannual variability of East Africa rainfall and its relationship with SST has been examined extensively using a statistical approach (e.g., Hastenrath *et al.*, 1993; Mutai *et al.*, 1998;

Ogallo, 1988; Diro *et al.*, 2008, 2011). These studies focus on the role of ENSO in controlling the East African rainfall. The general conclusion of the above studies was that ENSO exerts some control on equatorial East African short rains, with warm events being associated with high rainfall and cold events with low rainfall. The association was however weak, and there was a considerable spatial variability with the most influence in the north where the rainy season is strongly connected to the southwest monsoon (Black *et al.*, 2003). Moreover, Hastenrath *et al.* (1993) found that the causality of short rains anomalies is strongly related to the SO. They found from analysis of observed data that high SO phases correspond to low (high) pressure in the Eastern (Western) Indian Ocean in the short rains season. They also showed that strong westerlies over Tropical Indian Ocean (TIO) suppress atmospheric convection over western Indian Ocean. During negative SO phases opposite ocean-atmosphere condition takes place, and western Indian Ocean and the East African region receive abundant precipitation. These studies did not explicitly investigate the role of the Indian Ocean in influencing East African rainfall or they gave comparatively little attention (Behera *et al.*, 2005). Most studies on the climate of the Indian Ocean basin and of the countries around the border of the Indian Ocean have focused on the evolution of the Asian-Australian monsoon. Furthermore, it has usually been assumed that the effect of the Indian Ocean is secondary to ENSO in controlling the climate of India, Africa, and Indonesia.

4.3.3 The role of IOD

A number recent studies tried to compare the fractional influence of IOD and ENSO on short rains (Saji and Yamagata, 2003; Behera *et al.*, 2003). In addition, Goddard and Graham. (1999); Latif *et al.* (1999) concluded from their AGCM climate simulation experiment that Indian Ocean

SST anomalies rather than the Pacific SST anomalies forced the rainfall anomalies over eastern equatorial Africa. The modeling study by Latif *et al.* (1999) showed the importance of Indian Ocean anomalies in December-January 1997/98 in forcing climate anomalies over Eastern Africa. Moreover, Williams and Hanan (2011) studied the influence of IOD and ENSO on photosynthesis activity over Africa. In their composite analysis they point out that the response to SON ENSO over Tanzania is suppressed or changes sign when coincident with IOD activity, indicating the dominant role of IOD on the variation of climate and hence photosynthetic activity over Equatorial East Africa. Furthermore, Ummenhofer *et al.* (2009) in their AGCM ensemble experiments showed that increased East African short rains are mainly driven by a warming over western Indian Ocean. The physical mechanism identified by Ummenhofer *et al.* (2009) was that the western Indian Ocean warming leads to a local lowering of the pressure that extends to East Africa and induces westerly moisture flux anomalies to the west and easterly moisture flux anomalies over the Indian Ocean which converge over Eastern Africa and enhance rainfall. These modeling studies were conducted with prescribed idealized SST anomaly pattern to explain the mechanism for the atmospheric response over the Western Indian Ocean and Africa and hence for an enhanced rainfall over Eastern Africa.

4.4 Potential predictability of short rains

4.4.1 Statistical predictability

Following understanding of the influence tropical Ocean-Atmosphere phenomena on the variability of equatorial East Africa rainfall, statistical predictability and prediction of East Africa

short rains has been attempted. Mutai and co-workers (Mutai *et al.*, 1998; Mutai and Ward, 2000) used global SST as input for predicting the East African Short rains. The short rains of the East African coast have a concurrent correlation of -0.85 with the equatorial surface westerlies (Hastenrath *et al.*, 1993). Consequently, empirical circulation diagnostics has been applied by Philippon *et al.* (2002). Moreover, Hastenrath *et al.* (2004) explored the predictability of short rains using different indices derived from observation and reanalysis data, and found that the sudden development of the zonal circulation cell and the lack of long-lived precursors seriously hamper its usefulness as predictors for East African rainfall.

4.4.2 Dynamical predictability

During the last few decades, climate scientists have made tremendous advances to fully characterize climate forcing in particular, understanding and modeling the Earths climate system in general. With the advent of fully coupled Ocean-atmosphere models (Saha *et al.*, 2006; Weisheimer *et al.*, 2009), evidence that fully coupled GCMs can predict the evolution of SSTs to elevated levels of skill has been presented.

4.4.3 Multi model ensemble methods

Multi Model Ensemble (MME) are nearly always better than any of the individual models (Krishnamurti *et al.*, 2000). The benefits from combining ensembles are a result of the inclusion of complementary predictive information since the forecast scheme is able to extract useful information from the results of individual models from local regions where their skill is higher (Krishnamurti *et al.*, 2000). The idea behind the MME is that if the model parameterization schemes are independent of each other, the model errors associated with the model parameteri-

zation schemes may be random in nature; thus, an average approach may cancel out the model errors contained in individual models. Moreover, an increased ensemble size leads to further benefits (Brown and Murphy, 2007), but the multi- models approach is only beneficial if the individual models produce independent skillful information (Graham *et al.*, 2000)

This notion has been demonstrated conclusively through the DEMETER (Development of a European Multimodal Ensemble system for seasonal to interannual prediction) project (Palmer, 2004). Subsequently, prediction of seasonal variations and associated uncertainties using multiple dynamical models has become operational (Wang *et al.*, 2009). MME method is demonstrated to be a useful and practical approach for reducing errors and quantifying forecast uncertainty due to model formulation (Wang *et al.*, 2009; Desole and Shukla, 2012). In particular, since 2006, APCC has produced long-range seasonal forecasts with up to a six month lead time using MME of coupled ocean-atmosphere-land models for use by national hydrological and hydrometeorological services within the APEC regions (Lee *et al.*, 2010; Sohn *et al.*, 2012). The result on evaluation of APCC coupled dynamical forecast systems has been discussed on Chapter 6.

Chapter 5

ICTPAGCM Ensemble Experiments

This Chapter discuses the result on Interannual variability, physical mechanisms and potential predictability short rain over equatorial Africa using observational data and a series of ensembles of long ICTPAGCM simulations. Brief description of the model is given in Chapter 2 and examples of applications of the ICTPAGCM to the African monsoon can be found in Kucharski *et al.* (2012). The ICTPAGCM used here is configured with 8 vertical (sigma) levels and with a spectral truncation at total wave number 30.

5.1 Experimental set-up and methods

We have conducted three separate sets of AGCM experiments with 10 ensemble members each, where each member has been forced with observed SST over the Ocean basin of interest and set to monthly varying climatology elsewhere. The three experiments are as follows:

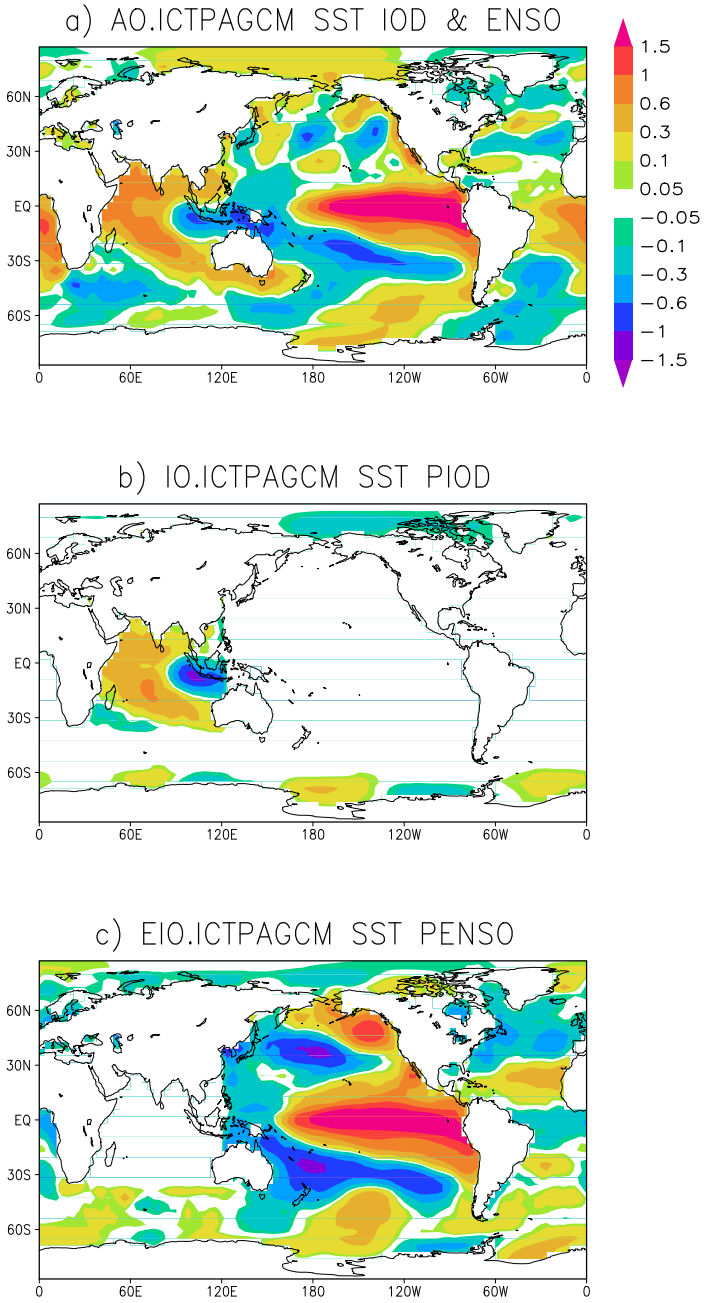

Figure 5.1: The three SST anomaly patterns (^oC) used in the response ensemble experiments with the ICTPAGCM. (a) AO.ICTPAGCM, (b) IO.ICTPAGCM, and (c) EIO.ICTPAGCM. SST anomaly used are derived from ERSST V3 during the period January 1919 - December 2010.

- In the First experiment (AO.ICTPAGCM: All Ocean-ICTPAGCM), 10 ensembles simulation of AGCM is carried by forcing global Ocean with observed time varying global SST.

- In the second ensemble experiment (IO.ICTPAGCM: Indian Ocean-ICTPAGCM), 10 simulations are conducted forcing in the Indian Ocean basin with time-varying observed SSTs, while in the other parts of the global ocean with climatological annual cycle of SSTs was prescribed.

- In contrast, the third ensemble experiment (EIO.ICTPAGCM: Except Indian Ocean-ICTPAGCM), was conducted by prescribing the climatological annual cycle of SSTs in the Indian Ocean basin, while the other parts of the global Ocean were forced by time varying observed SSTs.

The observed SST used in our experiment have been derived from NOAA ERSST V3 (Smith and Reynolds, 2004). The three experiments are composed of an ensemble of 10 integrations and each ensemble member has been created using different atmospheric initial conditions. Runs are initiated on January 1^{st} 1919 and run up to December 31^{st} 2010. The first year is treated as spin-up, thus the model outputs are analyzed from 1920 onwards. The analysis is performed based on the ensemble mean calculated separately from each experiment to demonstrate connection between SST anomalies and East African short rains variability.

The purpose of the AO.ICTPAGCM experiment is to provide best estimate for the mutual influence of ENSO and IOD (in addition to the remaining Oceanic regions) on East African short rains variability, to assess the potential predictability and to validate the model climatology with observation. Moreover, IO.ICTPAGCM experiment is used to investigate the role of Indian Ocean SST anomalies in driving East Africa short rains anomalies. On the other hand, EIO.ICTPAGCM experiment has been performed to assess how the short rains variability is affected by removing the Indian Ocean anomalous forcing and to evaluate the extent of the influence coming from ENSO and other Oceans on the variability of East African short rains.

We have applied the definition of IOD used by Saji and Yamagata (2003) and for ENSO we adopted the definition from Trenberth (1997). We have separated pure-IOD, pure-ENSO and joint ENSO-IOD depending on coexistence of both events. A pure positive (negative) IOD event is identified as an event when El Niño (La Niña) does not co-occur (Table 5.1), where PIOD represent positive IOD events and NIOD is for negative IOD events. In total, 9 independent IOD events, 10 independent ENSO events and 6 joint events are used as an input for composite analysis as shown in Table 5.1.

Table 5.1: Years of IOD and ENSO events considered in the composite analysis, and the asterisk indicates pure events while the bold years represent El Niño (La Niña) during a positive (negative) IOD events.

PIOD	NIOD	El Niño	La Niña
1961*	1958*	**1963**	**1964**
1963	1960*	1965*	1967*
1967*	**1964**	1969*	**1970**
1972	**1970**	**1972**	1971*
1977*	1989*	1976*	1973*
1982	1992*	**1982**	1975*
1994*	1996*	1986*	1988*
1997	-	1991*	-
-	-	**1997**	-

Our analysis concentrates on the September-November (SON) season. The results from the 10 ensemble members from each experiment have been averaged together and the resulting ensemble means provide an approximation of the response of the model to the prescribed SSTs. Simple statistical tools such as composite and correlation analysis are used to show the dynamical response generated by ICTPAGCM experiments forced by observed SST over different ocean basins. The

NCEP reanalysis dataset used in this study is available from 1948 to present; consequently, we have used the modeled and reanalysis data covering 1948-2002 for our climatology and composite analysis. However, we have used data both from observation and model simulation covering 1920-2009 period for the remaining analysis.

5.2 Seasonal cycle and model climatology

Since the focus of this study is on the short rains variability, potential predictability and its driving mechanism, we present model climatologies for the short rains season over Equatorial East Africa. ICTPAGCM resolution implemented in our experimental set ups were coarse with respect to reanalysis and observed dataset used and, therefore, interpolated onto a common 2.5^{o}X2.5^{o} grid prior to bias computation. The rainfall and low-level wind climatology derived from AO.ICTPAGCM simulation is compared with observations in Figure 5.2. As expected, all other experiments have very similar climatologies and are not shown. Figure 5.2 shows the observed, model simulated rainfall and the 925hPa wind distribution and the difference (bias) between the model and observation.

On the whole, the seasonal characteristics of wind and rainfall distribution are reasonably well reproduced. For example, rainfall distribution is well represented over India and south Asia, however, the model shows positive bias over the western part (between 10^{0}S and 5^{0}N) of equatorial East Africa especially west of 30^{0}E. Moreover, the model well replicated rainfall towards northern East Africa and over Somali coast. In general the model rainfall performance over Africa is comparable to typical Coupled Model Inter-comparison Phase 5 (not shown) and other GCM

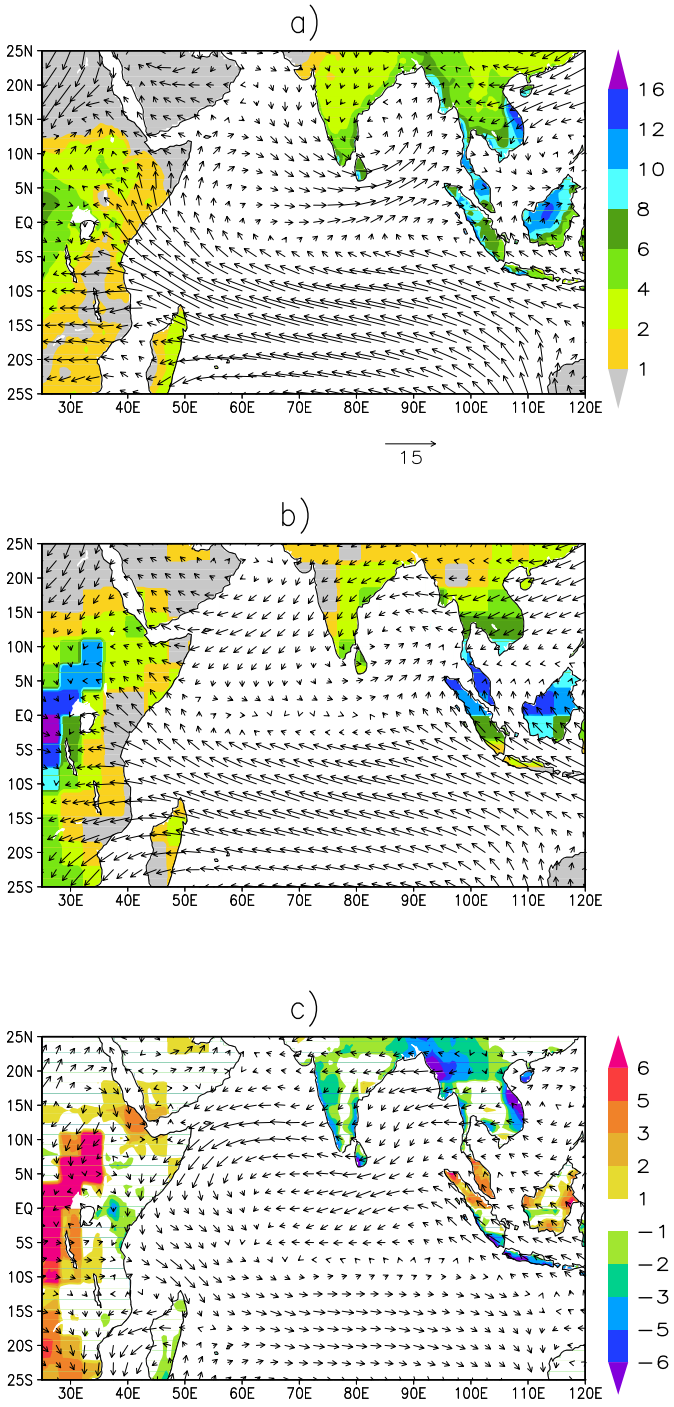

Figure 5.2: SON rainfall climatology (shaded) and 925hpa winds. (a) CRU rainfall and wind fields are derived from NCEP/NCAR reanalysis data, (b) Ensemble mean of AO.ICTPAGCM experiment (c) Bias (difference) between AO.ICTPAGCM and CRU precipitation, and Unit are $mm(day)^{-1}$ for rainfall and ms^{-1} for wind.

performances (e.g., Ummenhofer *et al.*, 2009).

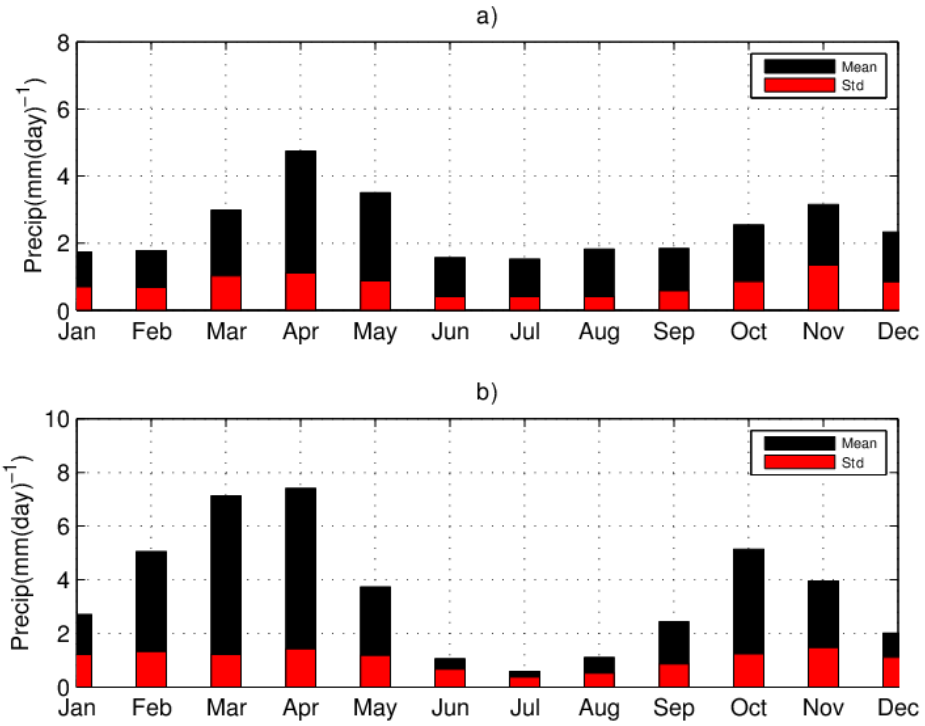

Figure 5.3: Annual cycle of the East African short rains averaged over (5^0S - 5^0N, 30 - 40^0E) along with monthly standard deviation derived from (a) observation results, and (b) AO.ICTPAGCM simulation. Rainfall units are given in $mm(day)^{-1}$.

The model also captures the 925 wind climatology fairly well compared to the NCEP re-analysis over the Indian Ocean basin during autumn, although with an underestimation of the southeasterly flow in the southern Indian Ocean, particularly north of Madagascar. As seen in Figure 5.2b surface winds are easterlies south of the equator in the eastern and central Indian Ocean but turn northwestward toward East Africa during the SON transition season.

Furthermore, Figure 5.3 designates mean and standard deviation of the annual cycle of EEARI, defined in this Chapter as an area averaged rainfall in the region (5^0S-5^0N, 30^0-40^0E). We have verified that the results presented in this study are robust with respect to small variations

in size and position of this index. The model simulation is comparable with the results shown in previous studies (Black *et al.*, 2003; Behera *et al.*, 2005). By comparing the upper and lower panel of Figure 5.3, we also find that the model simulates the seasonal rains and their variability reasonably well despite positive biases in the peak months of long rains and short rains. The peak of the short rains is shifted by a month. This model bias may be ignored here, as the main purpose of this study is to discuss the relation of short rains variability with IOD and ENSO.

5.3 Short rains interannual variability

The short rains season, which is also the peak season of the IOD (Saji *et al.*, 1999). However, there could be a delay between the IOD and the atmospheric response. In order to verify that the response in East Africa is indeed nearly instantaneous on a seasonal mean time scale we have calculated the lead-lag correlations between a 3-month moving average EEARI index (from observations and model) and the SON Dipole Mode Index (DMI; Saji *et al.*, 1999), which is representative of the IOD (Figure 5.4). Clearly, the SON DMI shows the largest correlation with SON EEARI in the CRU observations and in the AO.ICTPAGCM experiment. Correlations are still large for EEARI in OND, particularly for CRU, then they decrease as the lag becomes larger. Therefore, the short rains in the SON season shows statistically significant and relatively high correlation with SST anomalies in the Indian Ocean with large interannual fluctuation (Figure 5.4; Behera *et al.*, 2005; Williams and Hanan, 2011; Black *et al.*, 2003). The long rainfall regime over East Africa, however, is hardly relate to anomalies of the climate system and hence difficult to

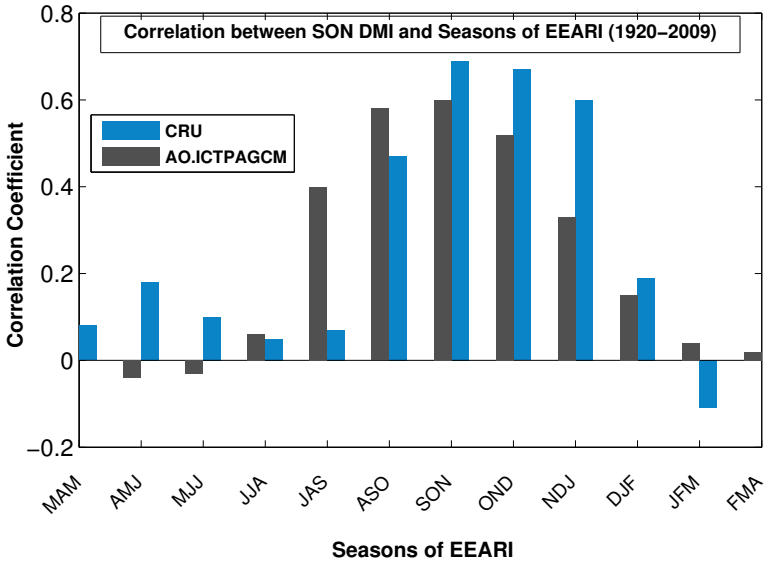

Figure 5.4: Time-lagged correlation between seasonal mean annual cycle of EEARI and SON mean DMI during the period 1920-2009. Rainfall is derived from CRU observation and AO.ICTPAGCM experiment where as the DMI is from ERSSTv3b.

predict (Figure 5.4; Camberlin and Philippon, 2002).

Figure 5.5a shows the EEARI time series from CRU (red line) and AO.ICTPAGCM (blue line). The observed and modeled rainfall are statistically significantly correlated at 99.9% confidence level, with a correlation coefficient of 0.6. This indicates that a substantial portion of East African short rains variability is SST forced, and that the model is reproducing this. Indeed, Figure 5.6 demonstrates the spatial distribution of correlation coefficients between the detrended EEARI derived from AO.ICTPAGCM simulation and SSTs. The detrending has been performed to avoid spurious correlations due to similar linear trends. The correlation map is dominated by a large correlation exceeding 0.5 in the western Indian Ocean. There is also an indication of significant at 95% confidence level, but small correlations in the eastern Indian Ocean. Our analysis supports the idea that enhanced short rains in East Africa are driven predominantly by

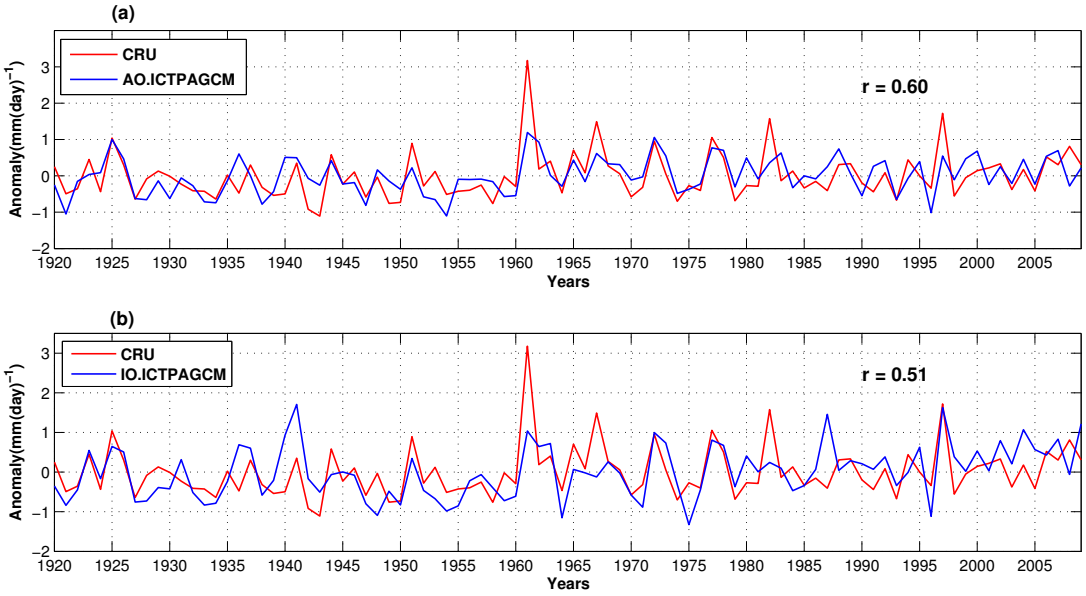

Figure 5.5: Interannual variability of the seasonal mean rainfall anomaly for SON over Equatorial East Africa (5S-5N, 30-40 E) since 1920. Plotted in blue, rainfall derived from a) AO-ICTPAGCM and b) IO-ICTPAGCM simulation and red is observed rainfall resulting from CRU, all rainfalls are given in $mm(day)^{-1}$.

the local warm SST anomalies in the western Indian Ocean, while the eastern cold pole is of lesser importance which is consistent with (Ummenhofer *et al.*, 2009).

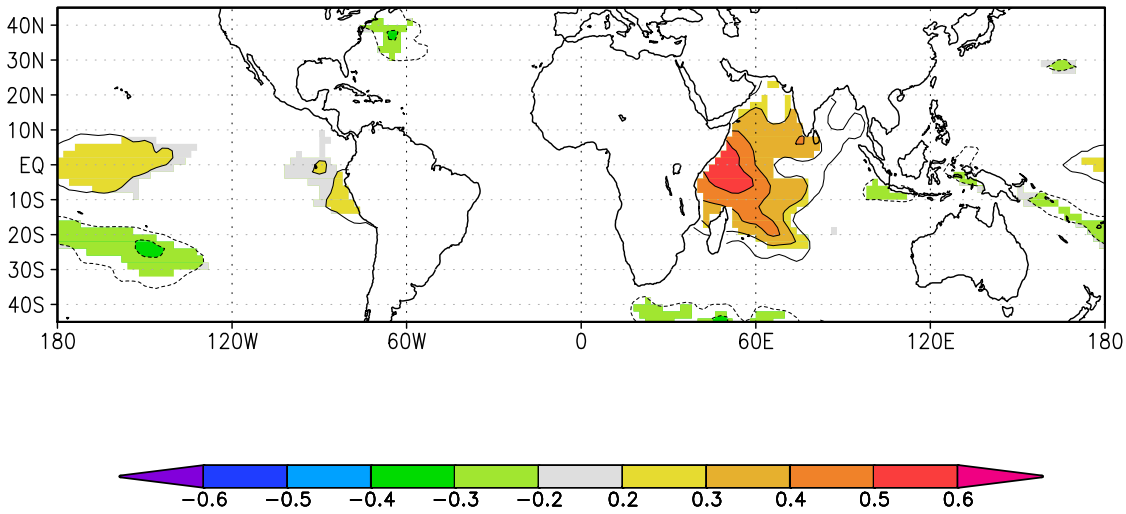

Figure 5.6: Concurrent correlations between SON short rains index derived from AO.ICTPAGCM experiment and SON season Sea Surface Temperature computed from ERSSTv3b. Shaded contours are statistically significant at 0.05 levels.

Certainly, the detrended IO.ICTPAGCM experiment (the ensemble forced in the Indian Ocean only; see Figure 5.5b) supports this and with a similar reproduction of the EEARI time series (correlation coefficient with the observed EEARI is 0.51, which is statistically significant at 99.9% confidence level). EIO.ICTPAGCM Experiment (not shown), on the other hand, shows that the modeled EEARI is slightly negative correlated with observed counterpart EEARI. In order to further analyze the SST forcing of East African short rains, we use composite analysis (selecting IOD and ENSO events as introduced in the data section), for the remaining of this section.

5.3.1 IOD, ENSO and combined influence on short rains interannual varaibilty

Previous studies also show that IOD events sometimes co-occur with the Pacific ENSO events (Yamagata *et al.*, 2004; Behera *et al.*, 2005). Moreover, the correlation between Dipole mode Index and Nino-3 index is 0.33 in the observation (Saji *et al.*, 1999). The correlation was obtained by considering all the months of the year and for the period of 1950-2002, here we have considered SON and annual mean SST anomalies for two climate periods based on ERSSTv3b dataset. We found correlations of 0.2 and 0.47 for annual mean and SON mean respectively for the period covering 1920-2009, whereas 0.25 and 0.51 for the 1948-2002 period. Therefore, there is a statistically significant relationship between the IOD and ENSO, particularly in SON. However, it is beyond the scope of this paper to analyze this connection. Instead, in this study we are concerned to investigate further whether the atmospheric influence of IOD is independent from ENSO in modulating rainfall anomalies over East Africa.

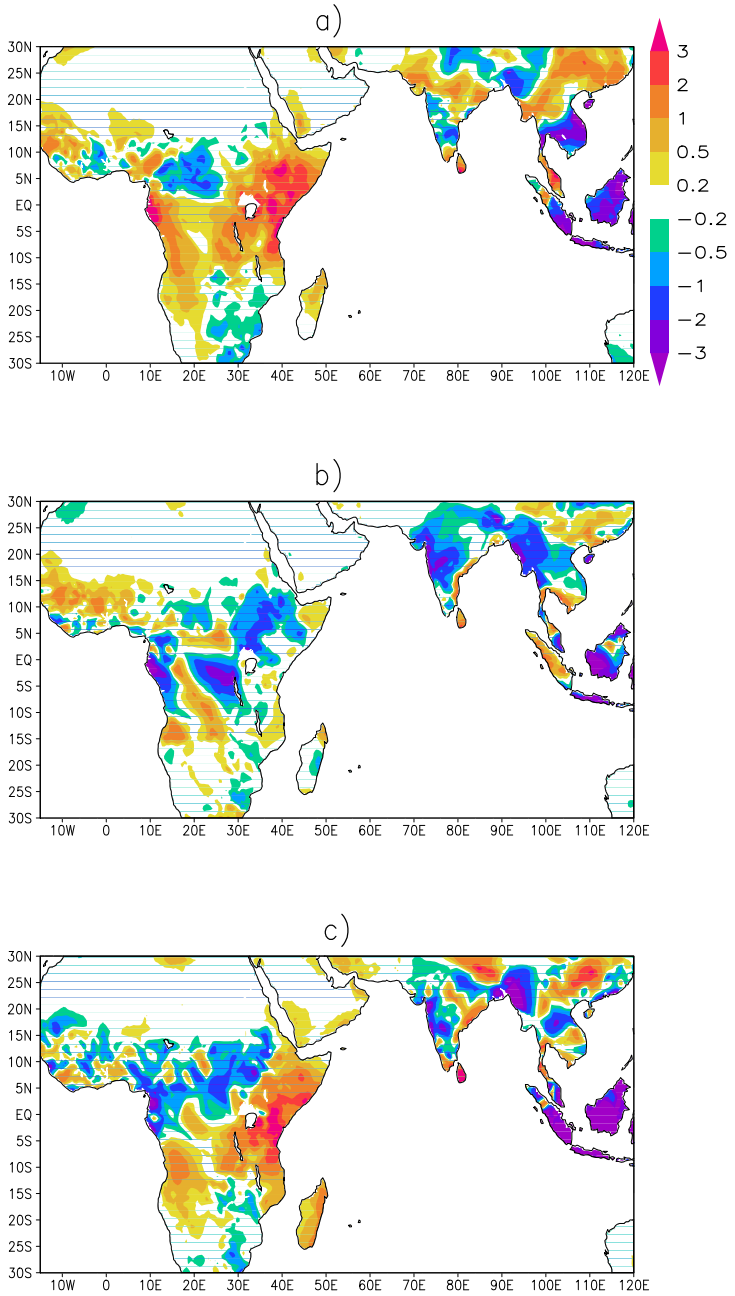

Figure 5.7: Composites of gridded precipitation anomalies derived from CRU for a) pure IOD events b) pure ENSO events c) Joint IOD and ENSO events. All panels are for SON season and the unit are given in $mm(day)^{-1}$.

Figure 5.7 demonstrates the result for the composite analysis of CRU gridded precipitation, the variability associated with either pure IOD (Figure 5.7a), pure ENSO (Figure 5.7b) and joint IOD-ENSO events (Figure 5.7c) for the SON season. The relative influence of pure IOD years and

pure ENSO years during the 1948-2002 period on short rains is calculated using the independent composite method (Saji and Yamagata, 2003). It is clear from Figure 5.7 that the pure IOD has a strong influence on the variability of short rains. The East African region receives above (below) normal rainfall during positive (negative) IOD events (Behera *et al.*, 2005; Ummenhofer *et al.*, 2009). For the pure ENSO composite, the response is rather noisy, but with a tendency for reduced rainfall over parts of East Africa specially north of the equator. The joint IOD and ENSO composite shows a rainfall response similar to the pure IOD composite over East Africa, with some contribution from the pure ENSO composite to the northwest of the region of interest. In a similar fashion Figure 5.8 displays composite of rainfall resulting from the simulation of AO.ICTPAGCM (Figure 5.8a and 5.8b), IO.ICTPAGCM (Figure 5.8c) for pure IOD cases, EIO.ICTPAGCM (Figure 5.8d) for pure ENSO cases as well as AO.ICTPAGCM (Figure 5.8e) for joint IOD-ENSO events. We have applied a two tailed t-test for our model composite analysis to identify the important patterns. Based on intra-ensemble variability of composites the dashed and solid contours in Figure 5.8 are statistically significant at 95% confidence level.

The distribution of the rainfall composite for pure IOD years from AO.ICTPAGCM experiment Figure 5.8a shows excess rainfall over equatorial East Africa and deficit over Sumatra which is a western part of Indonesia, as observed in CRU rainfall Figure 5.7a. On the other hand, the result from this experiment shows shortage of rainfall over the coast of equatorial East Africa for composite of pure ENSO year (Figure 5.8b) that is also seen in the observed rainfall (Figure 5.7b). However, the model is unable to produce excess of rainfall over Sumatra for ENSO years compared to observation (Figure 5.7b). The results from experiments IO.ICTPAGCM and EIO.ICTPAGCM are similar to pure IOD and pure ENSO, calculated from AO.ICTPAGCM simulation. This is

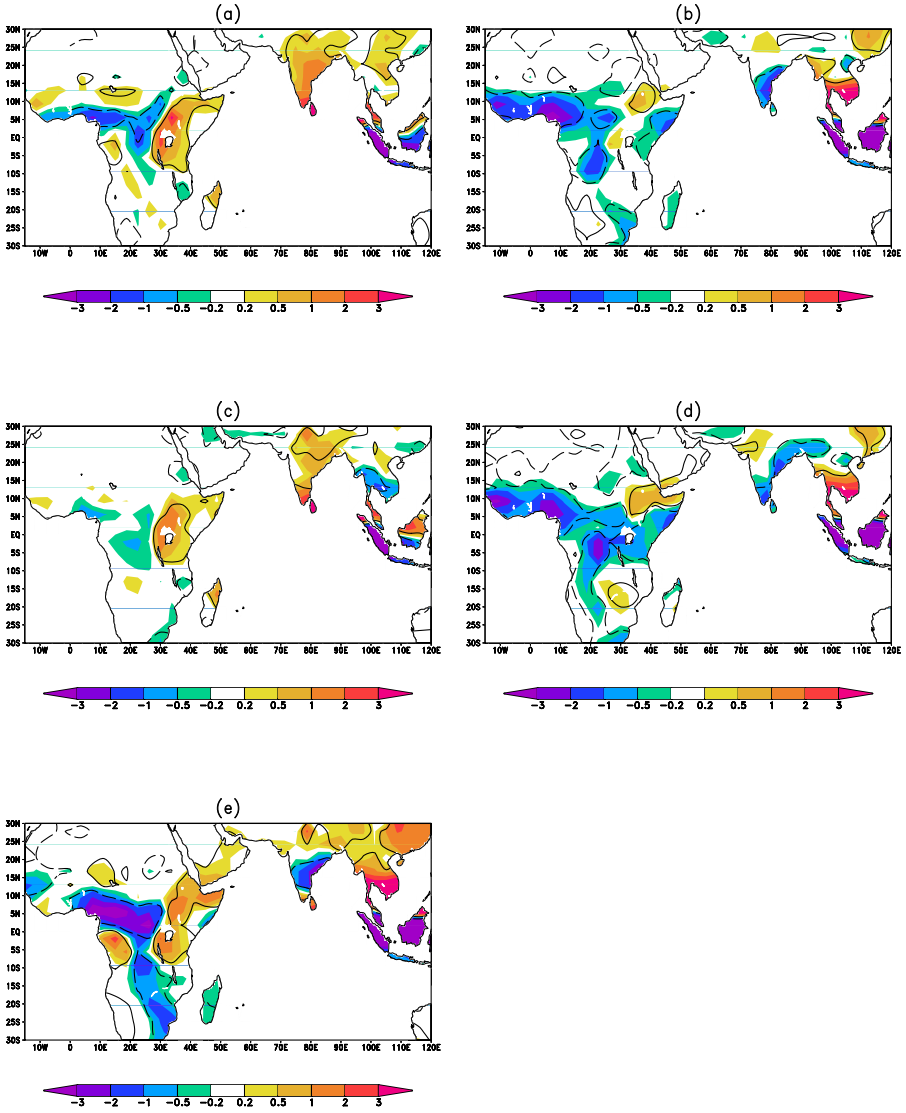

Figure 5.8: Composites of gridded precipitation anomalies in $mm(day)^{-1}$ resulting from ICTPAGCM. Where a) is pure IOD AO.ACTPAGCM b) the same as a, but pure ENSO, c) is pure IOD from IO.ICTPAGCM and d) Pure ENSO from EIO.ICTPAGCM, and e) joint IOD and ENSO events calculated from AO.ACTPAGCM experiment. All analyses are for SON season and the dashed and solid contours are significant at 95% confidence level.

supporting the composite of CRU and AO.ICTPAGCM rainfall anomalies based on pure IOD and pure ENSO over East Africa. As for the observations the model also shows a response that is similar to the pure IOD composite when joint IOD-ENSO events are considered, confirming the dominance of the IOD influence in the region of interest.

Overall, the model autumn rainfall composite patterns are consistent with the observed rainfall composites in the East African region; Pure positive IOD (ENSO) events are related to enhanced (reduced) short rains in East Africa.

5.3.2 Physical mechanism for Indian Ocean influence on East African short rains

In this section, we analyze the physical mechanism in the model for the Indian Ocean influence on East African short rains. The focus is on the Indian Ocean, as we have demonstrated above that SST forced signal is almost entirely due to the Indian Ocean influence. Therefore, we present results from the AO.ICTPAGCM experiment, but results are very similar if the same analysis is performed for the IO.ICTPAGCM experiment. We perform the analysis mainly on the model results, because it has comparative advantage in isolating the purely IOD forced signal due to the ensemble approach.

The observed surface pressure (SP) composites based on pure IOD events shows an extensive area of negative surface pressure anomalies over the warm western half of the Indian Ocean (Figure 5.9a), conversely an area of positive anomaly is observed over the eastern part of the basin. These features are reproduced by the AO.ICTPAGCM experiment (Figure 5.9b), but with increased amplitude. This increased amplitude may be partially explained by the fact that the ensemble mean represents the SST forced signal, whereas in the observations, the internal atmospheric variability may also play a role. The low-pressure anomaly over the western Indian

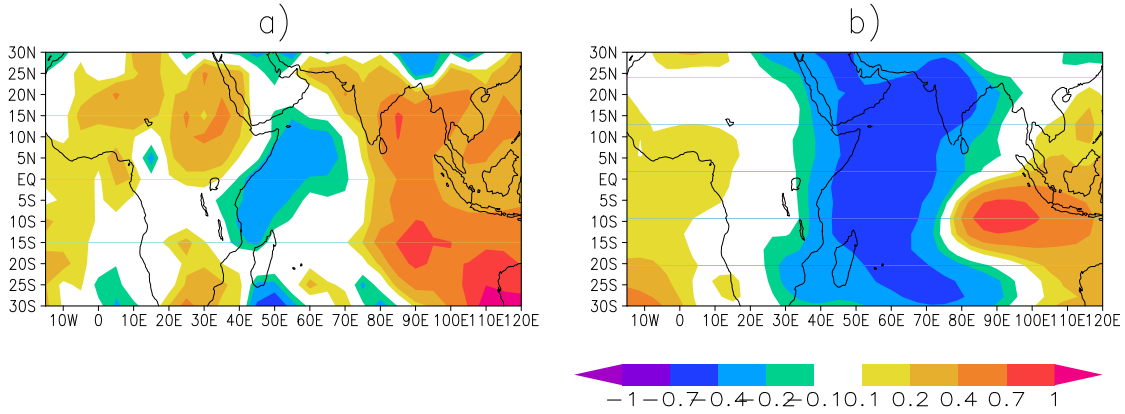

Figure 5.9: Composite of surface pressure anomalies (hpa) for SON season. (a) Pure IOD event derived from HadSLP, (b) Pure IOD event derived from AO-ICTPAGCM.

Ocean may be interpreted as a response induced by the warm pole of the pure IOD events.

Figure 5.10 shows the composites of wind at 850hPa and 200hPa level resulting from AO. ICTPAGCM experiment for pure IOD events. Consistent with the surface pressure response shown in Figure 5.9, there are easterly 850 hPa wind anomalies to the East and westerly anomalies to the west of the low pressure in the western Indian Ocean. This is in agreement with Ummenhofer *et al.* (2009). At 200 hPa, there are easterly wind anomalies to the west over western Indian Ocean and northwesterly to the East over the coast of sumatra, indicating a modulation of the Walker circulation up to the tropopause height during the dipole events (Hastenrath *et al.*, 2007; Goddard and Graham., 1999; Behera *et al.*, 2005). The westerly anomalies extend far into equatorial Africa. In general, such a response is consistent with a Gill-type response Gill (1980) to the western Indian Ocean SST anomalies. This interpretation is further supported by the composite analysis of 850 and 200 hPa velocity potential derived from AO.ICTPAGCM (Figure 5.11). Positive values indicate convergence, negative values divergence; therefore there is low-level convergence

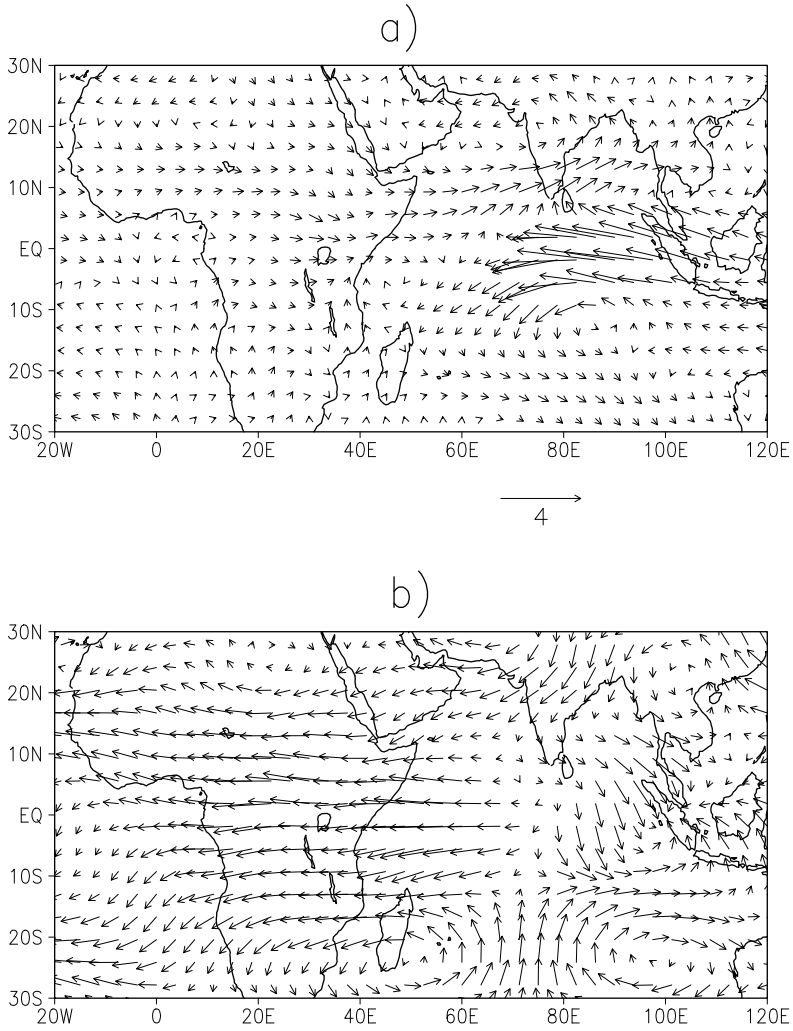

Figure 5.10: SON means composite anomalies of wind ms^{-1} for pure IOD events where (a) wind at 850hpa level and (b) wind at 200hpa level. Both wind composite anomalies are derived from AO.ICTPAGCM.

and upper-level divergence over the warm pole of the western Indian Ocean and East Africa. This is also consistent with previous works (Hastenrath *et al.*, 2007; Goddard and Graham., 1999; Behera *et al.*, 2005).

Moreover, we highlight here the importance of the low-level westerly wind anomalies over East Africa induced by the warm pole of the IOD, which according to our knowledge has not been stressed in the scientific literature. Ummenhofer *et al.* (2009) found that anomalous converging

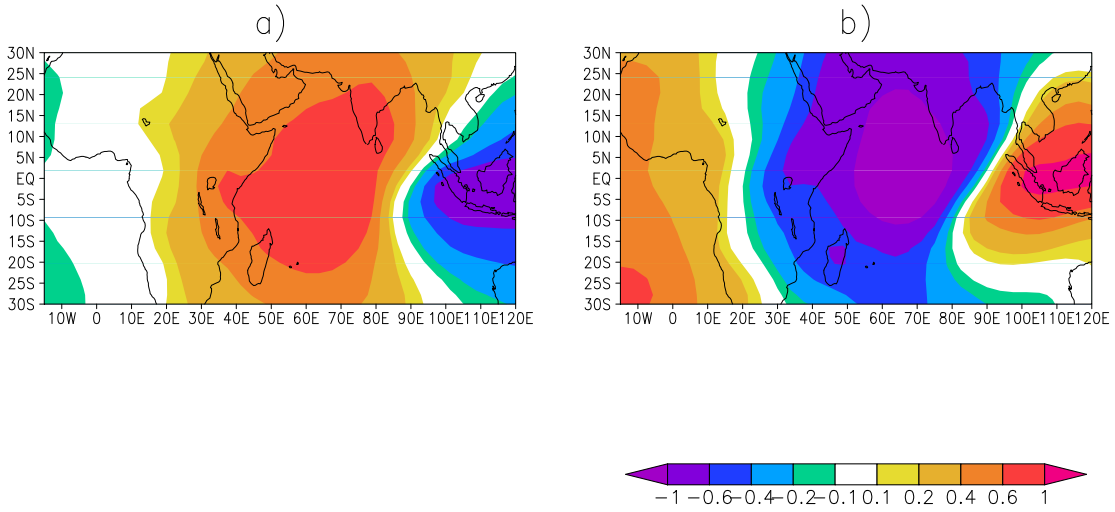

Figure 5.11: SON means composite anomalies of Velocity Potential ($10^6 m^2 s^{-1}$) (a) at 850 hPa, Pure IOD event, (b) Same as in Figure 10a but at 200hpa. Both composite anomalies derived from AO.ICTPAGCM.

westerly flow to the west of East Africa and easterly flow over the Indian Ocean are ingredients that cause an increase in East Africa short rains. Here we propose that the westerly flow anomaly over central Africa may be sufficient to cause an increase of rainfall in East Africa. Indeed, Figure 10 of Behera *et al.* (2005) also indicates only westerly wind anomalies near the coast of East Africa, but they did not further analyze this feature.

In order to further investigate the role of the low-level westerly wind anomalies over East Africa we perform an analysis of the moisture source for the rainfall anomalies (e.g., Peixoto and Oort, 1983). Figure 5.12a shows the total vertically integrated moisture flux and its convergence, indicating that the climatological mean moisture flux is easterly. But, there is also moisture in flux from the west and this only becomes visible when we restrict our integration to lower atmospheric column (Figure not shown), and the main reason is that integrating the whole atmospheric column hampers westerly influx by strong easterly in upper level.

On the other hand, Figure 5.12b shows the pure IOD composite of vertically integrated moisture flux and its convergence for IO.ICTPAGCM experiment. The anomalous moisture flux convergence can clearly explain the rainfall anomalies in East Africa, and the anomalous moisture flux is from west to East in this region, suggesting Congo air mass and the Atlantic region as moisture source, and not the Indian Ocean (Figure 5.12b; Chan *et al.*, 2008; Ummenhofer *et al.*, 2009). Given that the anomaly in the moisture flux shown in Figure 5.12b is smaller than the mean, an alternative interpretation of Figure 5.12b is that IOD events counteract the easterly climatological moisture flux in the African region and shifts the convergence zone to the east. This leads to an increased moisture flux convergence in the equatorial East Africa region.

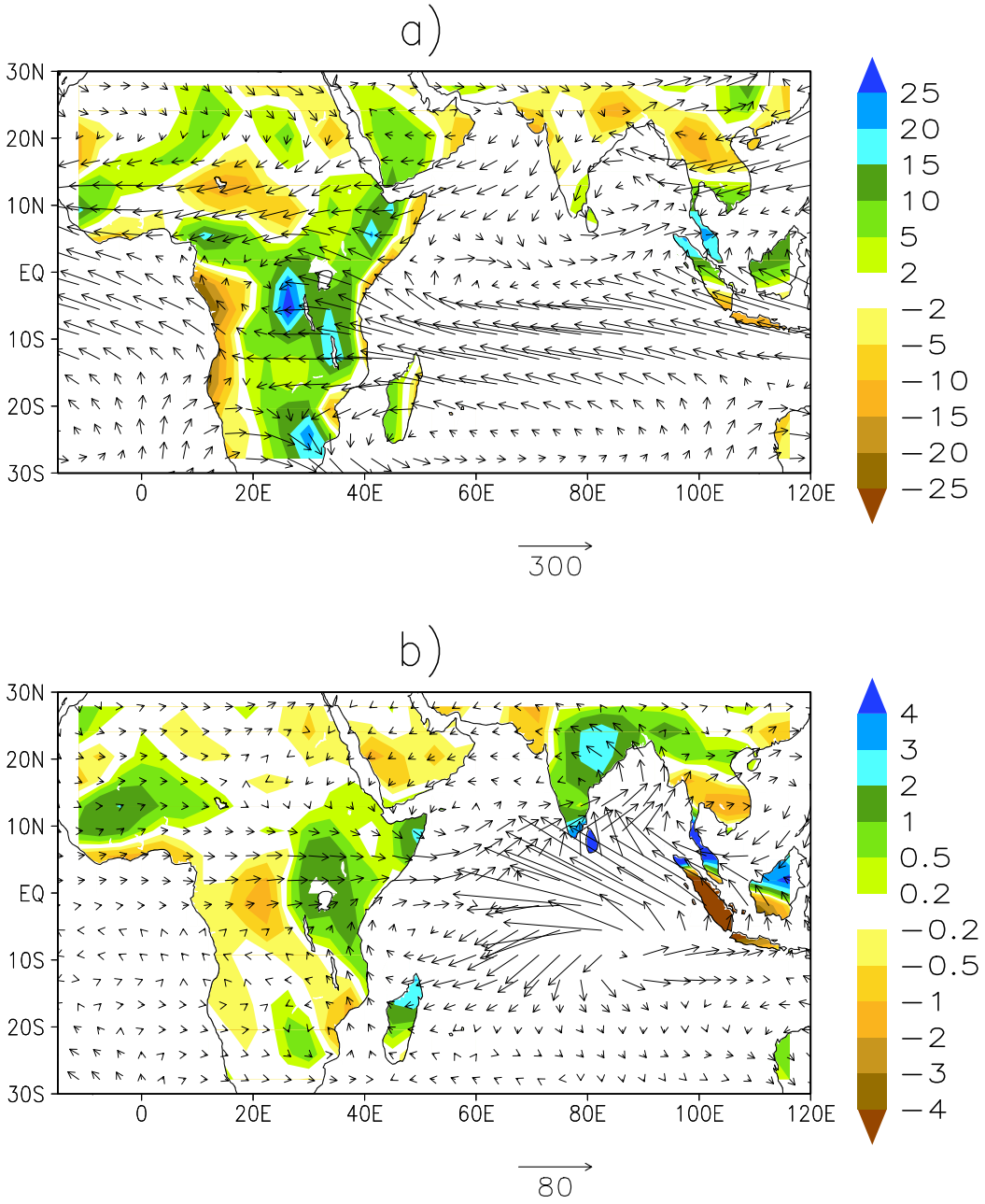

Figure 5.12: (a) Climatological mean vertically integrated moisture flux convergence (shaded) and vertically integrated moisture flux (vector) from the IO.ICTPAGCM experiment. (b) Pure IOD composite of vertically integrated moisture flux convergence (shaded) and vertically integrated moisture flux (vector) from the IO.ICTPAGCM experiment. Units are $mm(day)^{-1}$ for moisture flux convergence and kg $m(s^{-1})$ for moisture flux.

5.4 Potential predictability of short rains

In this section we further explore the potential predictability of short rains based on the ICTPAGCM ensemble experiments. Note that predictability in the context of an AGCM forced with observed SSTs means that it is assumed that the SSTs are known or predictable. In this respect, the predictability estimates provided here may be interpreted as an upper limit. We start the analysis of potential predictability with an analysis of the spatial distribution of SST forced and internal interannual standard deviation (STD) of SON rainfall derived from the ensemble of AO.ICTPAGCM experiment (Kucharski *et al.*, 2012). The SST forced STD is derived from the ensemble mean rainfall; whereas the internal STD is derived from deviations of individual ensemble members from the ensemble mean rainfall. Figure 5.13a shows the forced and Figure 5.13b the internal STD, whereas Figure 5.13c and 5.13d show the ratios of forced and internal STD to the total one, respectively. Such an analysis provide a spatial distribution of a potential predictability indicator, for example a ratio of forced to total STD of one means that all variability is SST forced, and therefore potentially predictable. Generally, the internal STD is larger than the forced one. There are only a few land regions where the forced standard deviation can attain significant amount compared to the internal variability. One of these regions is East Africa (Diro *et al.*, 2008), where the ratio of forced to total STD lies between 0.3-0.4.

Next we turn to the potential predictability of the EEARI index. Our analysis in section 4 showed a substantial skill in reproducing the observed EEARI variability both from AO.ICTPAGCM and IO.ICTPAGCM experiments. Furthermore, we have shown that in our simulations enhanced short rains in East Africa are derived mainly by the local warm SST anomalies in the western Indian Ocean, while the eastern cold pole is of lesser importance (Figure 5.8a; see also Ummen-

Table 5.2: Correlation of Western Indian Ocean SST Index (WIOI) derived from HadISST with observed and Model EEARI for total simulation and two climate periods.

Period	r(CRU,SST)	r(AO,SST)	r(IO,SST)
1920-2009	0.49	0.64	0.71
1920-1975	0.56	0.68	0.75
1976-2009	0.43	0.29	0.66

hofer *et al.* (2009)). Consequently we have analyzed the correlation between the EEARI derived from observation and model with a western Indian Ocean SST index (WIOI) averaged between 10^0S to 10^0N in latitude and 50^0E to 70^0E in longitude (Saji *et al.*, 1999). The correlation coefficients for the total period are 0.49 for observations and 0.64 for the AO.ICTPAGCM simulation (Table 5.2) for East African short rains predictions if Indian Ocean SSTs are known. We are also interested in low frequency changes of predictability, especially related to the Climate Shift of the mid 1970s, which has had global consequences (e.g., Zhang *et al.*, 1997; Trenberth and Hurrell, 1994; Miller *et al.*, 1994; Meehl *et al.*, 2009), and, for example lead to a reduction of predictability of the South Asian Monsoon based on ENSO (Kucharski *et al.*, 2007). Table 5.2 also reveals that the correlation between WIOI and observed and modelled rainfall are indeed reduced after the climate shift of the mid 1970s, even though they are still statistically significant. This reduction of correlation is more pronounced in the AO.ICTPAGCM experiment, whereas the reduction is less severe in IO.ICTPAGCM. This points to the hypothesis that SSTs outside the Indian Ocean could contribute to modify the relation between western Indian Ocean SSTs and East African

Table 5.3: Potential predictability of East Africa short rains index from correlation of ensemble members and ensemble mean for both AO.ICTPAGCM and IO.ICTPAGCM simulation over three climate period.

	AO.ICTPAGCM			IO.ICTPAGCM		
	1920-1975	1976-2009	1920-2009	1920-1975	1976-2009	1920-2009
r(M1,ENSM-1)	0.46	0.38	0.47	0.62	0.51	0.69
r(M2,ENSM-2)	0.51	0.47	0.51	0.62	0.48	0.66
r(M3,ENSM-3)	0.50	0.47	0.55	0.61	0.65	0.74
r(M4,ENSM-4)	0.60	0.49	0.55	0.69	0.62	0.74
r(M5,ENSM-5)	0.63	0.18	0.51	0.61	0.46	0.67
r(M6,ENSM-6)	0.54	0.26	0.49	0.61	0.53	0.67
r(M7,ENSM-7)	0.47	0.21	0.46	0.67	0.58	0.72
r(M8,ENSM-8)	0.44	0.45	0.49	0.64	0.53	0.70
r(M9,ENSM-9)	0.59	0.35	0.56	0.73	0.63	0.75
r(M10,ENSM-10)	0.45	0.48	0.51	0.69	0.74	0.73
P. P	**0.52**	**0.37**	**0.50**	**0.65**	**0.57**	**0.71**

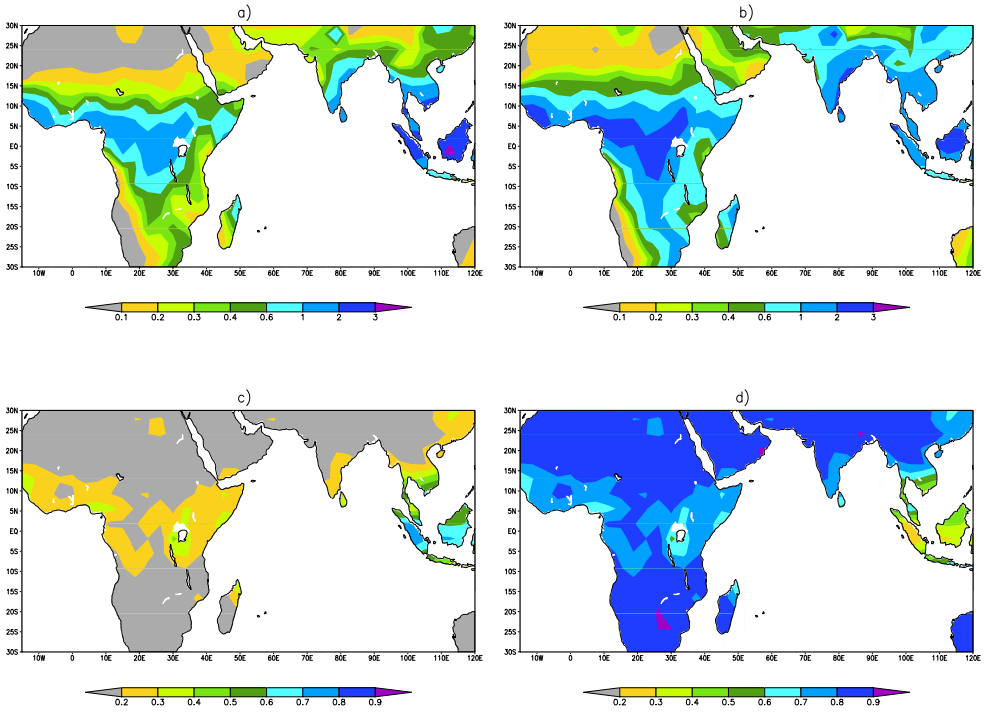

Figure 5.13: SON standard deviation of rainfall from AO.ICTPAGCM. (a) Forced component, (b) internal component, c) Forced STD $_{forced}$ / STD $_{total}$, d) internal contribution STD $_{intern}$/ STD $_{total}$ to the total variance. Units are $mm(day)^{-1}$ for (a) and (b).

short rains.

Now we analyze the potential predictability of East African short rains by considering one ensemble member as observation, and correlating all other remaining members with it (Table 5.3; see also e.g. Kucharski *et al.* (2009)). The mean of the correlation coefficients for EEARI can be considered as potential "correlation skill" and should be close to the correlation coefficient with the observed EEARI. The idea behind the concept of correlation skill is that in a perfect model framework each ensemble member is a single realization of climate and thus may be treated as comparable to an observation. Therefore, a single ensemble member should have a correlation with the ensemble mean of the remaining models that is consistent with the correlation of the observed rainfall time-series with the ensemble mean. Since this analysis can be repeated 10 times

in a 10-member ensemble, the 10 resulting correlation coefficients can be used to calculate the mean, which is the best estimate of the perfect model correlation skill. The mean correlation skill (0.5) is indeed close to the correlation coefficient of the model with the observed EEARI. On the other hand the potential correlation skill estimate from IO.ICTPAGCM is larger with 0.71 and the ensemble mean shows larger correlation with all ensemble members than with the observed EEARI. The interpretation of this result is that in the IO.ICTPAGCM experiment competing influences from other ocean basins (in particular from the Pacific) are excluded, and this may lead to a seemingly increased predictability of East African short rains.

The correlations in the AO.ICTPAGCM experiment drop after the Climate Shift by 0.15, whereas the correlations in IO.ICTPAGCM drop by less than (0.08), again indicating SSTs outside the Indian region contribute also to the reduced potential predictability seen in AO.ICTPAGCM.

The hypothesis that the interference of ENSO SST anomalies with IOD SST anomalies over East Africa (Williams and Hanan, 2011) may be responsible for the drop of correlation skill which is further supported by the analysis of SON standard deviation of Nino3.4 Index; and it has been increased from 0.71 before the climate shift to 0.95 afterwards, suggesting the ENSO related variability increased substantially after the 1970s climate shift. On the other hand, the WIOI standard deviations changes from 0.25 to 0.23, before and after climate shift respectively.

Chapter 6

Assessment of Coupled Dynamical Seasonal Forecast Systems

This Chapter focuses on the results generated from evaluation on performance of dynamical seasonal forecast systems for the prediction of SSTAs over tropical Indian Ocean and short rains anomalies over equatorial East Africa. Our evaluation is based on Asia-Pacific Climate Center (APCC) Ocean-Atmosphere coupled Multi-Model Ensemble (MME) hindcasts (Table 2.1). Individual models are initialized on 1^{st} of November, February, May and August for six month lead seasonal prediction. These forecast systems have different hindcast periods; in this study we have selected common years from 1982 to 2005. Hindcasts initialized on 1^{st} August from each year alone are considered, as these are the most relevant to short rains predictions. The ensembles of individual models and their MME mean are evaluated.

6.1 Verification and forecast quality measures

Evaluating the quality of seasonal predictions is an essential component of seasonal forecasting. Here we have used CMAP data to verify the skill of coupled dynamical models. Otieno and Anyah (2013) made a brief analysis on the performance of CMAP dataset in representation of rainfall distribution and intensity over East Africa compared against different satellite-gauge rainfall products and they have found agreement between observations over the region. Therefore, the choice of CMAP data is based on its availability over land and Ocean points, its data record match with the study period and its agreement with other gridded products. Similar to previous Chapters, here we have considered only the SON season for analysis input. The choice of SON (instead of October-November-December) is also motivated by the availability of seasonal hindcasts initialized close to the verification period. In this Chapter total rainfall and the equatorial East Africa SON short rainfall is defined area as averaged precipitation within (5S-5^{o}N, 35-46^{o}E) domain. The mean climate in East Africa varies in short distance, despite this inhomogeneity in the mean rainfall condition over the region, interannual variability of rainfall is coherent within selected domain. The details of verification data and reanalysis used here can be found in Chapter 2.

To measure the forecast quality of a deterministic forecast, MME mean prediction was constructed using the simple average of ten models ensemble means. The metrics used to measure and evaluate prediction skill of individual coupled models ensemble mean and MME mean forecast includes the anomaly correlation coefficient (ACC), linear regression and simple correlations. Calculation of these quantities is standard (e.g., Wilks, 1995) and uses anomaly data, whereby the observed seasonal cycle and the hindcast climatology (which is a function of start month and

lead time) are removed from the observations and forecasts, respectively. We have also calculated areal averaged temporal correlation between forecast and observation for EEARI and IOD.

6.2 Hindcast simulation of SON climatology and annual cycle

In the following we compare the performance of individual coupled model ensembles and MME mean hindcast of SON wind and precipitation climatology with observed precipitation and reanalysis wind over the equatorial Indian Ocean region. We also discuss the simulation of the annual cycle of rainfall over equatorial East Africa. The system under consideration provide forecasts with up to six moth lead with August initial conditions, therefore the modeled annual cycle includes only the months September to February. The observed rainfall and reanalysis 850 hPa wind climatology for SON season over a period of 1982 to 2005 are shown in Figure 6.1a.

The pattern of observed rainfall shows maxima over the eastern Indian Ocean near coast of Sumatra, Malaysia and around Vietnam. The observed climatological rainfall pattern over Africa shows high intensity around Equatorial Guinea and decreased towards the Equatorial East coast, where the retreat of southwest monsoon and westerlies from the Atlantic Ocean converge over the Congo air mass area. The corresponding rainfall and 850 hPa wind climatology for the ten coupled models ensemble mean forecasts, together with MME mean climatology, are shown in Figure 6.1b-l.

The coupled model hindcasts reproduce the observed spatial pattern with the rainfall maxima

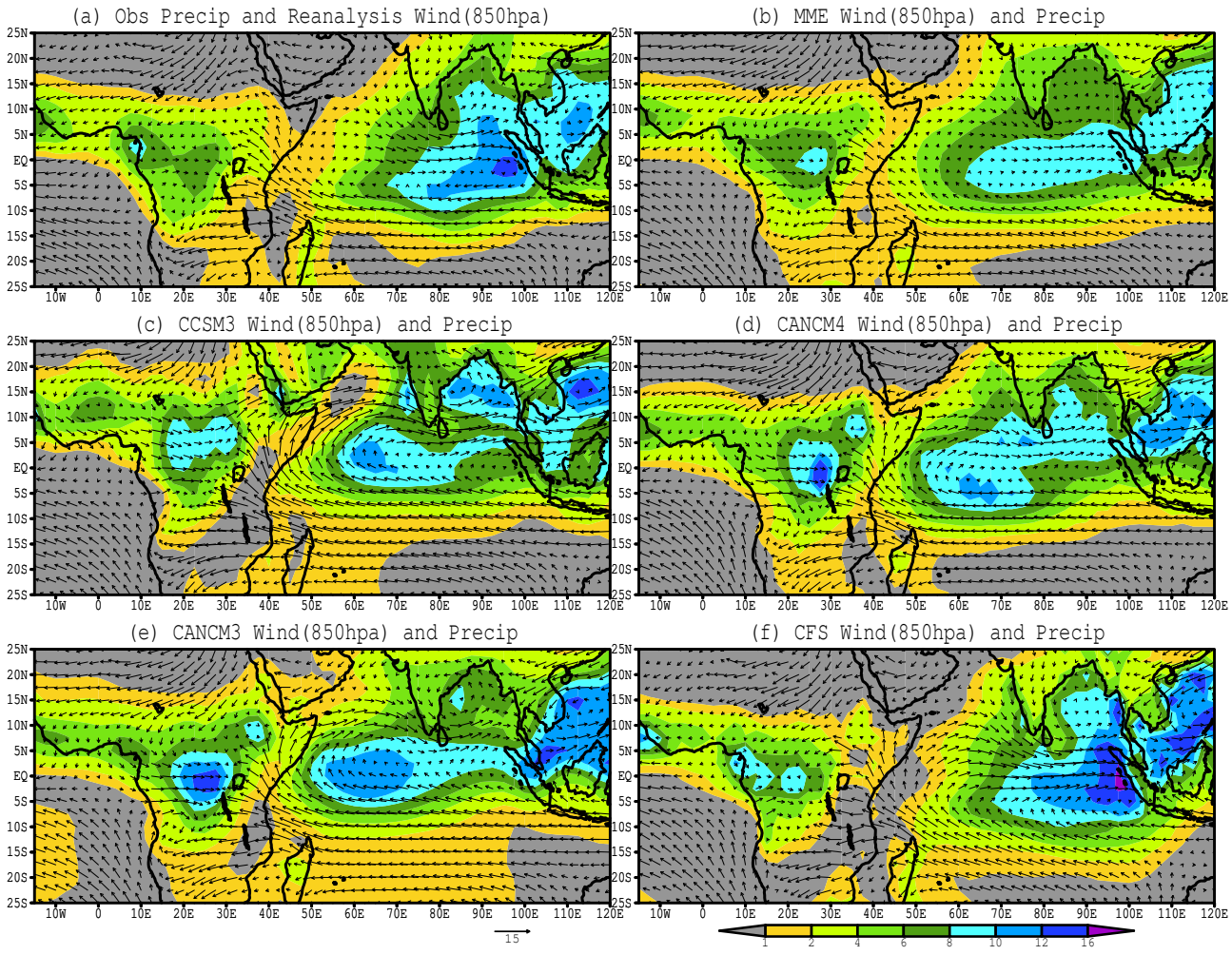

Figure 6.1: Rainfall $mm(day)^{-1}$ (shaded) and 850 hPa winds $m(s)^{-1}$ spatial climatology derived from observation and reanalysis respectively and APCC coupled models from 1982 - 2005 valid for SON. (a) Observed rainfall and reanalysis wind, (b) MME, (c) CCSM3, (d) CANCM4, (e) CANCM3, and (f) CFS.

generally well captured (Figure 6.1b-l). However, a few models show positive biases over the central Africa region and some underestimate rainfall over the coast of East Africa. The PNU, NASA and CFS models over estimate the rainfall intensity over the tropical eastern Indian Ocean (Figure 6.1h, b and f). On the other hand, the CCSM3 and CANCM3 coupled models rainfall band extends too far to the north towards Arabian Peninsula (Figure 6.1c and e), which is likely related the presence of a late summer monsoon in these models. The performance of the coupled

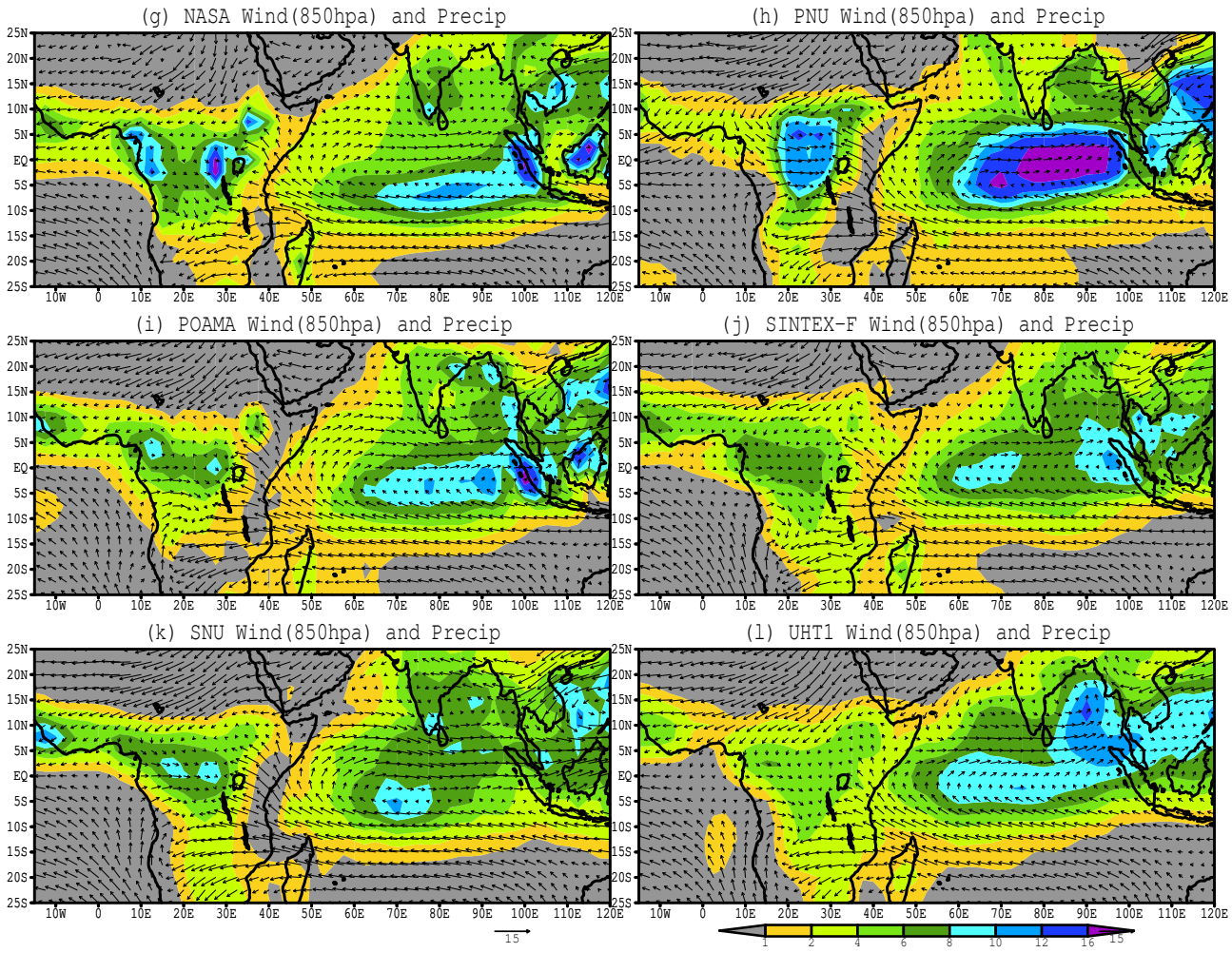

Figure 6.1: Continued, but g) NASA, h) PNU, i) POAMA, d) SINTEX-F, j) SNU, and k) UHT1. The unit for rainfall is in $mm(day)^{-1}$ and wind is given in $m(s^{-1})$.

model ensembles in capturing the SON climatology over the Indian Ocean region is enhanced in their MME mean (Figure 6.1b).

The climatological wind pattern are easterlies south of the equator in the eastern and central Indian Ocean but turn northwestward towards East Africa, conversely, there are strong westerlies north of the equator in the eastern Indian ocean towards Indonesia (Figure 6.1a-l). Overall, the coupled models reproduce the wind climatology over the Indian Ocean region fairly well compared

with reanalysis and is further improved in the MME mean, though there is weak flow into Africa and westerlies in east Indian Ocean (Figure 6.1b). However, two coupled models (CCSM3 and CANCM3) are unable to represent wind pattern and show over estimation over the Arabian Sea (Figure 6.1c and e).

Figure 6.2 shows the seasonal cycle of EEARI, defined as area averaged rainfall over the region (5S-5^{o}N, 35-46^{o}E), for the ten APCC coupled models, MME mean and observations. About half of coupled models initialized on first of August are unable to capture the phasing and amplitude of the seasonal cycle, but the phasing of the seasonal cycle in SINTEX-F, UHT1, CANCM4, CFS, CANCM3 is reasonably well simulated compared with observation and those shown in previous studies (e.g., Hastenrath *et al.*, 1993; Black *et al.*, 2003; Behera *et al.*, 2005). However, the PNU, CCSM3 and CANCM3 coupled models are unable to reproduce the peak month of the short rains and shift it towards December and January (Figure 6.2).

We also found that UHT1, CANCM4, and NASA simulate the seasonal rains and their variability relatively well, despite their over estimation in the peak phase of short rains. On the other hand, SNU, POAMA and CFS models show a dry bias in the short rains season. In spite of individual coupled models ensemble hindcast discrepancies compared with observation, MME mean shows a quite reasonable phasing and amplitude of the seasonal cycle of rainfall over equatorial East Africa, with the tendency of too much rainfall in December and January still present.

6.3 IOD prediction in coupled models and MME

The teleconnection of SST anomalies in the Indian Ocean and interannual fluctuation of short

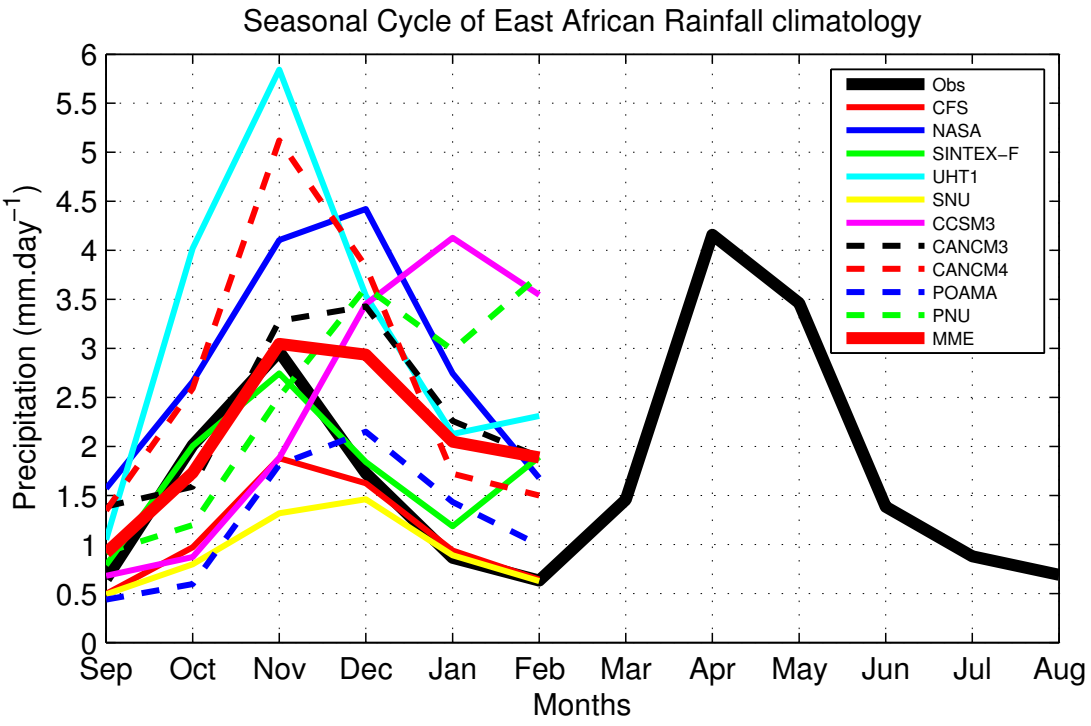

Figure 6.2: Seasonal cycle of the Equatorial East African rainfall averaged over (5S - 5N, 35 - 46 E), derived from ten APCC dynamical coupled models and MME mean. The unit of rainfall is given in mm/day.

rains over equatorial East Africa has recently been investigated (Black *et al.*, 2003; Yamagata *et al.*, 2004; Behera *et al.*, 2005; Ummenhofer *et al.*, 2009). SSTAs for IOD events start evolving during June and reach peak strength by October-November, and decay by the end of December (Rao *et al.*, 2007). In addition, Behera *et al.* (2005) has shown that the early signal of the IOD in the SST dipole mode index has high prediction skill for the variations of short rains. However, the relationships between the IOD and the East African short rains have not been documented in real seasonal forecasts.

In light of these research gaps and importance of IOD as seasonal rainfall prediction ingredient over equatorial East Africa, in this section we present the evaluation of the skill of coupled model ensembles and their MME mean in forecasting IOD. We consider SON mean SST anomalies for

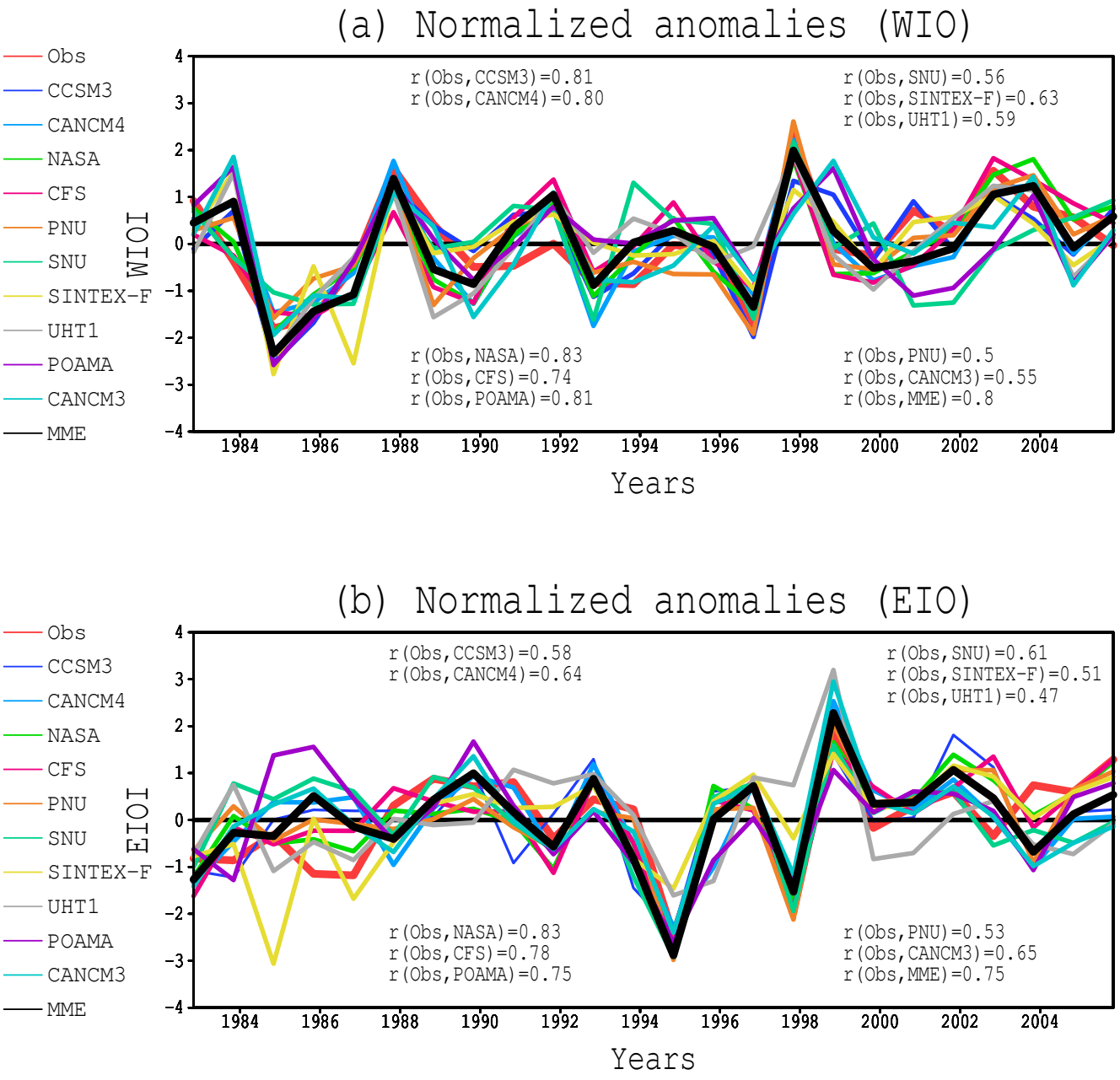

Figure 6.3: Year-to-year variation of SON seasonal mean observed, individual coupled models ensemble mean and MME mean hindcast SST anomalies normalized by standard deviation along with their correlatioon cofficient with respcet to verification data. (a) Normalized SST anomalies over western Indian Ocean index (WIOI), (b) normalized SST anomalies over south easternn Indian Ocean index (EIOI). All Hidcasts are intialized from 1^{st} August.

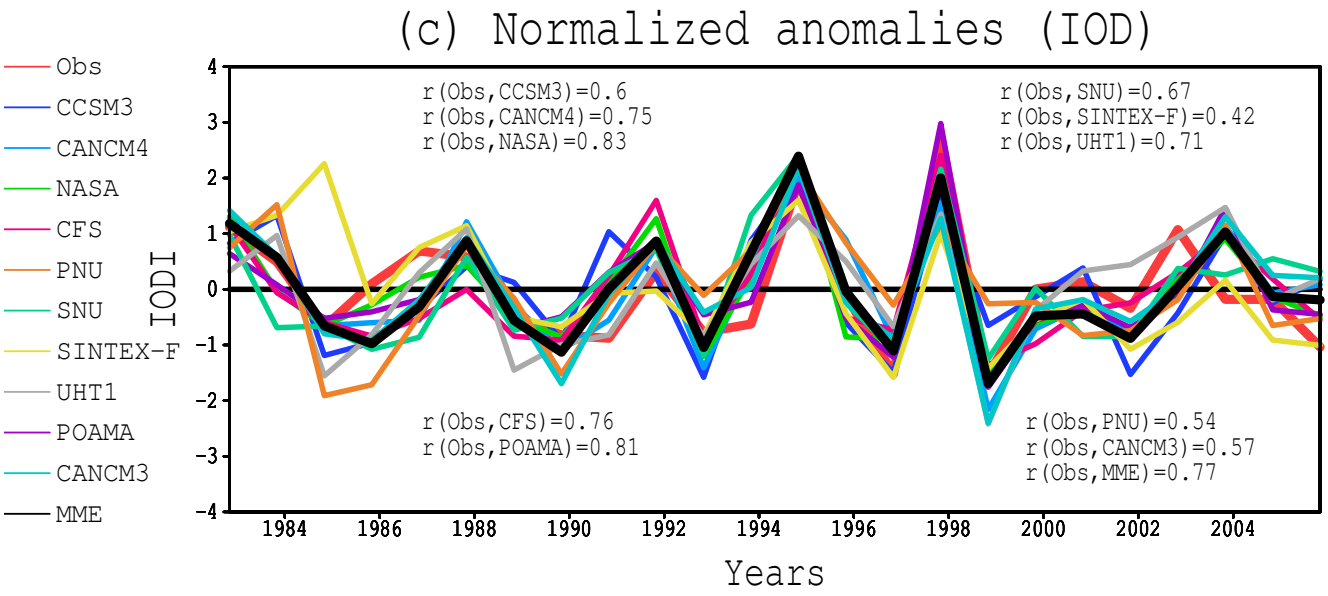

Figure 6.3: Continued, but (c) IOD. All Hidcasts are intialized from 1^{st} August.

hindcast verification, which is the peak season in the evolution of IOD. In addition, IOD and equatorial East Africa short rains have strong contemporaneous relations at this time of the year.

The performance of the SST prediction is investigated by analyzing the skill of forecast SST anomalies over the equatorial Indian Ocean. Figure 6.3 shows the forecast of interannual variation of SON season mean SST anomalies normalized by the corresponding standard deviation and derived from ten coupled models ensemble mean and MME mean hindcast initialized on the 1^{st} of August. The hindcasts are verified against the same indices derived from the ERSSTv3b, where a) WIO, b) EIO and c) IOD. It is seen from Figure 6.3a that there is a large skill of SST predictions over WIO for almost all models and their MME mean, as reflected in the large significant correlation of predicted SST with observation.

The skill of SST hindcasts over the EIO (Figure 6.3b) is relatively lower than over WIO (Figure 6.3a). On the other hand, the correlation skill of IOD (Figure 6.3c) predictions is in

between those of EIO and WIO, and is statistically significant at 99% confidence level for the MME mean. Previous studies have shown that the skill of long term prediction of IOD is predominately limited by the skill of predicting SST anomalies in the eastern Indian Ocean (Zhao and Hendon, 2009), but the difference is not significant in our analysis though there is slight reduction in skill for predicting the EIO compared to the WIO SST index (Figure 6.3).

Figure 6.3 also shows the correlation coefficients between observed and predicted SON WIO, EIO and IOD over the period of 1982-2005. In summary the forecast skill for the SST anomalies in almost all models exhibits skill greater than 0.5 and also highly significant above 99.9% level, except for the SINTX-F model (with a correlation of only 0.42; Shi *et al.* (2012)). Models with high IOD forecast skill are CFS, NASA, POAMA ensemble mean and MME mean. On the other hand, SNU, PNU, and CANCM3 are characterized by relatively lower correlation. POAMA and MME have the highest skills of all models with correlation coefficients close to 0.8 for IOD. Moreover, positive IOD prediction shows very good skills with the major IOD events like 1982, 1994 and 1997 captured well in nearly all forecasts (Figure 6.3). The high correlation coefficients further confirm the statistically significant skill of coupled models in forecasting SST anomalies over tropical India Ocean in the SON season.

In general, it can be concluded that the APCC coupled models and MME mean initialized on 1^{st} August produce excellent predictions of the temporal behavior of the SST anomalies over the Indian Ocean.

6.4 Equatorial East Africa short rains prediction

In this section the skill of the deterministic APCC coupled models ensemble and their MME

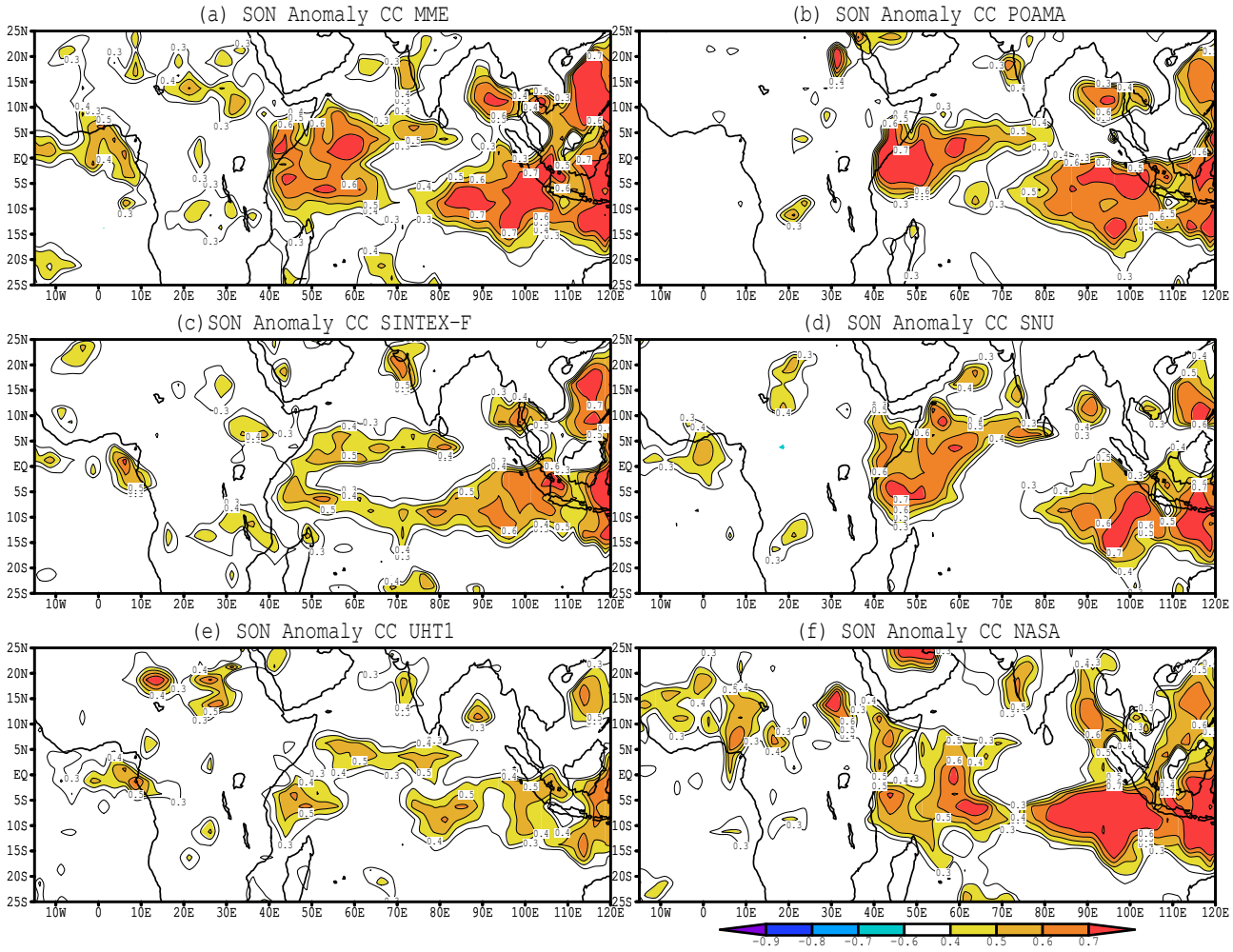

Figure 6.4: Anomaly correlation coefficient (ACC) between SON observed rainfall and forecast rainfall derived from coupled models ensemble and MME mean during the period of 1982-2005 with (a) MME, (b) POAMA, (c) SINTX-F, (d) SNU, (e) UHT1, and (f) NASA. All coupled system initialized on 1^{st} of August and shaded positive values are at 95% significant level

mean hindcast of SON rainfall is examined over the period 1982-2005. The assessment is made over the India Ocean region with particular emphasis on short rains anomalies over equatorial East Africa. Previous studies have demonstrated that IOD is the source of predictability for East African short rains (Behera *et al.*, 2005). Thus, we calculate correlation maps to demonstrate the fidelity of coupled models to capture the impact of IOD on the climate of surrounding region.

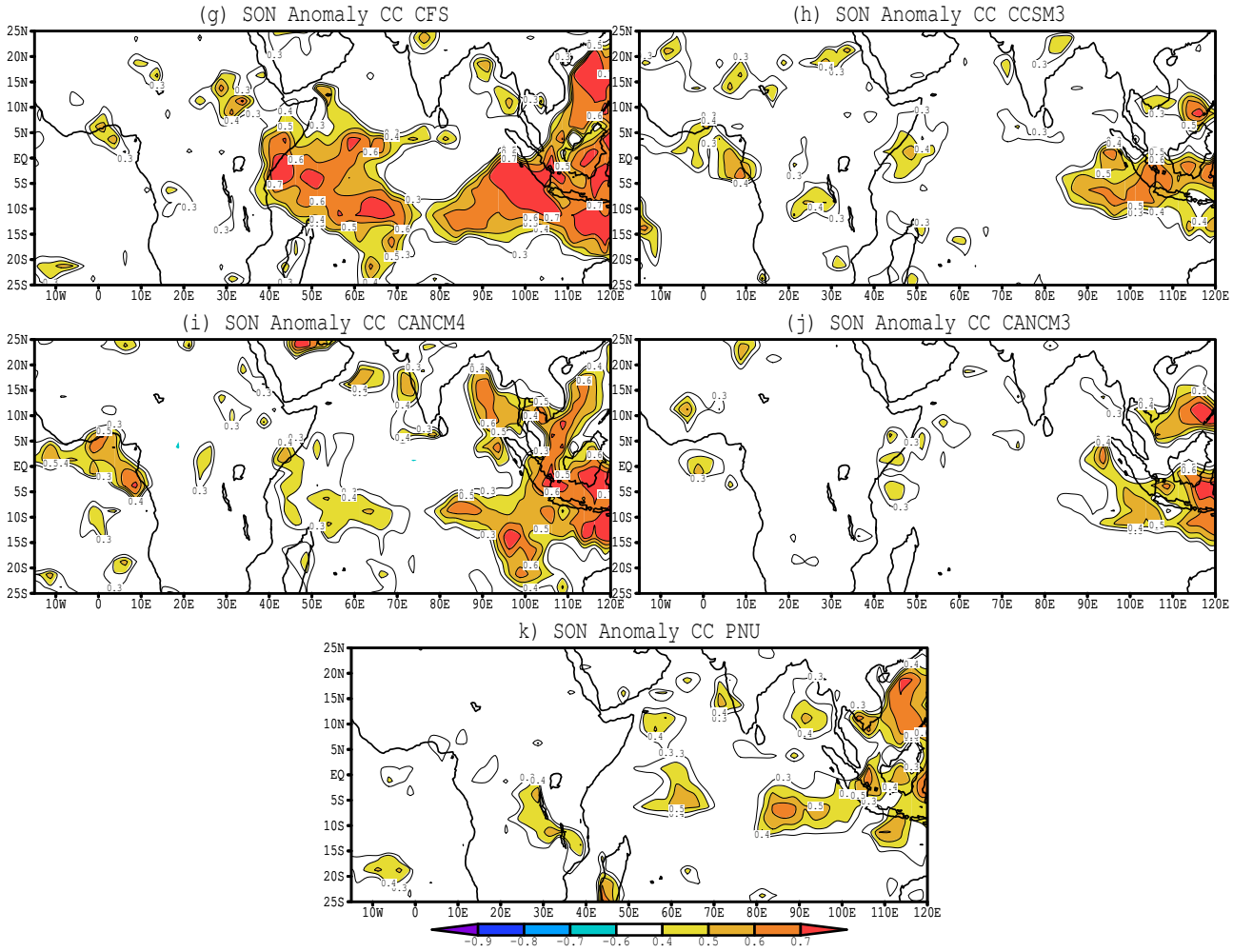

Figure 6.4: Continued, but (g) CFS, (h) CCSM3, (i) CANCM4, (j) CANCM3, and (k) PNU.

The skill of SON rainfall anomaly forecast is evaluated based on the Anomaly Correlation Coefficient (ACC) between the observation and coupled models forecast over Indian Ocean basin. The ACC maps for the coupled models and MME mean hindcast for SON season rainfall anomaly are shown in Figure 6.4. Overall, there is little or no skill found over most of land points, with the exception of the coast of East Africa and countries east of Tropical Indian Ocean region where significant skill can be identified.

A similar lack of rainfall predictability over most land regions has also been reported by

Wang *et al.* (2009). On the other hand, most coupled models and MME mean show significant skill over ocean points in the south eastern Indian Ocean and western Indian Ocean (Figure 6.4a-g). However, only SON rainfall hindcast derived from NASA, CFS, POAMA, SNU and MME show statistically significant skill for forecasting equatorial East Africa short rains, ACC between forecast rainfall anomaly and the observed rainfall anomaly for these models is high (almost of he order of 0.6) over coast of East Africa (Figure 6.4). CANCM4, CANCM3 and CCSM3 have ACC around 0.3 over coast of East Africa, the rest of the models less.

6.4.1 Skill for impacts of IOD on short rains variability

As shown in the previous section, APCC coupled models and MME mean hindcast are able to predict SST anomalies over the equatorial Indian Ocean at 1-month lead time. In this subsection, we briefly discuss the impact of IOD on East Africa short rains, and examine the coupled models performance in predicting the observed impacts. The relationship between SON rainfall variability and equatorial Indian Ocean SST anomalies is demonstrated by correlation maps between the time series of SON seasonal mean IOD derived from observations and the rainfall anomalies over the Indian Ocean region (Figure 6.5a). There are positive correlations over large parts of western Indian Ocean extending towards Arabian Sea and East Africa, indicating enhanced short rains in East Africa is driven predominantly by the local warm SST anomalies in the western Indian Ocean. Conversely, anomalously dry conditions are depicted in eastern Indian Ocean extending southern Sumatra, around Bay of Bengal and Southeast Asia. The physical mechanism determining the setting up of east-west gradient of SON seasonal rainfall anomalies can be explained by Walker cell modification over equatorial Indian Ocean (Saji *et al.*, 1999; Black *et al.*, 2003; Behera *et al.*, 2005).

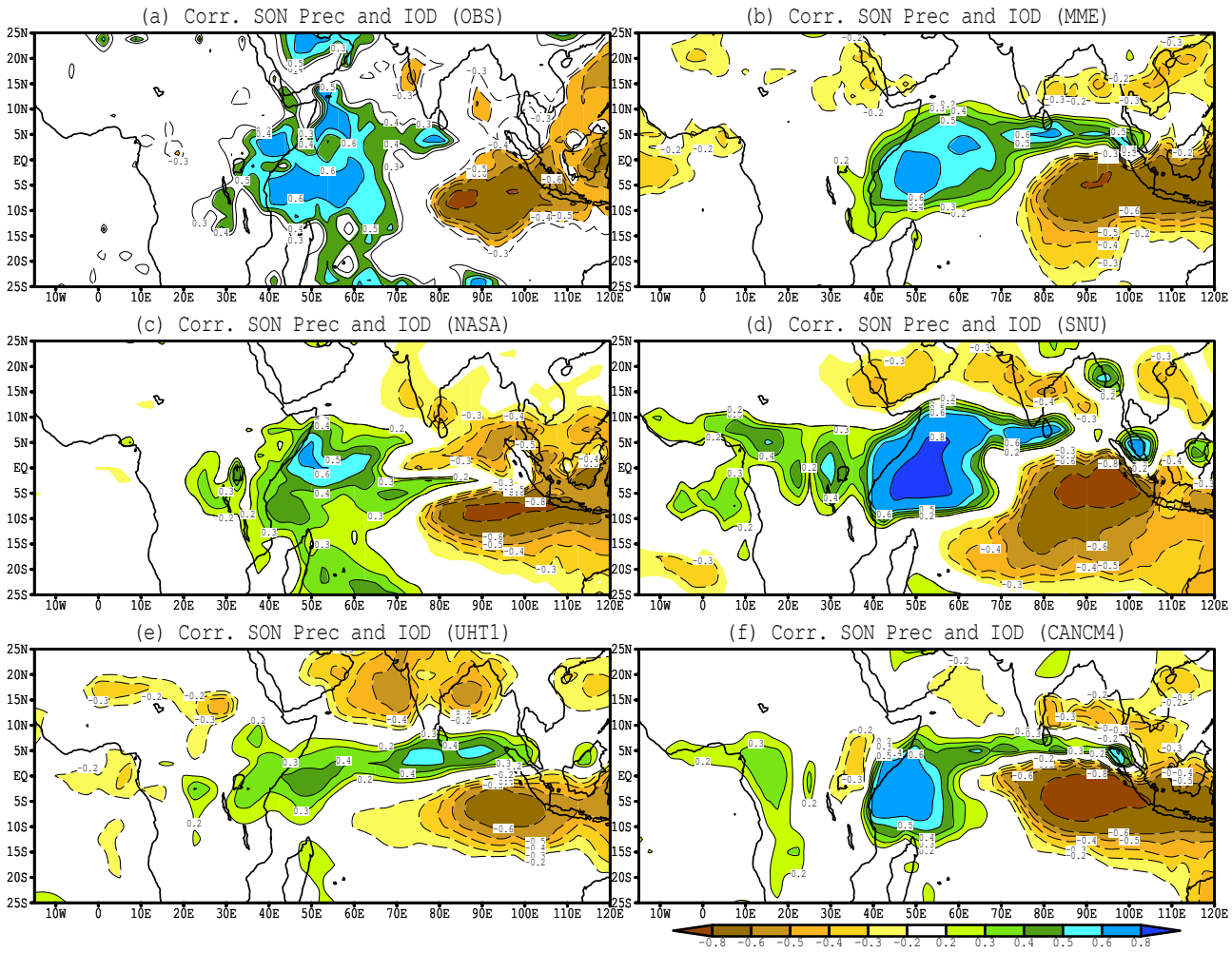

Figure 6.5: Correlation map between SON seasonal mean Dipole Mode Index and the corresponding SON seasonal mean standardized precipitation anomalies derived from observation, individual coupled models ensemble and MME mean where (a) Observation, (b) MME, (c) NASA, (d) SNU, (e) UHT1 and (f) CANCM4. All coupled models are initialized on 1^{st} August and estimated over 1982-2005 periods.

Now we estimate how well individual coupled models and MME mean predict the aforementioned rainfall variability associated with IOD. To demonstrate this relation we have created concatenated time series from individual model ensembles for both SST and precipitation. The pattern of correlation map between IOD and corresponding rainfall anomalies at 1-month lead time from concatenated series of individual model ensemble members, observation and MME are

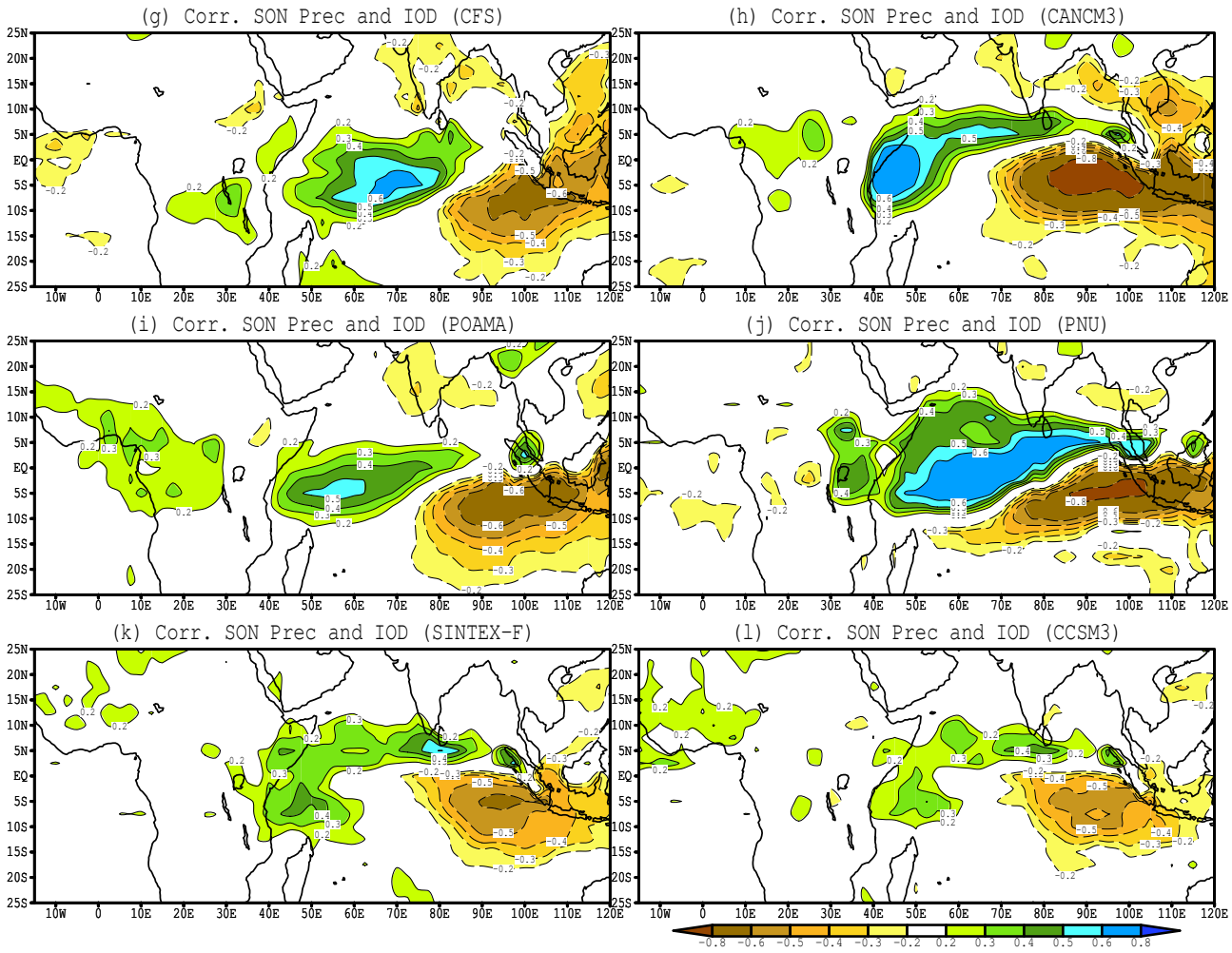

Figure 6.5: Continued, but (g) CFS, (h) CANCM3, (i) POAMA, (j) PNU, (k) SINTX-F and (l) CCSM3.

shown in Figure Figure 6.5. The MME correlation map has been calculated by using 5 members from each individual model (the minimum ensemble size) and concatenating all resulting 50 time series.

Consistent with previous discussion nearly all coupled models and MME predictions replicate the observed east-west dipole pattern fairly well (Figure 6.5b-l). For example, statistically significant at 95% confidence level positive correlation over western equatorial Indian Ocean, East Africa

and the northern part of the Indian Ocean along southern tip of India extending to north of Sumatra, and negative correlations over the equatorial south eastern Indian ocean, southern Sumatra and most parts of the southeast Asian region are well represented. However, three coupled models show relatively weak correlations over western Indian Ocean and East Africa (Figure 6.5g, i and l). Moreover, a better correlation patterns are found in MME, SINTEX-F and NASA (Figure 6.5b, c and k).

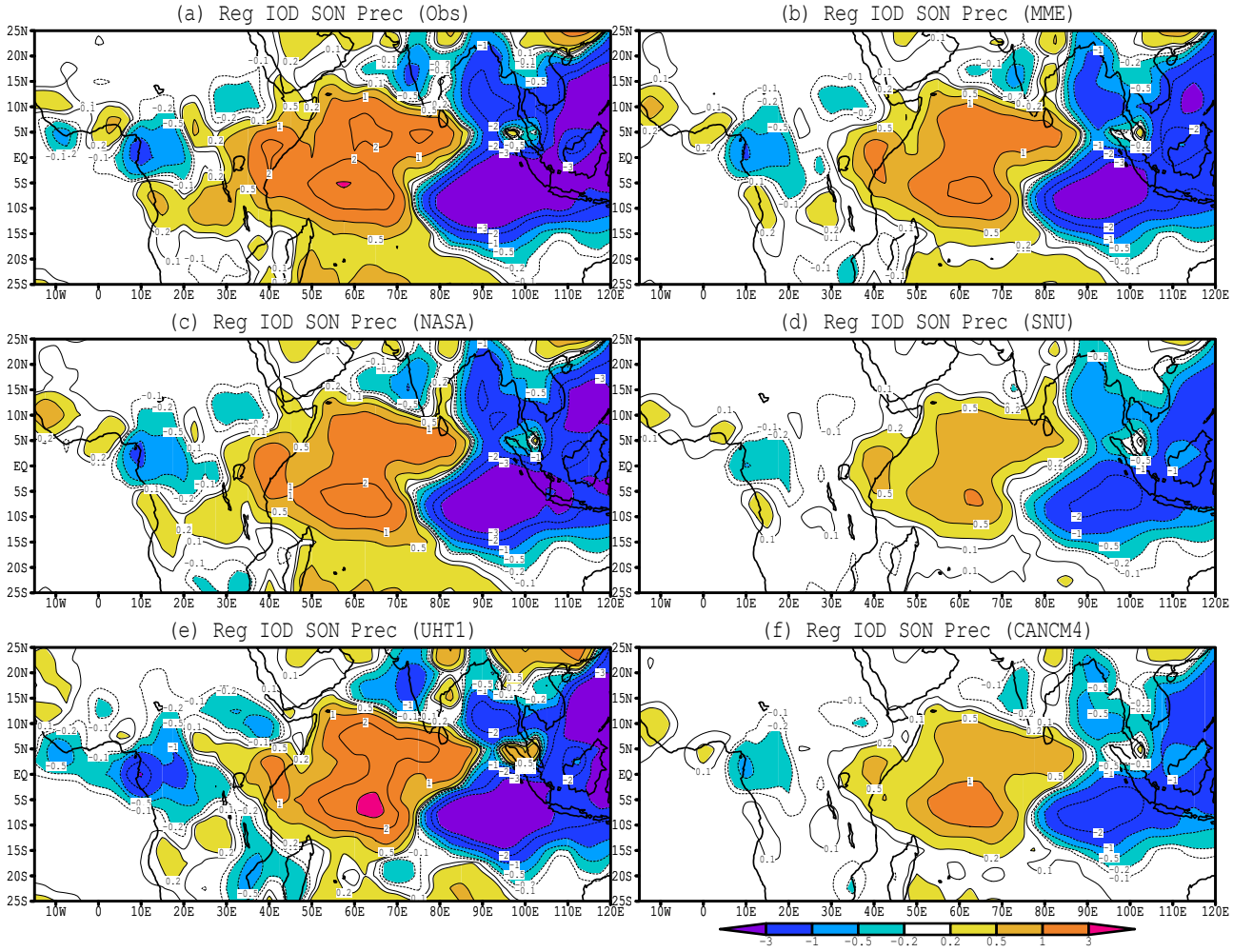

Figure 6.6: Regressions of SON seasonal mean observed rainfal on to Indian Ocean Dipole mode index (DMI) derived from APCC individual coupled model ensemble mean, observation and MME. (a) Observation, (b) MME, (c) NASA, (d) SNU, (e) UHT1 and f) CANCM4. All coupled model ensemble means are initialized on 1^{st} August for a period 1982-2005.

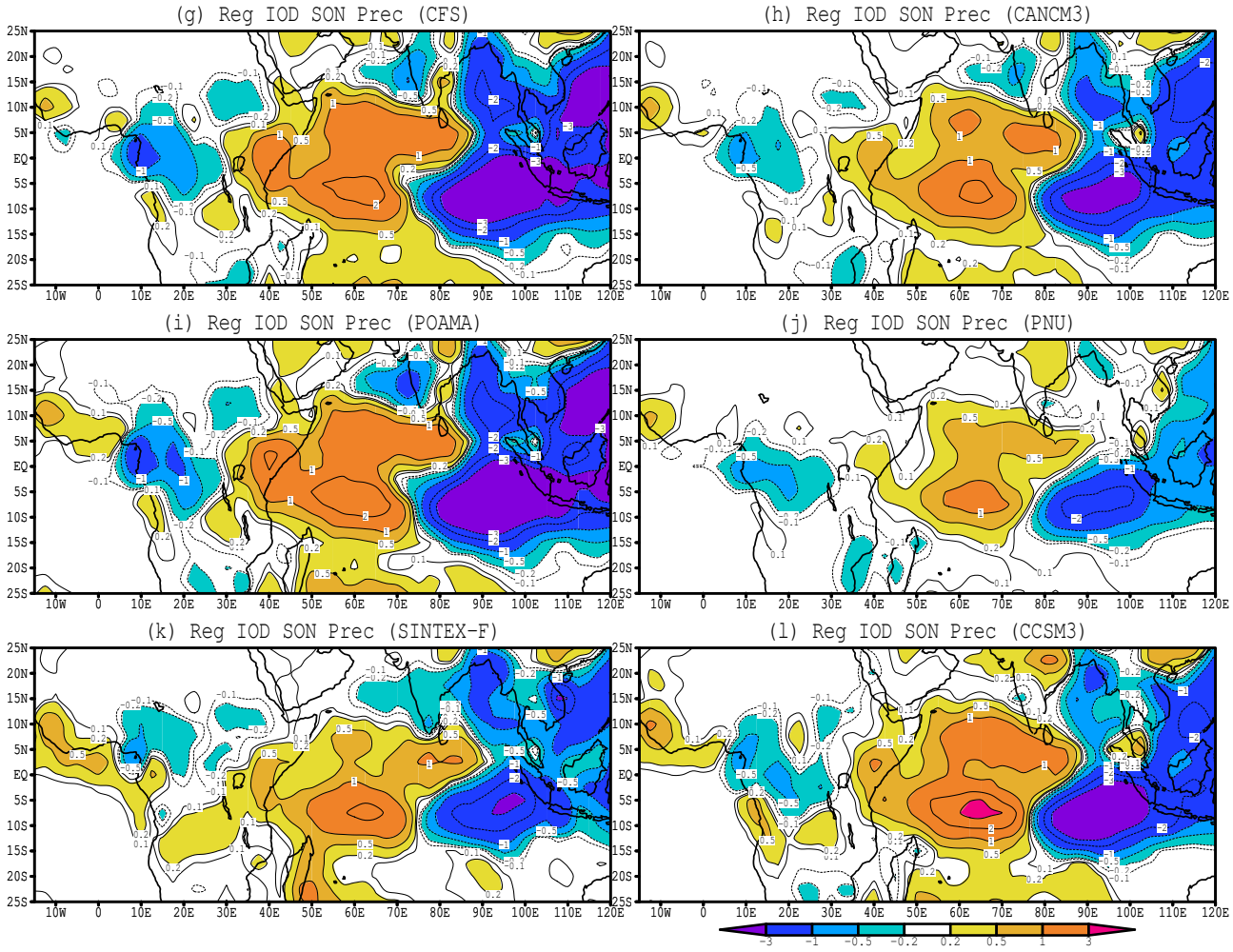

Figure 6.6: Continued, but (g) CFS, (h) CANCM3, (i) POAMA, (j) PNU, (k) SINTEX-F and (l) CCSM3.

In order to examine the possibility of using the APCC individual couple model predicted SSTs to predict the autumn rainfall over Indian Ocean basin and hence evaluate the skill of dynamical model performance in capturing observed relations in SSTAs and rainfall anomalies, SON seasonal mean observed rainfall regressed on to observed and forecast DMI during SON with 1^{st} August initial conditions (Figure 6.6). The regression maps demonstrate that IOD calculated from observation, most of coupled models and MME are produced statistically significant regression anomalies over tropical Indian Ocean basin.

The regression pattern in observation, almost all APCC coupled model ensemble and MME clearly shows a dipole in the Indian Ocean conditions (Figure 6.6). IOD, which is Ocean-Atmosphere coupling between east west contrast SST and zonal wind explained through precipitation. Associated with these changes the normal convection situated over the eastern Indian Ocean warm pool shifts to the west and brings heavy rainfall over the east Africa and severe droughts/forest fires over the Indonesia (Black *et al.*, 2003). Moreover, the out-of-phase relation between two sides of the basin is consistent with the previous findings, the fact that rainfall over East Africa (Indonesia) is increased (decreased) during a positive event IOD (Black *et al.*, 2003; Yamagata *et al.*, 2004; Behera *et al.*, 2005; Ummenhofer *et al.*, 2009). The above results are quite encouraging for the prospects of predicting East Africa short rains, but require forecasts from coupled Atmosphere-Ocean models. However, since the predictability of EEARI comes mainly from SSTAs over Indian Ocean, the question arises as to whether the predicted IOD index from coupled models can be used to derive skillful forecasts of EEARI.

6.4.2 Short rains forecast skill

We now consider hindcasts of short rains over East Africa produced by the coupled models. The interannual variation of equatorial East Africa rainfall index and the correlation between observed and each coupled models ensemble and MME mean is shown in Figure 6.7. The figure illustrates that five coupled models predict equatorial East Africa rainfall with statistically significant skill. CFS prediction giving the strongest correlation of all and SNU, UHT, POAMA and CANCM3 also show significant skill. The other models have relatively lower skill and unable are to produce significant correlations. Despite insignificant skill in some individual models, MME

mean produce the fourth largest significant correlation at 95% confidence level. Please note that the correlations could be influenced by sampling (given the relative small time series of 24 years), therefore, for example, that CFS gives the largest correlations could be by chance.

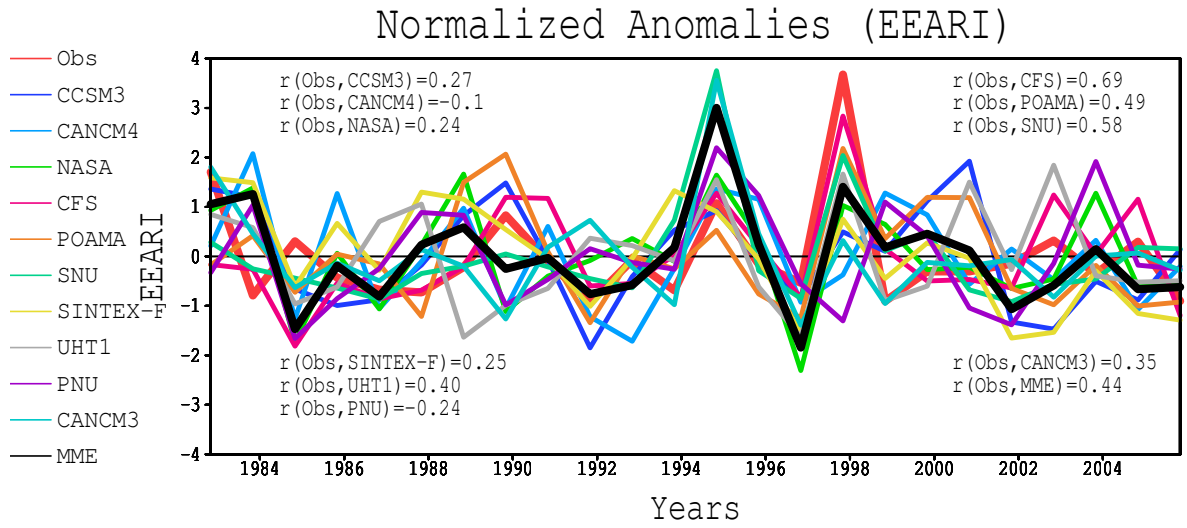

Figure 6.7: Interannual variation of SON normalized anomaly over equatorial East Africa in APCC coupled models hindcast and MME mean verified against observation along with the temporal correlation between observed and predicted SON equatorial east Africa rainfall index (5^0S-5^0N, 35-45^0E) for a period of 1982-2005. The ensembles mean EEARI is used from each models, while the mean of all models are used to compute the MME.

6.4.3 MME mean forecast skill improvements by model selection

Finally we consider improvements of forecast skill in the MME mean hindcasts of SON equatorial East Africa rainfall by selecting five good models according to their correlation skill in predicting the EEARI index (Figure 6.7). Only models that show at least 90% statistically significant correlations are selected. The resulting models are UHT1, CFS, POAMA, SNU and CANCM3. Such a selection should be revisited once more hindcast data is available. The correlation between

observed and ensemble mean of EEARI for the selected coupled models and their MME mean is shown in Figure 6.8. The 90% significant level is indicated by the horizontal dashed line. Thus the skill of the MME based on this model selection improves its skill from 0.44 for all models to 0.67.

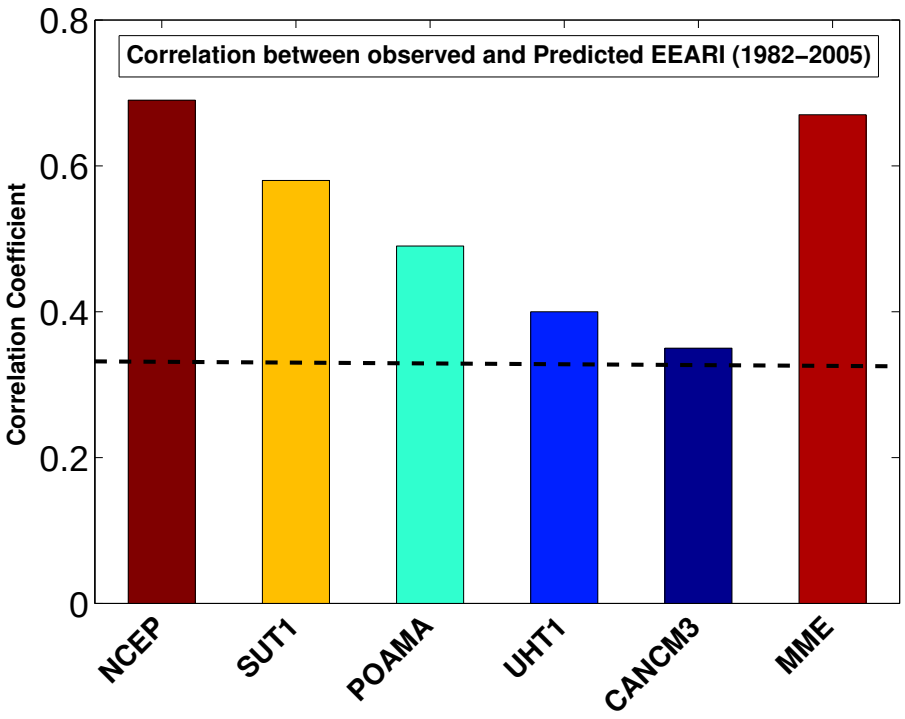

Figure 6.8: Correlation between observed and predicted SON Equatorial East Africa rainfall for hindcasts in APCC coupled models dataset for a period 1982-2005, East Africa rainfall index in a dynamical models and observation is defined as total precipitation within 35^o-46^{o}E and 5^{o}S-5^{o}N.

Chapter 7

Summary and Conclusions

The aim of this study has been to understand large scale influences on interannual variability, to scrutinize underlying physical mechanisms, to investigate the predictability and seasonal prediction of East African rainfall, with a focus on Equatorial East Africa. East Africa's climate is prone to extended rainfall deficits. In extreme cases these can lead to droughts and humanitarian disasters. Skilful prediction of seasonal rainfall would therefore bring sound humanitarian and economic benefits to countries over the region, that are highly dependent on rain-fed agriculture.

We first performed a detailed investigation on the roles of IOD and ENSO in the variability of equatorial East African short rains using observational data and a series of ensembles of long Atmospheric General Circulation Model (AGCM) simulations. Pure IOD and pure ENSO years are selected to differentiate the position of tropical Ocean-Atmosphere coupling over Indian Ocean and Pacific Ocean in influencing interannual short rains variability over equatorial East Africa. Composites of observed rainfall for pure IOD events show enhanced (reduced) precipitation over East African (Indonesia), on the other hand pure ENSO composites show a mixed signal with reduction of short rains over parts of East Africa see also (Black *et al.*, 2003; Behera *et al.*, 2005). In order to support the observational evidence of IOD and ENSO influences on East African

short rains, we have performed three sets of ICTPAGCM ensemble experiments, forced with interannually varying SSTs globally, in the Indian Ocean only, and everywhere outside the Indian Ocean.

We find that the main driver of East African short rains is the IOD, and ENSO provides only a minor contribution that opposes the IOD forced signal. The ENSO forcing does not lead to any predictable signal (Williams and Hanan, 2011). The physical mechanism for the IOD influence on East African short rains in our model is that the warm pole of a positive IOD leads to a Gill-type response that causes westerly wind anomalies over Africa, moving the moisture flux convergence zone towards East Africa. This finding is broadly consistent with previous findings (e.g., Ummenhofer *et al.*, 2009; Black *et al.*, 2003), but here we emphasis the role of the westerly wind anomalies over Africa, whereas the importance of the easterly wind anomalies over the Indian Ocean (or a combination of the two) have been emphasized previously.

There is a substantial potential predictability associated with an East African short rains index (EEARI), given that Indian Ocean SSTs can be predicted. The predictability of the EEARI, however, shows a decadal variation associated with the mid 1970s climate shift and is likely related to interfering influences of IOD and ENSO on East African short rains that increase after the climate shift due to increased ENSO variability.

We also made assessment of real predictability in seasonal hindcast products on predictive skill for short rains anomalies over East Africa. Our evaluation is based on observational datasets and the Asia-Pacific Climate Center (APCC) Ocean-Atmosphere-Land coupled Multi-Model Ensemble (MME) retrospective forecasts (hindcasts) (Kang *et al.*, 2009; Lee *et al.*, 2010; Min *et al.*, 2011; Sohn *et al.*, 2011). Coupled model hindcast also evaluated for prediction of SST anomalies over

tropical Indian Ocean.

Almost all Individual models and MME mean shows climatological pattern of rainfall and low level wind similar to observations. Though some models over estimate rainfall near the Equator at about 30 W, the MME reduces the errors and reasonably reproduces the observational pattern. Moreover, the usefulness of the MME method is further exemplified in analysis of seasonal cycle over equatorial East Africa. Moreover, assessment of the skill of individual coupled models and MME mean shows statistically significant skill in forecasting the peak phase of the IOD in the boreal autumn SON season, which is typically when the IOD is best defined and most climatically important (Zhao and Hendon, 2009). The skill for predicting IOD appears to be largely limited by the skill of predicting SST in the eastern Indian Ocean. Though coupled models and MME mean give a better skill for SST anomalies over western IOD relative to eastern IOD of equatorial Indian Ocean, a large predictive skill is found for the IOD. Furthermore, out of ten models five coupled models and MME mean show statistically significant skill in predicting equatorial East Africa short rains.

East African rainfall hindcast skill is further improved by selecting 5 models with the largest individual correlation skill. However, such a selection gives by definition an improved MME mean hindcast, and we are aware of the risk of eliminating or selecting models because of sampling, given the relatively short time series of 24 years. The models skills in predicting East African rainfall relies on the impact of the IOD on East African rainfall. Indeed, we have shown that most models and the MME mean show realistic correlations of the IOD index with rainfall, and in particular also positive correlations in the East African region. Moreover, coupled models skill over East Africa further confirmed by our regression maps showing dipole mode pattern that demonstrates

the control of IOD on the variation of East African short rains.

It is shown that the reproduction of the observed variability in the East African region is mainly due to a realistic relationship of East African rainfall with the Indian Ocean Dipole. Overall, the skill of the dynamical models is attributed to the fact that slowly evolving SSTs are the primary source of predictability, and to the fact that coupled climate models produce skillful predictions of SON SST anomalies over the tropical Indian Ocean. This information opens the possibility of using readily available seasonal forecasts as skillful predictions of equatorial East Africa short rains. An encouraging potential for real time forecasts of East African rainfall with about one month lead time is revealed. Such forecasts would be of substantial societal importance.

The results in this study therefore provide insight into interannual rainfall variability and predictability over East Africa, in view of tropical Indian Ocean-Atmosphere climate patterns and underlying mechanisms. In addition, the information on coupled forecast systems will open the possibility of using readily available seasonal forecasts as skillful predictions of equatorial East Africa short rains. The results can be fed into real-time monitoring and forecasting at seasonal to interannual timescales to enhance early warning and disaster preparedness activities and minimize the impacts of climate-related catastrophes that are prevalent in the region.

References

Allan R, Ansell T. 2006. A new globally complete monthly historical gridded mean sea level pressure dataset (HadSLP2): 1850-2004. *J. Clim.* **19**: 5816–5842. 10

Annamalai H, Potemra J, Murtugudde R, McCreary JP. 2005. Effect of preconditioning on the extreme climate events in the tropical indian ocean. *J. Clim.* **18**: 3450–3469. 38

Baquero-Bernal A, Latif M, Legutke S. 2002. Notes and correspondence on dipole like variability of sea surface temperature in the tropical Indian Ocean. *J. Clim.* **15**: 1358–1368. 42

Behera SK, Luo JJ, Masson S, Delecluse P, Gualdi S, Navarra A, Yagamata T. 2005. Paramount impact of the Indian Ocean dipole on the East African short rains: A CGCM study. *J. Clim.* **18**: 4514–4530. 2, 3, 27, 41, 44, 48, 59, 62, 64, 67, 68, 69, 82, 83, 87, 89, 94, 97

Behera SK, Rao SA, Saji HN, Yamagata T. 2003. Comments on "A cautionary note on the interpretation of EOFs". *J. Clim.* **16**: 1087–1093. 48

Behera SK, Yamagata T. 2003. Influence of the Indian Ocean dipole on the southern oscillation. *Journal of the Meteorological Society of Japan* **81**: 169–177. 43

Bjerknes J. 1966. A possible response of the atmospheric hadley circulation to equatorial anomalies of ocean temperature. *Tellus* : 820–828. 34

Black E, Slingo J, Sperber KR. 2003. An observational study of the relationship between excessively strong short rains in coastal East Africa and Indian Ocean SST. *Mon.Weather Rev.* **131**: 74–94. 2, 3, 23, 24, 34, 38, 41, 43, 44, 48, 59, 82, 83, 89, 94, 97, 98

Bourke W. 1974. A multilevel spectral model. i. formulation and hemispheric integrations. *Mon.Weather Rev.* **102**: 687–701. 12

Brown BG, Murphy A. 2007. Improving forecasting performance by combining forecasts: The example of road surface temperature forecasts. *Meteor Appl* **3**: 257–265. 51

Camberlin P, Philippon N. 2002. The East African March-May rainy season: associated atmospheric dynamics

and predictability over the 1968-97 period. *J. Clim.* **15**: 1002–1019. 60

Chan RY, Vuille M, Hardy DR, Bradley RS. 2008. Intraseasonal precipitation variability on kilimanjaro and the East Africa region and its relationship to the large-scale circulation. *Theor. Appl. Climatol.* **93**: 149–165. 70

Charney JG, Shukla J. 1981. Predictability of monsoons: Monsoon dynamics. *University Press, Cambridge* : 99–109. 4

Clark CO, Webster PJ, Cole JE. 2003. Interdecadal variability of the relationship between the indian ocean zonal mode and east african coastal rainfall anomalies. *J. Clim.* **16**: 548–554. 38

CLIVAR AR. 1999. Climate research for Africa. *WCRP Informal Rep* : 29–79. 2

Desole T, Shukla J. 2012. Climate models produce skillful predictions of indian summer monsoon rainfall. *Geophys Res Lett* **39**: L0973. 4, 51

Diro GT, Black E, Grimes DIF. 2008. Seasonal forecasting of Ethiopian spring rains. *Meteorol. Appl.* **15**: 73–83. 2, 4, 48, 72

Diro GT, Grimes DIF, Black E. 2011. Large scale features affecting Ethiopian rainfall. *In: Williams CJR, Kniveton DR (ed). Springer, Dordrecht* . 2, 48

Dommenget D, Latif M. 2002. A cautionary note on the interpretation of eofs. *J. Clim.* **15**: 216–225. 17

Fu X, Wang B. 2004. The boreal-summer intraseasonal oscillations simulated in a hybrid coupled atmosphere-ocean model. *Monthly Weather Review* **19**: 619–631. 16

Gibson JK, Kalberg P, Uppala S, A Hernandez AN, Serrano E. 1997. Ecmwf re-analysis. project report series. 1. era description. *European Centre for Medium-Range Weather Forecasts, Reading (U.K.)* . 13

Gill AE. 1980. Some simple solutions for heat-induced tropical circulations. *Q. J. R. Meteorol. Soc.* **106**: 447–462. 67

Gill AE. 1982. Atmosphere-ocean dynamic. *Academic Press* **30**: 978–0–12–283 522–3. 33

Gissila T, abd D I F Grimes EB, Slingo JM. 2004. Seasonal forecasting of the ethiopian summer rains. *Int. J. Climatol.* **24**: 1345–1358. 21

Glantz MH. 1988. Drought and hunger in africa. *Cambridge University Press, UK* . 20

Glantz MH. 2001. Currents of change: Impacts of el nio and la nia on climate and society. *Cambridge Univ.* . 31

Goddard L, Graham NE. 1999. Importance of the Indian Ocean for simulating rainfall anomalies over eastern and southern Africa. *J. Geophys. Res.* **104**: 99–116. 44, 48, 67, 68

Graham RJ, Evans ADL, Mylne KR, Harrison MSJ, Robertson KB. 2000. An assessment of seasonal predictability using atmospheric general circulation models. *Q. J. R. Meteorol. Soc.* **126**: 2211–2240. 51

Ham YG, Kang IS. 2010. Improvement of seasonal forecasts with inclusion of tropical instability waves on initial

conditions. *Clim. Dyn.* : 1277–1290. 16

Hastenrath S. 1991. Climate dynamics of the tropics. *Kluwer Academic Publishers* : 488. 20, 21

Hastenrath S, Nicklis A, Greischar L. 1993. Atmospheric - hydrospheric mechanisms of climate anomalies in the western equatorial Indian Ocean. *J. Geophys. Res.* **98**: 20,219–20,235. 2, 3, 27, 39, 47, 48, 50, 82

Hastenrath S, Polzin D, Camberlin P. 2004. Exploring the predictability of the $'short-rains'$ at the coast of East Africa. *Int. J. Climatol.* **24**: 1333–1343. 3, 23, 42, 50

Hastenrath S, Polzin D, Mutai C. 2007. Diagnosing the 2005 drought in equatorial East Africa. *J. Clim.* **20**: 4628–4637. 2, 67, 68

Held IM, Suarez MJ. 1994. A proposal for the intercomparison of the dynamical cores of atmospheric general circulation models. *Bull. Am. Meteorol. Soc.* **75**: 1825–1830. 12

Huang BH, Kinter JL. 2002. Interannual variability in the tropical indian ocean. *Journal of Geophysical Research-Oceans* **107**: C11. 38

Jeong HI, Ashok K, Song B, Min YM. 2008. Experimental 6-month hindcast and forecast simulation using CCSM3. *APCC 2008 Technical Report, APEC Climate Center.* . 16

Jury R. 2002. Economic impacts of climate variability in south africa and development of resource prediction models. *J Appl Meteor* **41**: 46–55. 1

Kalnay E, Kanamitsu M, Kistler R, Collins W, Deaven D, Gandin L, Iredell M, Saha S, G White J Woollen YZMC, Ebisuzaki W, WHiggins, Janowiak J, Mo KC, Ropelewski C, Wang J, Leetmaa A, Reynolds R, Jenne R, Joseph D. 1996. The NCEP/NCAR 40-year reanalysis project. *Bull Amer. Meteor. Soc.* **71**: 437–471. 10

Kang H, Park CK, Saji NH, Ashok K. 2009. Statistical downscaling of precipitation in korea using multimodel output as predictors. *Monthly Weather Review* **137**: 437–471. 14, 98

Kassie BT, Rtter RP, Hengsdijk H, Asseng S, van Ittersum MK, Kahiluto H, van Keulen H. 2013. Climate variability and change in the Central Rift Valley of Ethiopia: Challenges for rainfed crop production. *J. Agric. Sci* **52**: 58–74. 21

Krishnamurti T, Kishtawal CM, Shin DW, Williford CE. 2000. Multi-model superensemble forecasts for weather and seasonal climate. *J. Clim.* **13**: 4196–4216. 50

Kucharski F, Bracco A, Yoo JH, Molteni F. 2007. Low-frequency variability of the Indian Monsoon-ENSO relation and the Tropical Atlantic: The 'weakening' of the '80s and 90s. *J. Clim.* **20**: 4255–4266. 73

Kucharski F, Molteni F, Bracco A. 2006. Decadal interactions between the western tropical Pacific and the North Atlantic Oscillation. *Clim. Dyn.* **26**: 79–91. 11

Kucharski F, Molteni F, King MP, Farneti R, Kang IS, Feudale L. 2013. On the need of intermediate complexity

general circulation models: a SPEEDY example. BAMS **94**: 25–30. 11

Kucharski F, Scaife A, Yoo JH. 2009. The CLIVAR C20C project: skill of simulating Indian monsoon rainfall on interannual to decadal timescales. does GHG forcing play a role? *Clim. Dyn.* **10**: 615–627. 75

Kucharski F, Zeng N, Kalnay E. 2012. A further assessment of vegetation feedback on decadal Sahel rainfall variability. *Clim. Dyn.* **40**: 1453–1466. 45, 52, 72

Latif M, Barnett TP. 1995. Interactions of the tropical oceans. *J. Clim.* **8**: 952–964. 39

Latif M, Dommenget D, Dima M, Grotzner A. 1999. The role of indian Ocean sea surface temperature in forcing East African rainfall anomalies during December-January 1997/98. *J. Clim.* **12**: 3497–3504. 48, 49

Lee J, Wang B, Kang I, Shukla J. 2010. How are seasonal prediction skills related to models performance on mean state and annual cycle. *Clim. Dyn.* **35**: 267–283. 14, 51, 98

Liu Z, D O, W T, S K. 2012. Tropical rainfall measuring mission (trmm) precipitation data and services for research and applications. *Bull. Amer. Meteor. Soc.* **93**: 1317–1325. 8

Luo JJ, Masson S, Behera S, Shingu S, Yamagata T. 2005. Seasonal climate predictability in a coupled OAGCM using a different approach for ensemble forecasts. *J. Clim.* **18**: 4474–4494. 16

McFarlane N, Scinocca J, Lazare M, Harvey R, Verseghy D, Li J. 2005. The CCCma third generation atmospheric general circulation model. *CCCma Internal Rep* **25**. 16

Meehl GA, Hu A, Santer BD. 2009. Climate shift in the Pacific and the relative roles of forced versus inherent decadal variability. *J. Clim.* **22**: 780–792. 73

Mengistu Tsidu G. 2012. High-resolution monthly rainfall database for ethiopia: Homogenization, reconstruction, and gridding. *J. Clim.* **25**: 8422–8443. 23

Miller AJ, Cayan DR, Barnett TP, Graham NE, Oberhuber JM. 1994. Interdecadal variability of the Pacific Ocean: model response to observed heat fluxes and wind stress anomalies. *Clim. Dyn.* **9**: 187–302. 73

Min YM, Kryjov VN, Oh JH. 2011. Probabilistic interpretation of regression-based downscaled seasonal ensemble predictions with the estimation of uncertainty. *Journal of Geophysical Research* **116**: DOI:101 029/2010JD015 284. 14, 98

Mitchell TD, Jones PD. 2005. An improved method of constructing a database of monthly climate observations and associated high-resolution grids. *J. Clim.* **25**: 693–712. 7, 8

Molteni F. 2005. Atmospheric simulations using a GCM with simplified physical parameterizations. i: Model climatology and variability in multi-decadal experiments. *Climate Dyn.* **20**: 175–191. 11

Morse A, Hoshen M, Reyes FD, Thomson M. 2003. Towards forecasting epidemics in africa the use of seasonal forecasting. *CLIVAR Exchanges* **27**: 50–52. 2

Murphy S, Washington R, Downing T, Martin R, Ziervogel G, Todd APM, Butterfield R, Briden J. 2001. Seasonal forecasting for climate hazards: prospect and responses. *Natural Hazards* **23**: 171–196. 4

Mutai CC, Ward MN. 2000. East African rainfall and the tropical circulation/convection on intraseasonal to interannual time scales. *J. Clim.* **13**: 3915–3939. 3, 44, 50

Mutai CC, Ward MN, Colman AW. 1998. Towards the prediction of the East Africa short rains based on sea-surface temperature atmosphere coupling. *Int. J. Climatol.* **18**: 975–997. 2, 3, 47, 50

Nicholson SF, Hoopingarner J, Kim E. 1988. Atlas of african rainfall and its interannual variability. *Dept. of Meteorology, The Florida State University, Tallahassee* : 237 pp. 20, 24, 26, 27, 46

NMA. 1996. Climatic and agroclimatic resources of ethiopia. national meteorological agency of ethiopia (nma). *Meteorological Research Report Series* **1**: 1–137. 21

Ogallo LJ. 1988. Relationship between seasonal rainfall in East Africa and the Southern Oscillation. *Int. J. Climatol.* **8**: 31–43. 2, 44, 48

Otieno VO, Anyah RO. 2013. Cmip5 simulated climate conditions of the greater horn of africa (gha). part 1: contemporary climate. *Clim. Dyn.* **8**: DOI 10.1007/s00 382–012–1549–z. 78

Palmer TN, Anderson DLT. 1994. The prospects for seasonal forecasting a review paper. *Q. J. R. Meteorol. Soc.* **126**: 2013–2033. 4

Palmer TNea. 2004. Development of a european multi-model ensemble system for seasonal to interannual prediction (DEMETER). *Bull Am Meteorol Soc* **85**: 853–872. 51

Peixoto J, Oort AH. 1983. The atmospheric branch of the hydrological cycle and climate. in variations in the global water budget. *D. Reidel, Doredrechet* : 5–65. 69

Philippon N, Camberlin P, Faucherau N. 2002. Empirical predictability study of the October-December East Africa rainfall. *Q. J. R. Meteorol. Soc.* **128**: 2239–2256. 3, 50

Rao SA, Behera S, Masson S, Luo JJ. 2007. Global analyses of sea surface temperature, sea ice, and night marine air temperature since the late nineteenth century. *J. Clim.* . 83

Rayner NA, Parker DE, Horton EB, Folland CK, Alexander LV, ell DPR, Kent EC, Kaplan A. 2003. Global analyses of sea surface temperature, sea ice, and night marine air temperature since the late nineteenth century. *J. Geophys. Res* **108**: doi: 10.1029/2002JD002 670. 11

Reverdin G, Cadet DL, Gutzler D. 1986. Interannual displacements of convection and surface circulation over the equatorial Indian Ocean. *Q. J. R. Meteorol. Soc.* **112**: 43–67. 35, 39

Ropelewski CF, Halpert MS. 1987. Global and regional scale precipitation patterns associated with the el niño/southern oscillation. *Monthly Weather Review* **115**: 1606–1626. 2, 31, 34

Rowell DP. 1998. Assessing Potential Seasonal Predictability with an Ensemble of Multidecadal GCM simulations. *J. climate.* **11**: 109–120. 3

Saha S, Nadiga S, Thiaw C, Wang J, Zhang WWQ, den Dool HV, Pan H, Moorthi S, Behringer D, Stokes D, Pena M, Lord S, White G, Ebisuzki W, Peng P, Xie P. 2006. The ncep climate forecast system. *J. Clim.* **19**: 3483–3517. 16, 50

Saji HN, Yamagata T. 2003. Structure of SSt and surface wind variability during Indian Ocean dipole mode events: COADS observations. *J. Clim.* **16**: 2735–2751. 42, 43, 46, 48, 55, 64

Saji NH, Goswami BN, Vinayachandran PN, Yamagata T. 1999. A dipole mode in the tropical Indian Ocean. *Nature* **401**: 360–363. xvi, 2, 34, 35, 36, 37, 38, 39, 40, 41, 42, 43, 44, 59, 62, 73, 89

Sallinger J. 2005. Climate variability and change: past, present and future-an overview. *Climate Change* **70**. 32

Scinocca J, Mcfarlane NA, Lazare M, Li J, Plummer D. 2008. The CCCma third generation AGCM and its extension into the middle Atmospheres. *Atmos Chem and Phys.* **8**: 7055–70. 16

Segele ZT, Lamb PJ. 2005. Characterization and variability of Kiremt rainy season over ethiopia. *Atmos. Phys.* **89**: 153–180. 21

Segele ZT, Lamb PJ, Leslie L. 2009. Seasonal-to-interannual variability of Ethiopia/Horn of Africa monsoon. part I: associations of wavelet-filtered large-scale Atmospheric circulation and global sea surface temperature. *J. Clim.* **22**: 3396–3421. 4, 21, 23, 28

Shi L, Hendon H, Alves O. 2012. How predictable is the Indian Ocean dipole? *Mon Weather Rev* **140**: 3867–3884. 86

Smith T, Reynolds R, Peterson T, Lawrimore J. 2008. Improvements to NOAA's historical merged Land Ocean surface temperature analysis. *J. Clim.* **21**: 2283–2296. 10

Smith TM, Reynolds RW. 2004. Improved Extended Reconstruction of SST (1854-1997). *J. Clim.* **17**: 2466–2477. 54

Sohn SJ, Min YM, Lee JY, Tam CY, Kang IS, Wang B, Ahn JB, Yamagata T. 2011. Leading modes of east asian winter climate variability and their predictability: an assessment of the APCC multimodel ensemble. *Journal of the Meteorological Society of Japan* **89**: 455–474. 14, 98

Sohn SJ, Min YM, Lee JY, Tam CY, Kang IS, Wang B, Ahn JB, Yamagata T. 2012. Assessment of the long-lead probabilistic prediction for the asian summer monsoon precipitation (1983 - 2011) based on the APCC multimodel system and a statistical model. *J. Geophys. Res.* **117**: DOI: 10.1029/2011JD016 308. 14, 51

Sun J, Ahn J. 2011. AGCM-based forecasting model for the landfall of tropical cyclones in China. *Adv. Atmos. Sci.* **28**: 1049–1055. 16

Trenberth KE. 1997. The definition of El Niño. *Bull. Am. Meteorol. Soc.* **78**: 2771–2777. 55

Trenberth KE, Hurrell JW. 1994. Decadal Atmosphere-Ocean variations in the Pacific. *Clim Dyn* **9**: 303–309. 73

Ummenhofer CC, Gupta AS, England MH, Reason CJC. 2009. Contributions of Indian Ocean Sea Surface Temperatures to Enhanced East African Rainfall. *J. Clim.* **22**: 993–1013. 3, 41, 49, 58, 61, 64, 67, 68, 70, 72, 83, 94, 98

Vintzileos A, Rienecker MM, Suarez MJ, Miller SK, Pegion PJ, Bacmeister JT. 2003. Simulation of the El Niño interannual prediction project coupled general circulation model. *CLIVAR Exchanges,International CLIVAR Project Office, Southampton, United Kingdom* **8**: 25–27. 16

Walker GT. 1924. Correlation in seasonal variations of weather, ix: A further study of world weather. *Memoirs of the Indian Meteorological Department XIV* . 32

Wang B, Lee JY, Kang IS, et al. 2009. Advance and prospectus of seasonal prediction: Assessment of the APCC/CLIPAS 14-model ensemble retrospective seasonal prediction (1980 - 2004). *Clim. Dyn.* **33**: 93–117. 14, 51, 89

Webster PJ, Moore AM, Loschnigg JP, Leben RR. 1999. Coupled Ocean-temperature dynamics in the Indian Ocean during 1997-98. *Nature* **401**: 356–360. 34, 35, 38, 39

Weisheimer A, Doblas-Reyes FJ, Palmer TN, Alessandri A, Arribas A, que N Keenlyside M MacVean A Navarra P Rogel MD. 2009. Ensembles: A new multi-model ensemble for seasonal-to-annual predictions-skill and progress beyond demeter in forecasting tropical pacific ssts. *Geophys Res Lett* **36**: 21 711. 50

Wilks D. 1995. Statistical Methods in the Atmospheric sciences: An introduction. *Academic Press.* . 78

Williams CA, Hanan NP. 2011. ENSO and IOD teleconnections for African ecosystems: evidence of destructive interference between climate oscillations. *Biogeosciences* **8**: 27–40. 49, 59, 76, 98

Wyrtki K. 1973. An Equatorial Jet in the Indian Ocean. *Science* **181**: 262–264. 34

Xie P, Arkin PA. 1996. Analysis of global monthly precipitation using gauge observations, satellite estimates, and numerical model predictions. *J. Clim.* **9**: 840–858. 7, 9

Xie SP, Annamalai H. 2002. Structure and mechanisms of south Indian Ocean climate variability. *J. Clim.* **15**: 864–878. 34, 36, 42, 44

Yamagata T, Behera SK, Luo JJ, Masson S, Jury M, Rao SA. 2004. Coupled Ocean-Atmosphere variability in the tropical Indian Ocean. Earth Climate: The Ocean-Atmosphere Interaction, geophys. monogr. *Amer. Geophys. Union* **147**: 189–212. 3, 39, 41, 62, 83, 94

Zhang Y, Wallace JM, Battisti DS. 1997. ENSO-like Interdecadal Variability: 1900-93. *J. Clim.* **10**: 1004–1020. 73

Zhao M, Hendon H. 2009. Representation and prediction of the Indian Ocean dipole in the poama seasonal forecast

model. *Q. J. R. Meteorol. Soc.* **135**: 337–352. 86, 99

Zhong A, Hendon H, Alves O. 2005. Indian Ocean variability and its association with ENSO in a global coupled model. *Nature* **18**: 3634–3649. 16